**DOKUZ EYLÜL UNIVERSITY**

**GRADUATE SCHOOL OF NATURAL AND APPLIED SCIENCES**

# DETERMINATION OF DISPERSIVITY VALUES FROM EXPERIMENTS IN HOMOGENEOUS AND NON HOMOGENEOUS POROUS MEDIA

**by**

**Ayşegül ÖZGENÇ AKSOY**

**September, 2008**

**İZMİR**

# DETERMINATION OF DISPERSIVITY VALUES FROM EXPERIMENTS IN HOMOGENEOUS AND NON HOMOGENEOUS POROUS MEDIA

**A Thesis Submitted to the**
**Graduate School of Natural and Applied Sciences of Dokuz Eylül University**
**In Partial Fulfillment of the Requirements for the Degree of Doctor of Philosophy**
**in Civil Engineering, Hydraulics Hydrology Water Resources Program**

**by**

**Ayşegül ÖZGENÇ AKSOY**

**September, 2008**
**İZMİR**

**Ph.D. THESIS EXAMINATION RESULT FORM**

We have read the thesis entitled **"DETERMINATION OF DISPERSIVITY VALUES FROM EXPERIMENTS IN HOMOGENEOUS AND NON HOMOGENEOUS POROUS MEDIA"** completed by **AYŞEGÜL ÖZGENÇ AKSOY** under supervision of **PROF. DR. MEHMET ŞÜKRÜ GÜNEY** and we certify that in our opinion it is fully adequate, in scope and in quality, as a thesis for the degree of Doctor of Philosophy.

Prof. Dr. Mehmet Şükrü GÜNEY

Supervisor

Prof. Dr. Yalçın ARISOY

Committee Member

Prof. Dr. Gültekin TARCAN

Committee Member

Prof. Dr. Halil ÖNDER

Jury Member

Assist. Prof. Dr. Birol KAYA

Jury Member

Prof.Dr. Cahit HELVACI
Director
Graduate School of Natural and Applied Sciences

## ACKNOWLEDGMENTS

I would like to thank my advisor Prof. Dr. M. Şükrü GÜNEY for his patience, guidance, and support during my PhD.

I would like to express my sincere appreciation to retired Prof. Dr. Turhan ACATAY, for his precious advices and suggestions.

I am grateful to our technician İsa ÜSTÜNDAĞ who constructed the flume and for his contribution.

I am especially indebted to my husband for his unfailing support and patience. I would like to thank my family to encourage me during my PhD.

I would like to thank my friends and my colleagues at Hydraulic Laboratory for their helps when I needed. I wish them a successful career.

The financial support provided by the TÜBİTAK is gratefully acknowledged.

**DETERMINATION OF DISPERSIVITY VALUES FROM EXPERIMENTS IN HOMOGENEOUS AND NON HOMOGENEOUS POROUS MEDIA**

## ABSTRACT

In this study, an elaborate experimental system is designed and constructed in Hydraulics Laboratory of the Civil Engineering Department of Dokuz Eylül University, in order to study contaminant transport in homogeneous as well as heterogeneous porous media.

A flume 12 m long, 135 cm wide and 60 cm high is built 70 cm over the floor, within Hydraulics Laboratory of Civil Engineering Department of Dokuz Eylül University. The porous media in the channel are constituted by sands of different size, and the tracer tests are carried out by using NaCl as contaminant. The concentrations in various directions are measured and their distributions are determined. Accordingly, the dispersivity values along the flow and in the two directions vertical to flow are determined applying the trial and error method to the relevant theoretical equation, by using Mass Transport 3 Dimensional (MT3DMS) software.

The heterogeneous medium is constituted from three horizontal layers with different kind of granular material. The concentration pattern is observed and dispersivity values are determined by trial and error method applied to the advection-dispersion equation.

The best match for 3-5 mm quartz sand is obtained for longitudinal dispersivity value of 12.2 cm. The ratios of horizontal transverse dispersivity to longitudinal dispersivity and vertical transverse dispersivity to longitudinal dispersivity are 0.21 and 0.05, respectively. The corresponding values for 1-3 mm quartz sand are 5.5 cm, 0.25 and 0.07 for 1-3 mm quartz sand and for 0.6-1.2 mm quartz sand 3 cm, 0.18 and 0.055. These ratios are in the order of magnitude with those obtained from in-situ tests, given in the related literature.

This experimental system is designed to investigate contaminant transport in steady as well as unsteady flow, provided that some required measurement devices are supplied. It will also be beneficial to procure necessary instruments and pursue this study in the case of unsteady flow.

**Keywords:** Groundwater flow, Contaminant transport, 3D dispersivity

# DİSPERSİVİTE DEĞERLERİNİN HOMOJEN VE HETEROJEN GÖZENEKLİ ORTAMLARDA DENEYLER YARDIMIYLA BELİRLENMESİ

## ÖZ

Bu çalışmada hem homojen hem de heterojen gözenekli ortamlarda kirliliğin taşınmasını araştırmak için Dokuz Eylül Üniversitesi Mühendislik Fakültesi İnşaat Mühendisliği Bölümü Hidrolik Laboratuarında kapsamlı bir deney sistemi tasarlanmış ve inşa edilmiştir. Yeraltısuyunda kirliliğin yayılmasında önemli bir rol oynayan dispersivite değerleri homojen ve heterojen ortamların her ikisi için üç boyutlu yeraltısuyu akımı durumunda deneysel olarak belirlenmişlerdir.

İnşaat Mühendisliği Bölümü Hidrolik Laboratuarında 12 m uzunluğunda, 135 cm genişliğinde ve 60 cm yüksekliğinde yerden 70 cm yukarıda bir kanal inşa edilmiştir. Kanaldaki gözenekli ortamlar farklı boyutlarda kumlar vasıtasıyla oluşturulmuş ve izleyici deneyleri kirletici olarak NaCl kullanılarak gerçekleştirilmiştir. Değişik doğrultulardaki konsantrasyonlar ölçülmüş ve dağılımları belirlenmiştir. Buna bağlı olarak akım boyunca ve akıma dik yönlerdeki dispersivite değerleri deneme yanılma yöntemi ilgili teorik bağıntılara uygulanarak Mass Transport 3 Dimensional (MT3DMS) yazılımının kullanımıyla belirlenmiştir.

Heterojen ortam farklı daneli malzemeler içeren üç yatay tabakayla oluşturulmuştur. Konsantrasyon dağılımı gözlenmiş ve dispersivite değerleri adveksiyon-dispersiyon denklemine deneme yanılma yöntemi uygulanarak belirlenmiştir.

3-5 mm kuvars kumu için en iyi uyum boyuna dispersivite değeri 12.2 cm, yatay dispersivite değerinin boyuna dispersivite değerine oranı 0.21 ve düşey dispersivitenin boyuna dispersivite değerine oranı 0.05 değerleri ile elde edilirken, bu değerler 1-3 mm kuvars kumu için 5.5 cm, 0.25 ve 0.07; 0.6-1.2 mm kuvars kumu için de 3 cm, 0.18 ve

0.055 olarak belirlenmiştir. Bu oranlar arazi çalışmaları sonucu elde edilen ve literatürde verilen değerlerle aynı büyüklüktedir.

Deney sistemi gerekli ölçüm cihazları sağlanması şartıyla kararlı rejimde olduğu kadar kararsız akım durumunda da kirlilik taşınmasını araştırmak için tasarlanmıştır. Gerekli ölçüm cihazlarının temin edilip bu araştırmaya kararsız akım durumunda da devam edilmesi faydalı olacaktır.

**Anahtar Kelimeler:** Yeraltısuyu akımı, Kirlilik taşınımı, 3B dispersivite

**CONTENTS**

**Page**

# CHAPTER ONE
# INTRODUCTION

## 1.1 Importance of Groundwater

In planet groundwater is the safest and most important sources of available freshwater. It is essential for life-sustaining, but is in grave hazard. It is threatened by pollution, over extraction, water mismanagement and rising populations. Namely groundwater sources are endangered.

Only 3% of all water on earth is freshwater. 97% is salt water as shown in Figure 1.1. 68.4% of the freshwater is glaciers, polar ice caps and permanent snow cover. Lakes and rivers are only 0.2% of freshwater. The remaining 32.4% comes from natural underground sources.

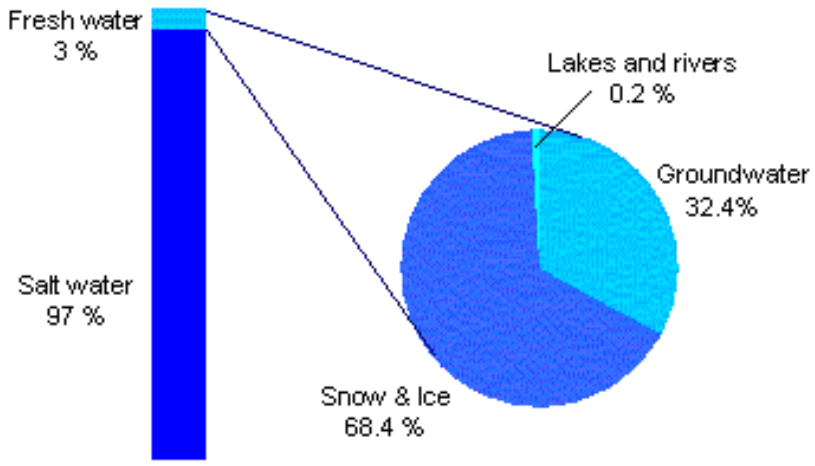


Figure 1.1 Distribution of earth water (Wikipedia)

Groundwater is generally more reliable for use than surface water. One of the reason is surface water is more easily polluted than groundwater. However once groundwater is contaminated, remedial options are extremely costly and difficult process. At the same time, since groundwater is invisible, the dangers are disregarded at most places around the world.

Contaminates can reach wells which are used for drinking, irrigation and other purposes. For example, a chemical spill at an industrial area located away from residential area could infiltrate the ground and finally enter the aquifer and can reach residential area. In this situation health of people is threatened.

In the world approximately one-fifth of all people do not have access to safe drinking water. Furthermore groundwater resources are withdrawn faster than it can be replenished. They are also contaminated by human, industrial and agricultural wastes. These unfavorable conditions can deprive future generations from using groundwater resources. Monitoring of the water at industrial, waste disposal, residential and agricultural sites must be improved.

**1.2 Literature Review**

Huang K., Toride N. and Genuchten Van (1995) conducted laboratory tracer experiments to determine values of dispersivity. 12.5 m long, 10 cm wide and 10 cm high channel constructed for this purpose. The length dimension of 12.5 m is chosen to allow for a scale-dependent dispersion process. Medium-textured sand is packed as uniformly as possible in the channel. NaCl solution of concentration $C_0$=6 g/l is injected into the sandy soil column and concentrations are estimated by electrical conductivity probes inserted at 100 cm intervals. According to experimental results dispersivity values ranged from 0.1 to 5.0 cm. They indicated that dispersivity increased with travel distance.

Kim D., Kim J., Yun S. and Lee S. (2002) determined longitudinal dispersivity in an unconfined sandy aquifer at laboratory scale. Model dimensions are 200 cm long, 50 cm width and 150 cm height. They indicated that dispersivity is proportional to the travel distance and the proportionality constant is equal to 0.3. This value is given as 0.1 in literature.

Kim S., Jo, Kim D. and Jury (2004) determined two-dimensional dispersivities in laboratory. A physical aquifer chamber 110 cm long, 25 cm wide and 71 cm high is constructed and KCl solution with chloride concentration of 1.5 g/l is applied at the upper left corner of the chamber. Samples are taken by using 1 ml syringes at predetermined sampling ports in two dimensions to obtain two-dimensional chloride distribution. Samples are taken 9 hours and 16 hours after injection of the solution. Chloride concentrations of samples are measured by using ion chromatography. A numerical transport model (MT3D) is established to estimate dispersive parameters by matching observed and calculated chloride concentrations. The best match is obtained for longitudinal dispersivity of 0.25 cm and for the ratio of transverse to longitudinal dispersivity of 0.2.

Maineult A., Bernabe Y and Ackerer P. (2004) investigated electrical response of flow and advection in a laboratory sand box. Sand box has dimensions 44.25 cm by 23.75 cm by 26.5 cm. NaCl solution is given into the sand box and electrical potential differences are measured between custom made electrodes. After the experiments they observed that electric signal is proportional to the salinity. They indicated that monitoring potential differences allows to determine the concentration in sand box.

Mascioli S., Benavente M., and Martinez D.E. (2005) estimated dispersivity value in laboratory for selected undisturbed sediment from Buenos Aires in Argentina. Experimental curves of arrival for chloride are adjusted with those obtained from numerical simulation. The best adjustment is obtained when dispersivity value is 1 cm. They indicated that the determination of this parameter is very important since it is needed to predict contaminant migration for numerical simulations.

Ham, Prommer, Olsson, Schotting and Grathwohl (2007) determined transversal dispersivity by using acrylic glass tanks filled with silica glass beads of uniform grain diameter. The smaller tank, of dimensions 28.0 cm×14.0 cm×1.05 cm, was used initially

for the non-reactive tracer experiments. Fluorescein is used as a tracer. According to the experimental results the transversal dispersivity was determines as 0.25 cm.

The dispersivity values are determined by neglecting diffusion since groundwater flow velocity is relatively high. The experimental determination of the dispersivity values in three dimensions has not been yet encountered.

### 1.3 Scope of this study

Mathematical models for groundwater flow and contaminant transport should be established to predict future conditions of the groundwater levels and contamination values. The various mathematical models obtained under different scenarios can be used in order to determine the precautions to take, if necessary. The results of the model are more meaningful and reliable only if all parameters for flow and transport process are known. Dispersivity is one of the most important parameter for transport modeling.

In this study dispersivity values are determined for sandy aquifers in three-dimensions by means of an experimental system built in the Hydraulics Laboratory of Civil Engineering Department. A channel 1320 cm long, 190 cm wide and 60 cm high is constructed.

3-5 mm quartz sand is used to constitute the homogeneous porous medium.

The layered porous medium is constituted by using 0.6-1.2 mm (upper layer), 1-3 mm (intermediate layer) and 3-5 mm (lower layer) quartz sands.

# CHAPTER TWO
# THEORY OF CONTAMINANT TRANSPORT

## 2.1 Equation of Groundwater Flow

According to Darcy Law, the flow rate in a porous medium maybe written as follows:

$$Q = -K\,A\frac{dh}{dx} \tag{2.1}$$

where x represents distance along the flow, dh/dx is the hydraulic gradient, A is the cross sectional area and K is the hydraulic conductivity of the porous material.

The head is

$$h = z + \frac{P}{\rho\, g} \tag{2.2}$$

where P is the pressure, ρ is the mass density of the water, g is the gravitational acceleration and z is the elevation. The kinetic term ($v^2/2g$) is negligible since the velocity is generally low enough.

Average seepage velocity can be defined as

$$v = \frac{Q}{n\,A} \tag{2.3}$$

where n is the effective porosity.

Substituting Eq. 2.1 into Eq. 2.3 yields

$$v = -\frac{K}{n}\frac{dh}{dx} \tag{2.4}$$

Darcy velocity is

$$q = \frac{Q}{A} = -K\frac{dh}{dx} \tag{2.5}$$

For three-dimensional problem the Darcy velocity is expressed as a vector namely,

$$\vec{q} = q_x\vec{i} + q_y\vec{j} + q_z\vec{k} \tag{2.6}$$

where $\vec{i}$, $\vec{j}$, $\vec{k}$ are the conventional unit vectors in the x, y and z directions, respectively and $q_x$, $q_y$ and $q_z$ are the scalar components of the Darcy velocity (Zheng&Bennett, 2002).

Darcy velocity components (for the water of constant density and viscosity) are

$$\begin{aligned} q_x &= -K_x\frac{\partial h}{\partial x} \\ q_y &= -K_y\frac{\partial h}{\partial y} \\ q_z &= -K_z\frac{\partial h}{\partial z} \end{aligned} \tag{2.7}$$

where $K_x$, $K_y$ and $K_z$ are the components of hydraulic conductivity.

If the principal components of hydraulic conductivity are not aligned with horizontal and vertical coordinate axes, each velocity component is a function of head in all three dimensions rather than solely in the direction of the velocity component. Therefore Eq. 2.7 becomes

$$\begin{aligned} q_x &= -K_x\frac{\partial h}{\partial x} - K_{xy}\frac{\partial h}{\partial y} - K_{xz}\frac{\partial h}{\partial z} \\ q_y &= -K_{yx}\frac{\partial h}{\partial x} - K_y\frac{\partial h}{\partial y} - K_{yz}\frac{\partial h}{\partial z} \\ q_z &= -K_{zx}\frac{\partial h}{\partial x} - K_{zy}\frac{\partial h}{\partial y} - K_z\frac{\partial h}{\partial z} \end{aligned} \tag{2.8}$$

where $K_x$, $K_y$, $K_z$ are principal components of the hydraulic conductivity tensor and $K_{xy}, K_{yx}, K_{xz}, K_{zx}, K_{yz}, K_{zy}$ are the cross-terms of the same tensor.

In practice the principal components of the hydraulic conductivity tensor can be aligned with horizontal and vertical coordinate axes, thus the cross-terms become zero.

The equation of groundwater flow is written as

$$\frac{\partial}{\partial x}\left(K_x \frac{\partial h}{\partial x}\right)+\frac{\partial}{\partial y}\left(K_y \frac{\partial h}{\partial y}\right)+\frac{\partial}{\partial z}\left(K_z \frac{\partial h}{\partial z}\right)+q_s = S_s \frac{\partial h}{\partial t} \tag{2.9}$$

## 2.2 Contaminant Transport Mechanisms in Saturated Porous Media

The movement of a contaminant with the flowing groundwater according to the seepage velocity, or average linear velocity in the pore space is referred to as **advection**. Seepage velocity is

$$v_x = \frac{K}{n}\frac{dh}{dx} \tag{2.10}$$

where n is effective porosity, K is hydraulic conductivity, dh/dl is hydraulic gradient.

Solute in water is moving from an area of higher concentration to an area of lower concentration. This is known as **diffusion**. Diffusion can occur even if there is no groundwater flow.

Heterogeneities in the medium create variations in flow velocities and flow paths. These variations are due to friction within a single pore channel, to velocity differences from one channel to another, or to variable path lengths. Water which contains solute is not traveling at the same velocity so mixing occurs along the flow path. This is called as

**mechanical dispersion**. Laboratory column studies have shown that dispersion is a function of average linear velocity and a factor α, called dispersivity.

Diffusion and mechanical dispersion can not be separated from each other and these two processes are called as **hydrodynamic dispersion** which is described by a tensor named hydrodynamic dispersion coefficient (D) with components $D_x$, $D_{xy}$,… as follows:

$$D = \begin{pmatrix} D_x & D_{xy} & D_{xz} \\ D_{yx} & D_y & D_{yz} \\ D_{zx} & D_{zy} & D_z \end{pmatrix} \tag{2.11}$$

where

$$D_x = \alpha_L \frac{v_x^2}{|v|} + \alpha_{TH} \frac{v_y^2}{|v|} + \alpha_{TV} \frac{v_z^2}{|v|} + D^* \tag{2.12}$$

$$D_y = \alpha_L \frac{v_y^2}{|v|} + \alpha_{TH} \frac{v_x^2}{|v|} + \alpha_{TV} \frac{v_z^2}{|v|} + D^* \tag{2.13}$$

$$D_z = \alpha_L \frac{v_z^2}{|v|} + \alpha_{TH} \frac{v_y^2}{|v|} + \alpha_{TV} \frac{v_x^2}{|v|} + D^* \tag{2.14}$$

$$D_{xy} = D_{yx} = (\alpha_L - \alpha_{TH}) \frac{v_x v_y}{|v|} \tag{2.15}$$

$$D_{xz} = D_{zx} = (\alpha_L - \alpha_{TV}) \frac{v_x v_z}{|v|} \tag{2.16}$$

$$D_{yz} = D_{zy} = (\alpha_L - \alpha_{TV}) \frac{v_y v_z}{|v|} \tag{2.17}$$

$$|v| = \sqrt{v_x^2 + v_y^2 + v_z^2} \tag{2.18}$$

where

$D_x, D_{xy}, D_{yx}, D_y, D_{xz}, D_{zx}, D_z, D_{yz}, D_{zy}$ are dispersion coefficient tensor components

$\alpha_L$ is longitudinal dispersivity

$\alpha_{TH}$ is horizontal transverse dispersivity

$\alpha_{TV}$ is vertical transverse dispersivity

$D^*$ is diffusion coefficient

$v_x, v_y, v_z$ are the components of the average linear velocity (Zheng&Bennett, 2002).

Diffusion is a process slower than the mechanical dispersion. Diffusion is dominant only when the groundwater velocity is too slow.

**2.3 Derivation of Advection-Dispersion Equation**

The difference between the mass of solute which enters and leaves the representative elementary volume will be equal to the rate of mass change in the representative elementary volume (Figure 2.1) (Zheng&Bennett, 2002).

The mass flux (F) of solute in the x direction for the two mechanisms of solute transport is given by

Advective transport: $v_x nCdA_x$

Dispersive transport: $-n\left(D_x \frac{\partial C}{\partial x} + D_{xy} \frac{\partial C}{\partial y} + D_{xz} \frac{\partial C}{\partial z}\right) dA_x$

where $dA_x$ is the elemental cross-sectional area of the cubic element normal to x direction and C is concentration of the tracer.

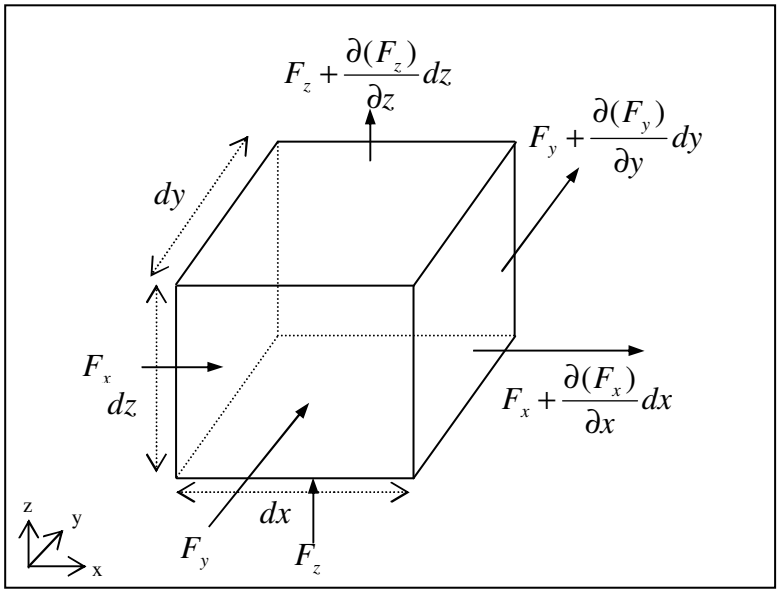


Figure 2.1 The representative elementary volume

The total mass of solute per unit cross-sectional area per unit time

$$F_x = v_x nC - nD_x \frac{\partial C}{\partial x} - nD_{xy} \frac{\partial C}{\partial y} - nD_{xz} \frac{\partial C}{\partial z} \tag{2.19}$$

and similarly

$$F_y = v_y nC - nD_{yx} \frac{\partial C}{\partial x} - nD_y \frac{\partial C}{\partial y} - nD_{yz} \frac{\partial C}{\partial z} \tag{2.20}$$

$$F_z = v_z nC - nD_{zx} \frac{\partial C}{\partial x} - nD_{zy} \frac{\partial C}{\partial y} - nD_z \frac{\partial C}{\partial z} \tag{2.21}$$

The negative sign indicates that the concentration decreases along the flow.

Thus the solute entering the representative elementary volume for three directions can be expressed as

$$F_x \, dy \, dz + F_y \, dx \, dz + F_z \, dx \, dy \tag{2.22}$$

The solute leaving the representative elementary volume corresponds to

$$(F_x + \frac{\partial F_x}{\partial x} dx) dy\, dz + (F_y + \frac{\partial F_y}{\partial y} dy)\, dx\, dz + (F_z + \frac{\partial F_z}{\partial z} dz)\, dx\, dy \tag{2.23}$$

The difference in the amount solute entering and leaving the elementary volume is equal to

$$-\left( \frac{\partial F_x}{\partial x} + \frac{\partial F_y}{\partial y} + \frac{\partial F_z}{\partial z} \right) dx\, dy\, dz \tag{2.24}$$

The rate of mass change in the elementary volume can be written as

$$n \frac{\partial C}{\partial t} dx\ dy\ dz \tag{2.25}$$

By the law of mass conservation Eq. 2.24 is equal to Eq. 2.25

$$\left( \frac{\partial F_x}{\partial x} + \frac{\partial F_y}{\partial y} + \frac{\partial F_z}{\partial z} \right) = -n \frac{\partial C}{\partial t} \tag{2.26}$$

By substituting Eqs. 2.19, 2.20 and 2.21 in Eq. 2.26, three dimensional advective-dispersion equation can be expressed as

$$\begin{aligned} &\frac{\partial}{\partial x}\left( D_x \frac{\partial C}{\partial x} + D_{xy} \frac{\partial C}{\partial y} + D_{xz} \frac{\partial C}{\partial z} \right) - \frac{\partial}{\partial x}(v_x C) + \frac{\partial}{\partial y}\left( D_{yx} \frac{\partial C}{\partial x} + D_y \frac{\partial C}{\partial y} + D_{yz} \frac{\partial C}{\partial z} \right) - \frac{\partial}{\partial y}(v_y C) \\ &+ \frac{\partial}{\partial z}\left( D_{zx} \frac{\partial C}{\partial x} + D_{zy} \frac{\partial C}{\partial y} + D_z \frac{\partial C}{\partial z} \right) - \frac{\partial}{\partial z}(v_z C) = \frac{\partial C}{\partial t} \end{aligned} \tag{2.27}$$

or in subscript form as

$$\frac{\partial}{\partial x_i}\left( D_{ij} \frac{\partial C}{\partial x_j} \right) - \frac{\partial}{\partial x_i}(v_i C) = \frac{\partial C}{\partial t} \tag{2.28}$$

## 2.4 Initial and Boundary Conditions

The solution of the Eq. 2.28 is the concentration distribution which is dependent on position and time. Initial and boundary conditions must be specified before mathematical solution, in order to obtain a solution.

The initial condition is the concentration distribution at t=0 and in general form it can be written as

$$C(x, y, z, t)=C^0(x, y, z) \quad \text{on R} \tag{2.29}$$

where $C^0(x, y, z)$ is a known concentration and R denotes the space domain.

There are three types of boundary condition.

The first one called Dirichlet condition where concentration distribution is specified along a boundary for a specified time;

$$C(x, y, z, t)=c(x, y, z) \qquad \text{on } B_1, \text{ for } t > 0 \tag{2.30}$$

where $B_1$ is a part of the boundary of R, c(x,y,z) is a known function.

The second type of boundary condition is called Neumann condition and gives a known dispersion flux along the boundary;

$$-D_{ij}\frac{\partial C}{\partial x_j} = f_i(x, y, z) \qquad \text{on } B_2, \text{ for } t > 0 \tag{2.31}$$

where $B_2$ is a part of the boundary of R and $f_i(x,y,z)$ is a known function.

The third type is known as Cauchy boundary condition and defines both the concentration along the boundary and the concentration gradient across the boundary.

$$-D_{ij}\frac{\partial C}{\partial x_j}+v_i C = g_i(x,y,z) \qquad \text{on } B_3, \text{ for } t > 0 \qquad (2.32)$$

where $B_3$ is a part of the boundary of R and $g_i(x,y,z)$ is a known function.

# CHAPTER THREE
# NUMERICAL SOLUTIONS

In this study, Mass Transport 3 Dimensional (Zheng and Wang, 1999, MT3DMS code) which is a three-dimensional solute transport simulation model incorporating various methods such as finite differences, third-order TVD, mixed eulerian-lagrangian is used to solve the three dimensional advective-dispersive transport equation. The different methods are all performed and similar results are obtained. Accordingly the Finite differences method is reviewed and applied to solve Eq. 2.28. The term related to diffusion is neglected since its contribution is negligibly small.

## 3.1 Finite Difference Scheme for Advection-Dispersion Equation

An aquifer system is discretized into a mesh of cells and the locations are described in terms of rows (i), columns (j), and layers (k) as illustrated in Figure 3.1.

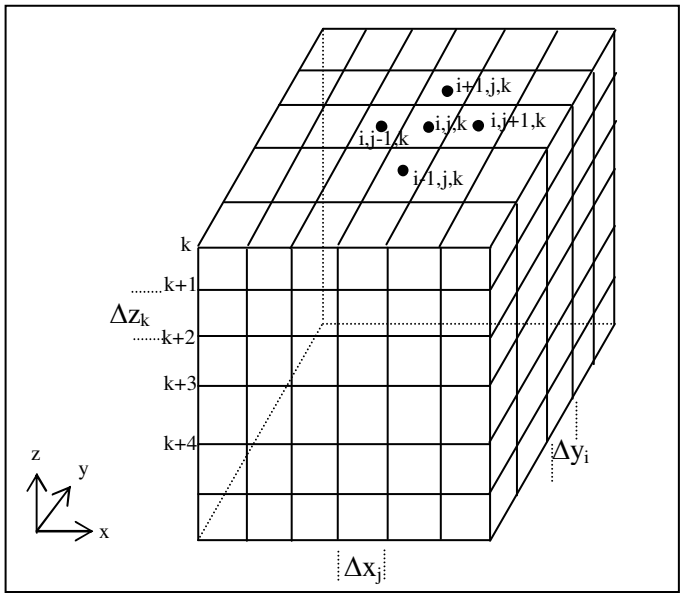


Figure 3.1 Mesh-centered finite differences grid

Applying the implicit finite-difference algorithm with notations given in Figure 3.1, some derivatives in Eq. 2.27 can be expressed in as follows:

$$\frac{\partial C}{\partial t} = \frac{C_{i,j,k}^{n+1} - C_{i,j,k}^{n}}{\Delta t} \tag{3.1}$$

in which the superscript n corresponds to time.

$$\begin{aligned}\frac{\partial}{\partial x}(v_x C) = {} & v_{x\,i,j+1/2,k}\,\frac{\alpha_{x\,j+1/2}\,C_{i,j,k}^{n+1} + (1-\alpha_{x\,j+1/2})C_{i,j+1,k}^{n+1}}{\Delta x_j} \\ & - v_{x\,i,j+1/2,k}\,\frac{\alpha_{x\,j-1/2}\,C_{i,j-1,k}^{n+1} + (1-\alpha_{x\,j-1/2})C_{i,j,k}^{n+1}}{\Delta x_j}\end{aligned} \tag{3.2}$$

where $j \pm 1/2$ denotes cell interfaces normal to the x direction and $\alpha_{x\,j\pm1/2}$ is the spatial weighting factor for the advection term defined as $\alpha_{x\,j+1/2} = \dfrac{\Delta x_{j+1}}{\Delta x_j + \Delta x_{j+1}}$.

$$\frac{\partial}{\partial x}\left(D_x \frac{\partial C}{\partial x}\right) = D_{x\,i,j+1/2,k}\,\frac{C_{i,j+1,k}^{n+1} - C_{i,j,k}^{n+1}}{\Delta x_j (0.5\Delta x_j + \Delta x_{j+1})} - D_{x\,i,j-1/2,k}\,\frac{C_{i,j,k}^{n+1} - C_{i,j-1,k}^{n+1}}{\Delta x_j (0.5\Delta x_{j-1} + \Delta x_j)} \tag{3.3}$$

$$\begin{aligned}&\frac{\partial}{\partial x}\left(D_{xy} \frac{\partial C}{\partial y}\right) = \\ &D_{xy,i,j+1/2,k}\,\frac{\omega_{x\,j+1/2} C_{i+1,j,k}^{n+1} + (1-\omega_{x\,j+1/2})C_{i+1,j+1,k}^{n+1} - \omega_{x\,j+1/2} C_{i-1,j,k}^{n+1} - (1-\omega_{x\,j+1/2})C_{i-1,j+1,k}^{n+1}}{\Delta x_j (0.5\Delta y_{i-1} + \Delta y_i + 0.5\Delta y_{i+1})} \\ &- D_{xy,i,j-1/2,k}\,\frac{\omega_{x\,j-1/2} C_{i+1,j-1,k}^{n+1} + (1-\omega_{x\,j-1/2})C_{i+1,j,k}^{n+1} - \omega_{x\,j-1/2} C_{i-1,j-1,k}^{n+1} - (1-\omega_{x\,j-1/2})C_{i-1,j,k}^{n+1}}{\Delta x_j (0.5\Delta y_{i-1} + \Delta y_i + 0.5\Delta y_{i+1})}\end{aligned} \tag{3.4}$$

where $\omega_x$ is the spatial weighting factors.

The other derivatives in Eq. 2.27 can be written in a similar fashion, and this equation is solved by taking into consideration also initial and boundary conditions.

Initial and boundary conditions for the steady state groundwater flow and contaminant transport models are given below.

Groundwater flow model:

Initial condition: $h(x,y,z,0)=h_0(x)$

Boundary condition: $h(0,y,z,t) = h_1 = \text{constant}$

$h(L,y,z,t) = h_2 = \text{constant}$

where L is the channel length.

Contaminant transport model :

Initial condition: $C(x,y,z,0) = 0$

Boundary condition: $C(0,y,z,t) = C_0$

# CHAPTER FOUR
# CONSTRUCTION OF THE EXPERIMENTAL SETUP AND MEASUREMENT TECHNIQUE

## 4.1 Design and Construction of the Experimental System

Dispersivity is one of the most important parameter to model and describe solute transport in porous media. The determination of the longitudinal, tranversal and vertical dispersivity for an aquifer is important to understand the shape of the distribution of a contaminant in two and three dimensions (Fetter, 1993). However its estimation is difficult since longitudinal and two transversal components are required. If sufficient observation data exist, dispersivity can be determined until the compatibility between the observed and calculated concentrations obtained from solute transport model is acceptable. They can be also determined from field tracer experiments but this method is extremely expensive and time consuming. Alternatively, the experiments carried out in laboratory can be used to determine the dispersivities.

A flume is constructed in the Hydraulic Laboratory of Civil Engineering Department in Dokuz Eylül University in order to investigate contaminant transport. This flume is 12 m long, 1.35 m wide and 0.60 m high. Its height from the ground level is approximately 70 cm in order to place and reach easily piezometer tubes which are located at the bottom of the channel. The weight of the channel is approximately 30 tons including the weight of the granular material and concrete plaque. So it was necessary to determine the bearing capacity. Three bricks are tested and the average bearing capacity of a brick is determined as 932 $kN/m^2$ which is sufficient for supporting the channel.

Homogeneous porous medium is prepared with 3-5 mm quartz coarse sand. The layered porous medium is constituted by using 0.6-1.2 mm (upper layer), 1-3 mm (intermediate layer) and 3-5 mm (lower layer) quartz sands.

Two constant level reservoirs are placed at upstream and downstream part of the channel. Plan view and cross section of the channel are shown in Figures 4.1a, 4.1b and 4.1c.

50 piezometers are placed in the channel to determine groundwater hydraulic heads. The observed heads are compared with those obtained from numerical solution of groundwater flow equation.

NaCl solution is used as tracer to investigate contaminant transport in the channel to determine the dispersivities for 3 dimensions. The measurements are carried out at 220 points in order to determine the dispersivities for 3 dimensions. Before placing the porous material in the channel, a chrome-nickel plate is placed at its bottom. Once the porous material is placed in the channel, copper wires are installed at measurement points. Then an electrical signal is applied to the plate and wires. The conductivities are read by using a data card and these values are transferred to the computer. These conductivity values are converted to concentration values by means of the calibration curve which is generated prior to experiments.

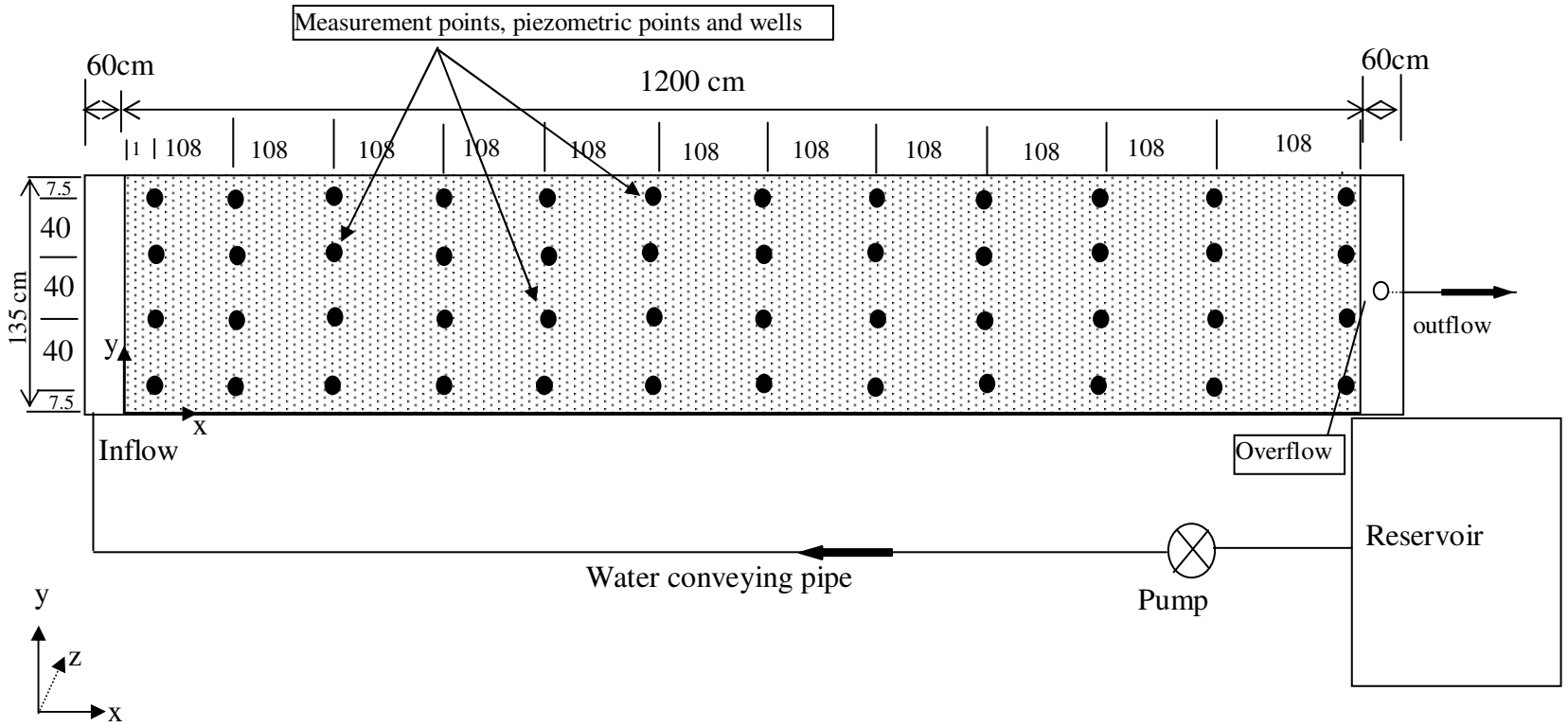


Figure 4.1a The plan view of the channel

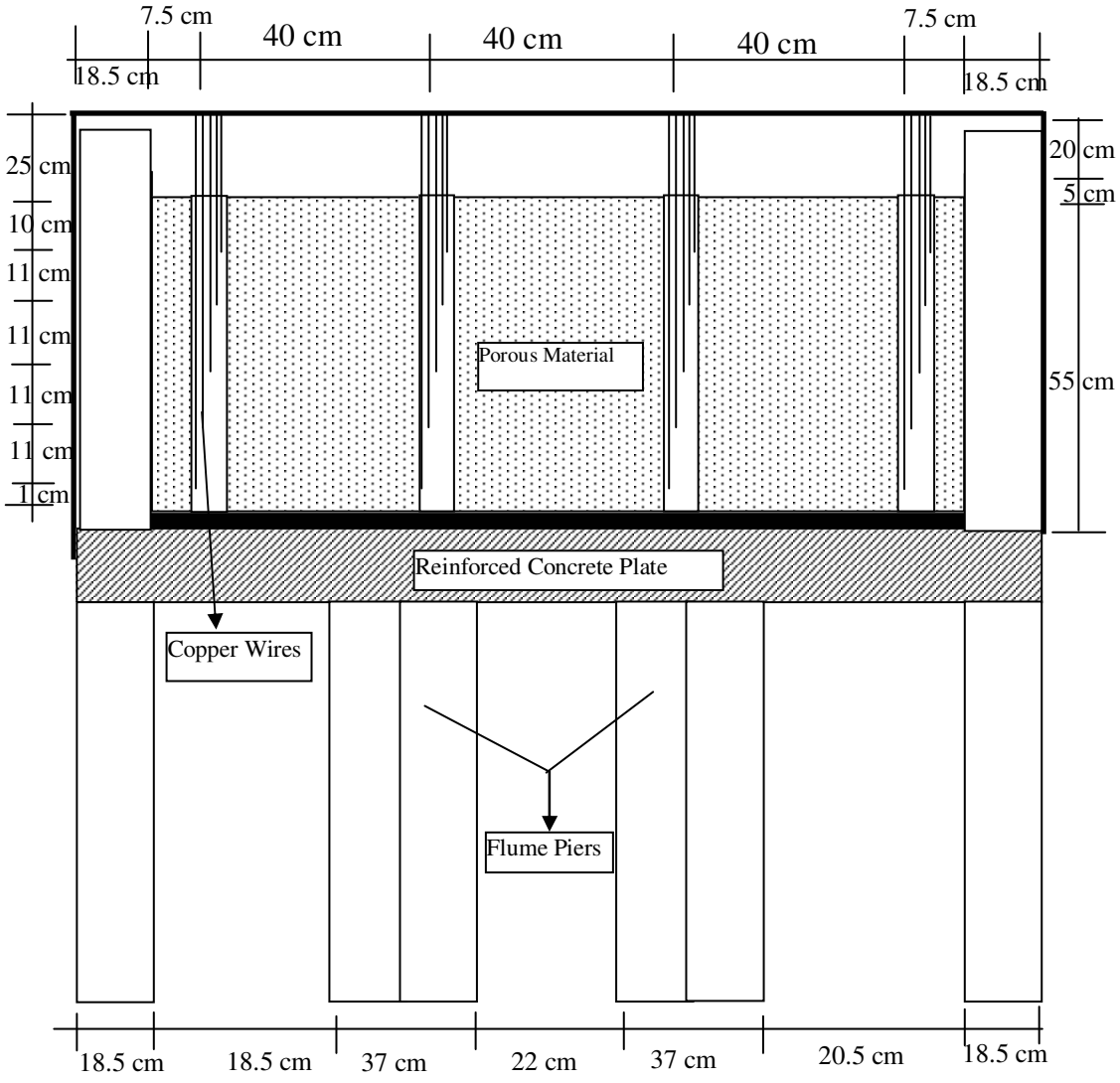


Figure 4.1b The transversal-section of the channel

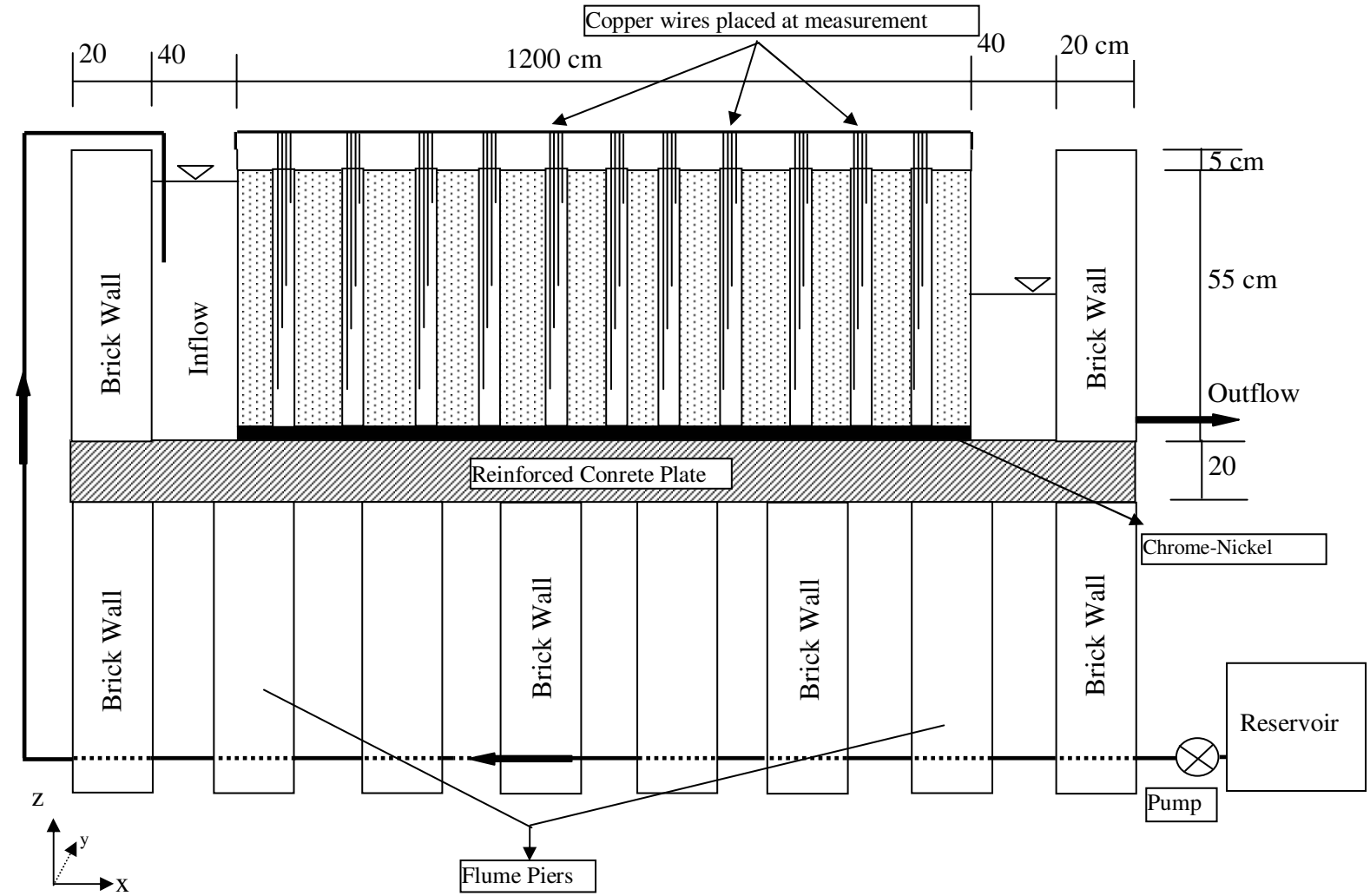


Figure 4.1c The longitudial-section of the channel

The general view of the constructed channel is given in Figure 4.2. The construction stages of the channel are given in the appendix.

Figure 4.2 The general view of the channel

A scanner is manufactured with 236 inputs to detect the electrical signals from the measurement points as shown in Figure 4.3.


Figure 4.3 The manufactured scanner

## 4.2 Measurement Technique

### *4.2.1 Discharge measurement*

Since groundwater flow is at steady state, the discharge is measured at the downstream end of the channel by using scaled container (Figure 4.4). Discharge is the volume of the scaled container divided by the time elapsed for filling it.


Figure 4.4 The discharge measurement tools

### *4.2.2 Water Level Measurement*

Water levels in the channel are read from the piezometer tubes by means of straightedges located at both side of the panel (Figure 4.5).


Figure 4.5 The panel of piezometers for reading the water levels

### *4.2.3 Conductivity of the water*

The WPA CM35 is a compact portable analogue device to measure conductivity (the inverse of resistance), suitable for field or laboratory use (Figure 4.6). It has an input which is used to transmit signals and read the conductivity values and, an output used to transfer the conductivity values to computer as shown in Figure 4.6. The cables which are fastened to the chrome-nickel plate and copper wires are connected to input whereas the cables fixed to data card are attached to output of the conductivity meter.


Figure 4.6 The conductivity Meter

The electrical scheme of the system is shown in Figure 4.7. R corresponds to the porous medium between the end of the probe (copper wire) and the chrome-nickel plate.

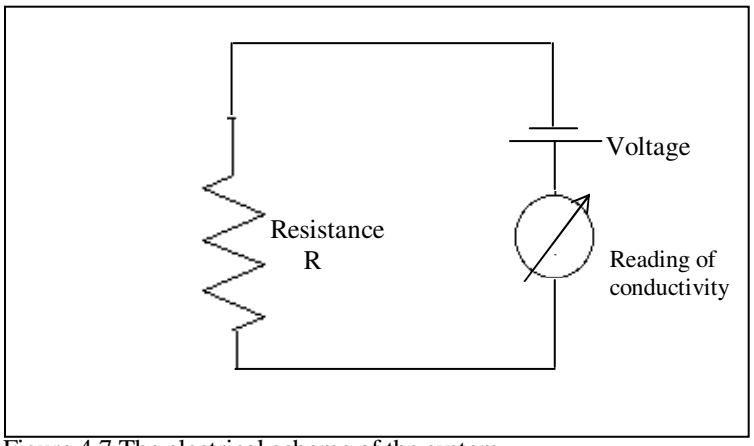


Figure 4.7 The electrical scheme of the system

Electrical conductivity is the inverse of the electrical resistance which is expressed as $R = \rho\, l / A$ where $\rho$ is resistivity, $l$ is vertical length and A is the cross sectional area of the conductor. Since resistance is proportional with length $l$ its effect is investigated and conductivity values of the water with different NaCl concentration are read for different lengths. Measured conductivities sketched in Figure 4.8 show that the effect of length can be neglected compared to the effect of the NaCl solution, since the conductivity values for different lengths are similar one to another. Measured conductivity values (therefore concentrations) are assumed to be uniform through the length $l$.

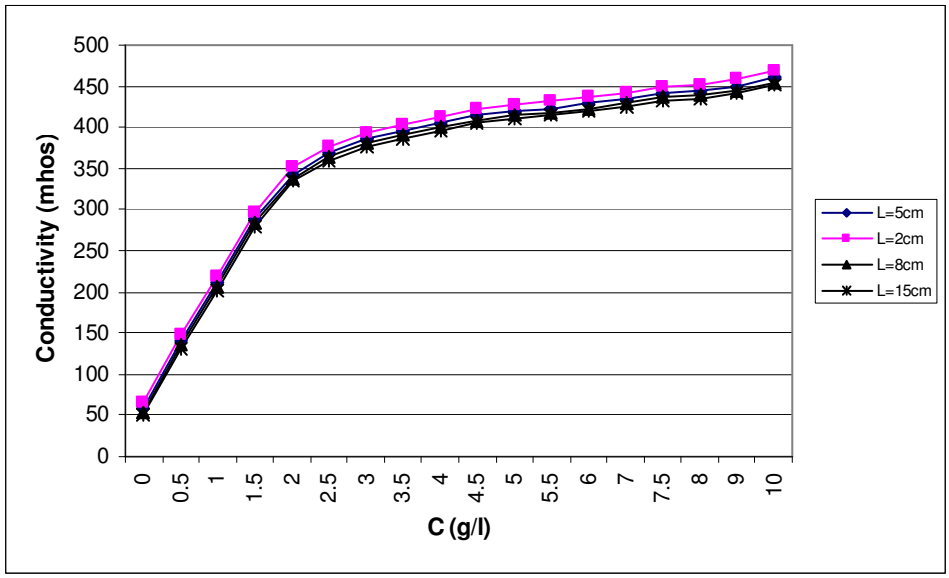


Figure 4.8 The conductivity values for different vertical distance values ($l$)

The digitalized conductivity values are transferred to the computer by using data card and a programme written in Visual basic language. With the aid of this programme the conductivity values can be read and stored every specified time interval. This interval may be chosen in the range of millisecond to second. Figure 4.9 shows the data card connections.

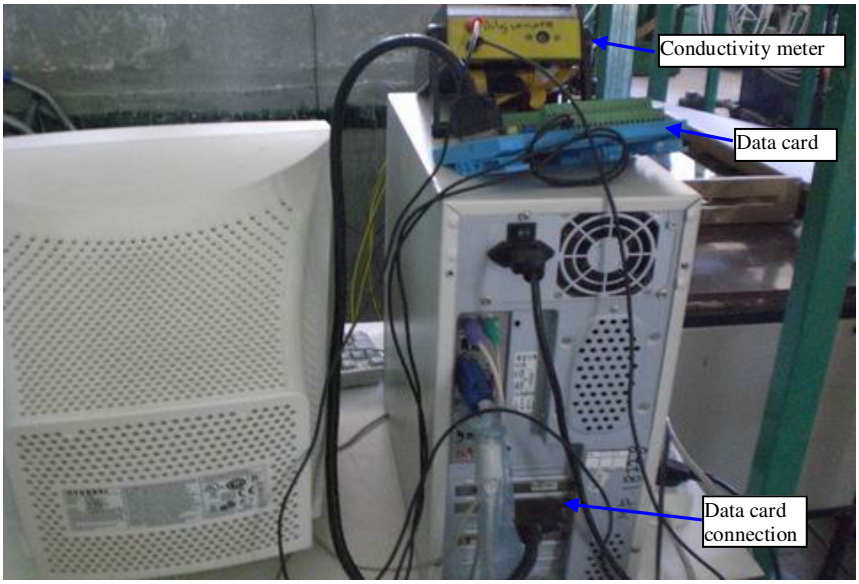


Figure 4.9 The connections of the data card

The apparatus (scanner) with 236 inputs shown in Figure 4.3 transmits the electrical signal to measurement points one by one. The transmission interval can be selected as 1 second, 5 seconds, 10 seconds or 20 seconds by using the switches mounted on the apparatus as shown in Figure 4.10.

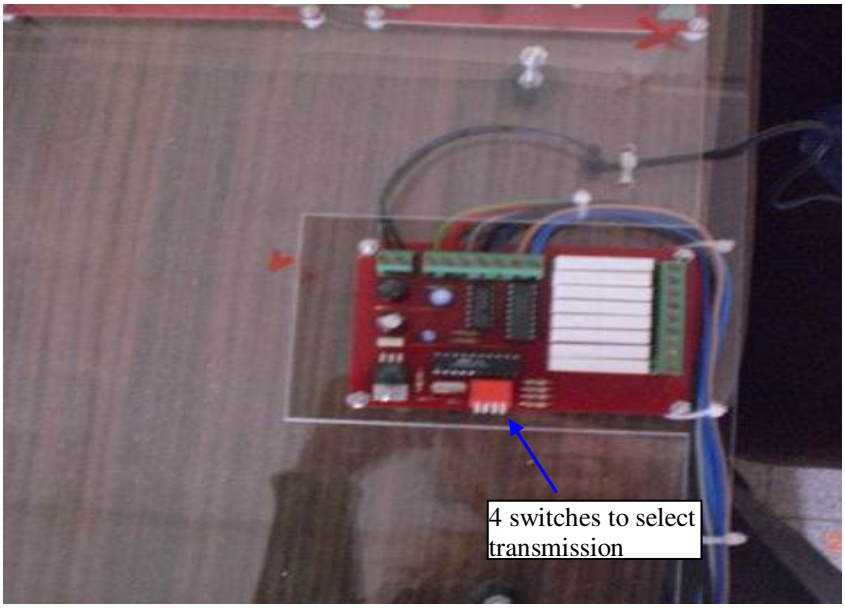


Figure 4.10 The arrangement designed to select the interval of transmission

# CHAPTER FIVE
# EXPERIMENTAL RESULTS

## 5.1 Determination of the hydraulic conductivity (K)

Hydraulic conductivity value is determined by using a permeameter based on Darcy experiment and manufactured in the laboratory (Figure 5.1). Discharge is measured by using scaled container. The values of discharge, hydraulic gradient and cross sectional area are given in Table 5.1. According to experimental results hydraulic conductivity value of the 3-5 mm quartz sand is found as approximately 10 cm/sec according to Darcy Law given by equation 5.1.

$$Q = K\,A\,\frac{\Delta h}{L} \tag{5.1}$$

where Q is discharge, K is hydraulic conductivity, A is the cross-sectional area and Δh/L is the hydraulic gradient.

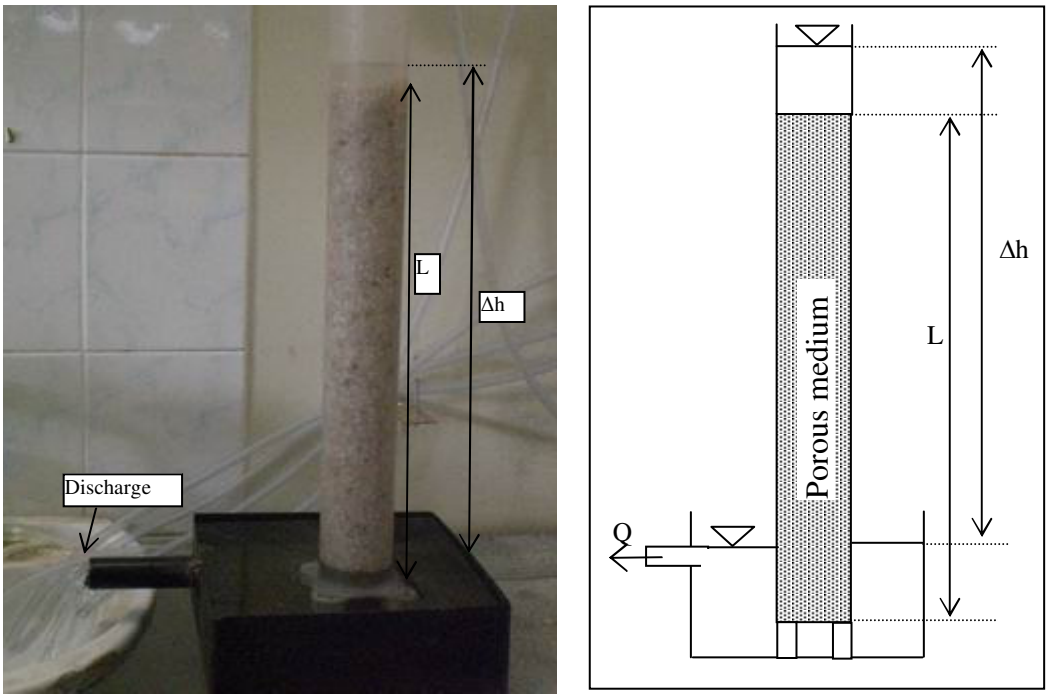


Figure 5.1 The device manufactured to measure hydraulic conductivity

Table 5.1 Hydraulic conductivity values determined by using permeameter

| Discharge (lt/sec) | Hydraulic gradient Δh /L | Cross sectional area ($cm^2$) | Hydraulic Conductivity (cm/sec) |
|---|---|---|---|
| 0.305 | 0.92 | 33.2 | 10 |
| 0.304 | 0.94 | 33.2 | 9.75 |
| 0.309 | 0.91 | 33.2 | 10.25 |

The determined value is checked by means of observed water levels in the channel. Water levels in upstream and downstream reservoirs are kept constant by adjusting the position of the gate at the downstream reservoir to establish steady-state condition. Then the water levels for each section are read by using the piezometer panel. The discharge of the system is measured by means of a scaled container at the downstream end of the channel. The hydraulic gradients are computed for each interval by dividing water level differences to the lengths between two subsequent sections. Consequently the hydraulic conductivity values are found from the Darcy Law. These experiments are repeated for 3 different discharges and the average hydraulic conductivity for the medium is determined as 10.02 cm/sec. By using the mean diameter of 4 mm Reynolds number is computed. The results are given in Table 5.2.

Table 5.2 Hydraulic conductivity values determined from sand tank model

| Discharge (lt/sec) | Water level in upstream end (cm) | Water level in downstream end (cm) | Hydraulic Conductivity (cm/sec) | Velocity (cm/sec) | Reynolds number |
|---|---|---|---|---|---|
| 0.82 | 36 | 6.2 | 10 | 0.25 | 10 |
| 0.65 | 35.2 | 6 | 10.11 | 0.24 | 9.6 |
| 1.24 | 50 | 16.9 | 9.96 | 0.27 | 10.8 |

Darcy's law is valid as long as the Reynolds number is smaller than 1 to 10 (Bear, Verruijt, 1987). Accordingly, one can say that Darcy's law is valid for the present study.

MODFLOW software is also used to verify the hydraulic conductivity value. The channel is presented in the software and the hydraulic heads are computed by using the

hydraulic conductivity value obtained from Darcy experiment. The computed heads are in good agreement with those observed in the channel as shown in Figure 5.2.

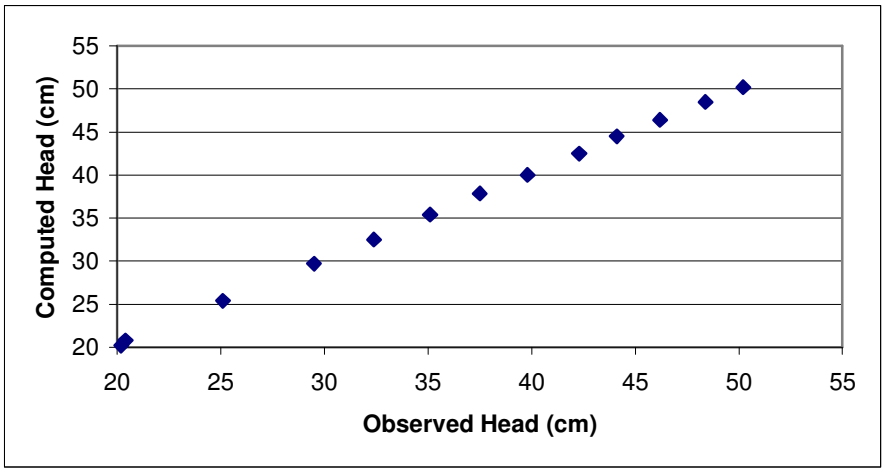


Figure 5.2 The observed and computed heads

The hydraulic conductivity is also determined by using the following formula (Küreksiz, 2008).

$$K = \frac{2QL}{(h_1^2 - h_2^2)W} \tag{5.2}$$

where L is the channel length, W is the channel width and $H_1$ and $H_2$ are the water levels at upstream and downstream ends of the channel, respectively.

If the values at sections i and i+1 are considered the relation above may be written as

$$K = \frac{2Q}{mW} \tag{5.3}$$

where $m = \left(h_i^2 - h_{i+1}^2\right)/\left(x_{i+1} - x_i\right)$. The calculated hydraulic conductivity values by using equations 5.2 and 5.3 are given in Table 5.3.

Table 5.3 Hydraulic conductivity values determined by using equations 5.2 and 5.3

| | Q ($cm^3$/sec) | $H_1$ (cm) | $H_2$ (m) | $m_{average}$ | K (cm/sec) |
|---|---|---|---|---|---|
| Equation (5.2) | 435.8 | 51 | 42.5 | | 9.75 |
| | 1168.4 | 50.2 | 20.2 | | 9.84 |
| | 1465.2 | 51.5 | 6 | | 9.96 |
| Equation (5.3) | 435.8 | | | 0.66 | 9.75 |
| | 1168.4 | | | 1.75 | 9.9 |
| | 1465.2 | | | 2.15 | 10.11 |

## 5.2 Determination of the calibration curve

The calibration curve is generated by reading conductivity values of the water in the porous medium having different NaCl concentration by means of the conductivity meter shown in Figure 4.6. First the conductivity value of the clear water is read and then 0.5 gram NaCl is added into the 1 lt water before reading the conductivity values. This process of adding 0.5 gr of NaCl is repeated until the concentration becomes 10 gr/lt. After sketching the conductivity values versus concentrations, curve fitting analysis is performed to obtain an analytical expression between them. The obtained calibration curve and the analytical expression are given in Figure 5.3. Later, during the experiments the given analytical expression is used to convert the read conductivity values into the concentrations.

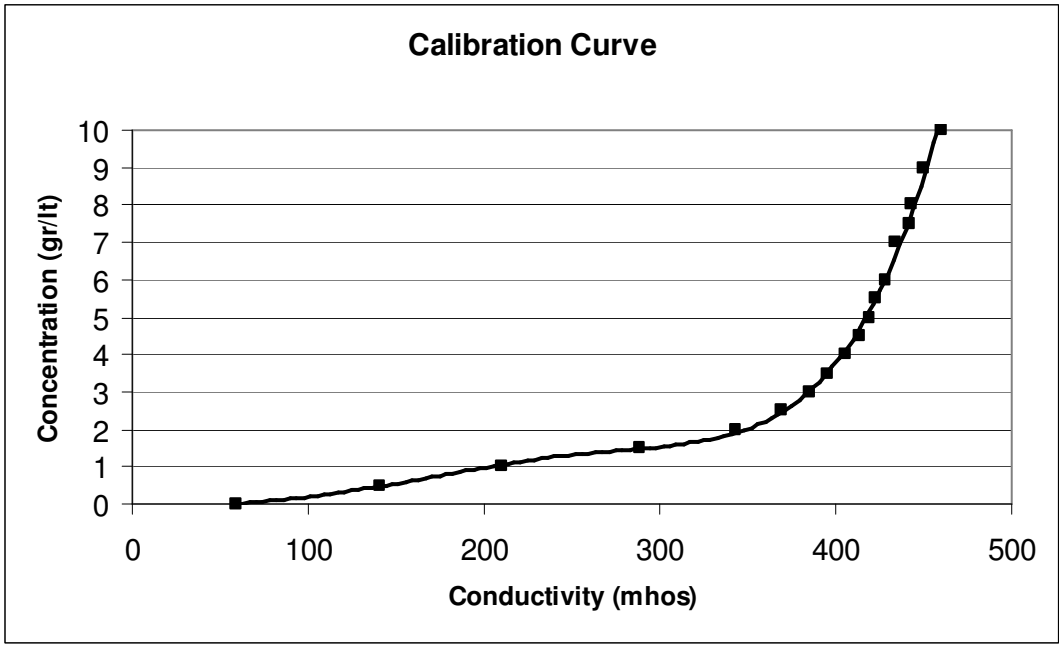


Figure 5.3 The calibration curve

The equation of the calibration curve is

$$C = a * EC^3 - b * EC^2 + c * EC - d \tag{5.4}$$

where $a$ = 1.7116*10$^{-6}$, b = 2.0328*10$^{-4}$, c = 1.4543*10$^{-2}$ and d = 0.43186.

### 5.3 Contaminant transport experiments in homogenous porous medium

Homogeneous porous medium is prepared with 3-5 mm quartz coarse sand. The porosity of the material is determined by provider as 0.38.

The tank which is located at downstream end is used as a contaminant supply reservoir and water is supplied from another pipe at upstream end. The solution is pumped with a rate of 0.1 l/sec into the box which is placed at the upstream end of the channel during the experiment and the conductivities are measured. The box is 55 cm long, 15 cm wide and 30 cm high and its all sides are constructed by perforated plates except back side. The conductivity of the water into the box is also measured to determine the initial concentration and during the first, second and third experiments the

concentrations are measured as 5 g/l, 4.8 g/l and 4.8 g/l, respectively in the box which is placed at the entrance of the channel.

The transmission interval is selected as 1 second, implying that the scanner which transmits the electrical signal changes the measurement point every second. The conductivity values of each wire are read and stored for each 0.1 second. Since the scanner has 236 inputs, the signal returns to the starting point 236 seconds later. This period is quite sufficient for groundwater flow experiments since the flow velocity is quite slow.

Figure 5.4 illustrates the positions of all measurement points. They are arranged so that there are 11 points in the longitudinal direction $(x = i\,\Delta x\ ;\ i = 1,11\ ;\ \Delta x = 108\ cm)$, 4 points in the transversal direction $(y = j\ \Delta y\ ;\ j = 1,4\ \ ;\ \Delta y = 40\ cm)$, and 5 points in the vertical direction $(z = k\ \Delta z\ ;\ k = 1,5\ \ ;\ \Delta z = 11\ cm)$.

The measurement points are designated by using the indices (i, j, k) related to their coordinates x, y and z, respectively, as shown in Table 5.4.

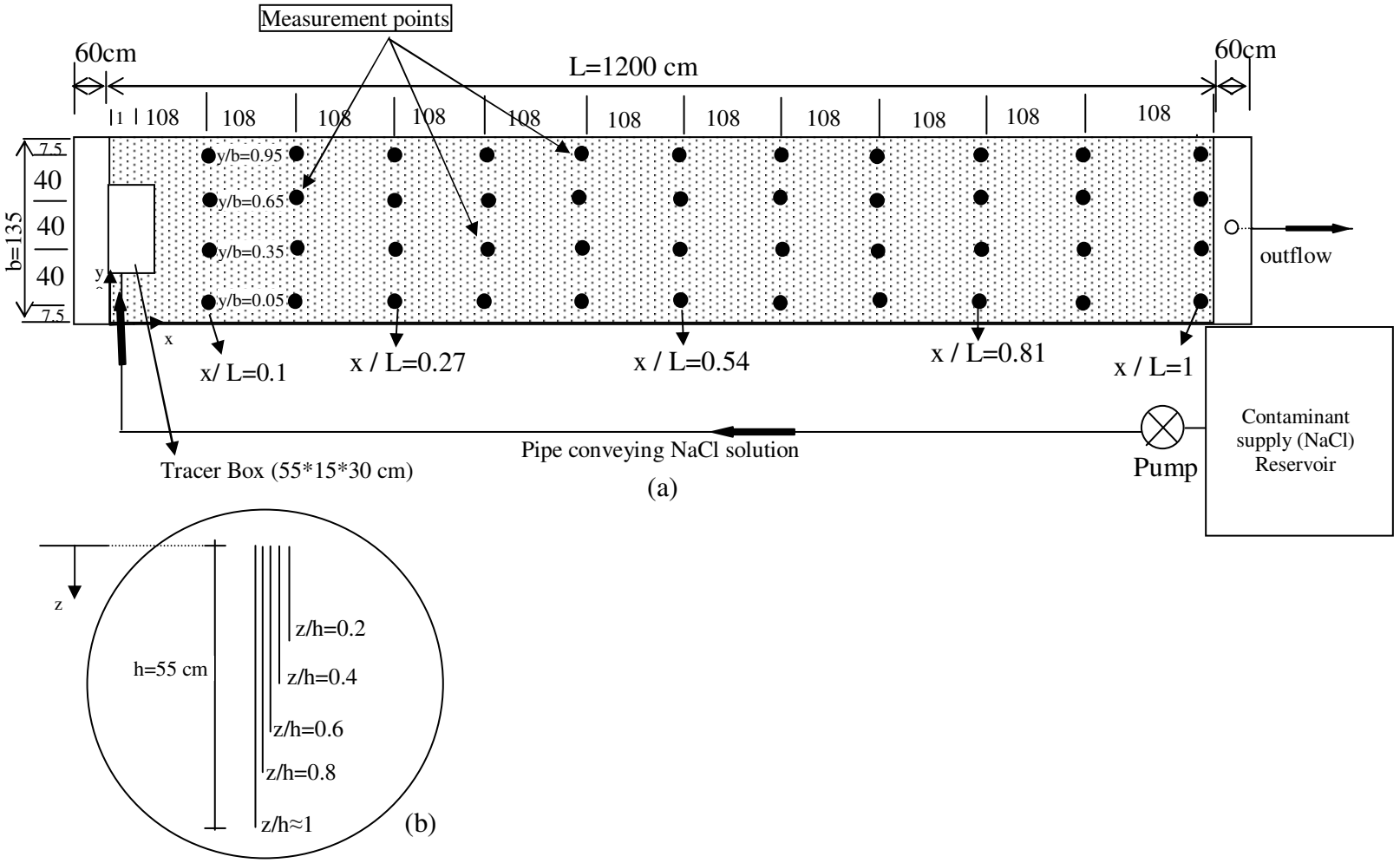


Figure 5.4 Arrangement of the measurement points (a) plan view (b) their locations in the vertical direction

Table 5.4 Identification of the measurement points

| Point No | i | j | k | Point No | i | j | k | Point No | i | j | k | Point No | i | j | k | Point No | i | j | k |
|---|---|---|---|---|---|---|---|---|---|---|---|---|---|---|---|---|---|---|---|
| ***1*** | 1 | 1 | 1 | ***2*** | 1 | 1 | 2 | ***3*** | 1 | 1 | 3 | ***4*** | 1 | 1 | 4 | ***5*** | 1 | 1 | 5 |
| ***6*** | 1 | 2 | 1 | ***7*** | 1 | 2 | 2 | ***8*** | 1 | 2 | 3 | ***9*** | 1 | 2 | 4 | ***10*** | 1 | 2 | 5 |
| ***11*** | 1 | 3 | 1 | ***12*** | 1 | 3 | 2 | ***13*** | 1 | 3 | 3 | ***14*** | 1 | 3 | 4 | ***15*** | 1 | 3 | 5 |
| ***16*** | 1 | 4 | 1 | ***17*** | 1 | 4 | 2 | ***18*** | 1 | 4 | 3 | ***19*** | 1 | 4 | 4 | ***20*** | 1 | 4 | 5 |
| ***21*** | 2 | 1 | 1 | ***22*** | 2 | 1 | 2 | ***23*** | 2 | 1 | 3 | ***24*** | 2 | 1 | 4 | ***25*** | 2 | 1 | 5 |
| ***26*** | 2 | 2 | 1 | ***27*** | 2 | 2 | 2 | ***28*** | 2 | 2 | 3 | ***29*** | 2 | 2 | 4 | ***30*** | 2 | 2 | 5 |
| ***31*** | 2 | 3 | 1 | ***32*** | 2 | 3 | 2 | ***33*** | 2 | 3 | 3 | ***34*** | 2 | 3 | 4 | ***35*** | 2 | 3 | 5 |
| ***36*** | 2 | 4 | 1 | ***37*** | 2 | 4 | 2 | ***38*** | 2 | 4 | 3 | ***39*** | 2 | 4 | 4 | ***40*** | 2 | 4 | 5 |
| ***41*** | 3 | 1 | 1 | ***42*** | 3 | 1 | 2 | ***43*** | 3 | 1 | 3 | ***44*** | 3 | 1 | 4 | ***45*** | 3 | 1 | 5 |
| ***46*** | 3 | 2 | 1 | ***47*** | 3 | 2 | 2 | ***48*** | 3 | 2 | 3 | ***49*** | 3 | 2 | 4 | ***50*** | 3 | 2 | 5 |
| ***51*** | 3 | 3 | 1 | ***52*** | 3 | 3 | 2 | ***53*** | 3 | 3 | 3 | ***54*** | 3 | 3 | 4 | ***55*** | 3 | 3 | 5 |
| ***56*** | 3 | 4 | 1 | ***57*** | 3 | 4 | 2 | ***58*** | 3 | 4 | 3 | ***59*** | 3 | 4 | 4 | ***60*** | 3 | 4 | 5 |
| ***61*** | 4 | 1 | 1 | ***62*** | 4 | 1 | 2 | ***63*** | 4 | 1 | 3 | ***64*** | 4 | 1 | 4 | ***65*** | 4 | 1 | 5 |
| ***66*** | 4 | 2 | 1 | ***67*** | 4 | 2 | 2 | ***68*** | 4 | 2 | 3 | ***69*** | 4 | 2 | 4 | ***70*** | 4 | 2 | 5 |
| ***71*** | 4 | 3 | 1 | ***72*** | 4 | 3 | 2 | ***73*** | 4 | 3 | 3 | ***74*** | 4 | 3 | 4 | ***75*** | 4 | 3 | 5 |
| ***76*** | 4 | 4 | 1 | ***77*** | 4 | 4 | 2 | ***78*** | 4 | 4 | 3 | ***79*** | 4 | 4 | 4 | ***80*** | 4 | 4 | 5 |
| ***81*** | 5 | 1 | 1 | ***82*** | 5 | 1 | 2 | ***83*** | 5 | 1 | 3 | ***84*** | 5 | 1 | 4 | ***85*** | 5 | 1 | 5 |
| ***86*** | 5 | 2 | 1 | ***87*** | 5 | 2 | 2 | ***88*** | 5 | 2 | 3 | ***89*** | 5 | 2 | 4 | ***90*** | 5 | 2 | 5 |
| ***91*** | 5 | 3 | 1 | ***92*** | 5 | 3 | 2 | ***93*** | 5 | 3 | 3 | ***94*** | 5 | 3 | 4 | ***95*** | 5 | 3 | 5 |
| ***96*** | 5 | 4 | 1 | ***97*** | 5 | 4 | 2 | ***98*** | 5 | 4 | 3 | ***99*** | 5 | 4 | 4 | ***100*** | 5 | 4 | 5 |
| ***101*** | 6 | 1 | 1 | ***102*** | 6 | 1 | 2 | ***103*** | 6 | 1 | 3 | ***104*** | 6 | 1 | 4 | ***105*** | 6 | 1 | 5 |
| ***106*** | 6 | 2 | 1 | ***107*** | 6 | 2 | 2 | ***108*** | 6 | 2 | 3 | ***109*** | 6 | 2 | 4 | ***110*** | 6 | 2 | 5 |
| ***111*** | 6 | 3 | 1 | ***112*** | 6 | 3 | 2 | ***113*** | 6 | 3 | 3 | ***114*** | 6 | 3 | 4 | ***115*** | 6 | 3 | 5 |
| ***116*** | 6 | 4 | 1 | ***117*** | 6 | 4 | 2 | ***118*** | 6 | 4 | 3 | ***119*** | 6 | 4 | 4 | ***120*** | 6 | 4 | 5 |
| ***121*** | 7 | 1 | 1 | ***122*** | 7 | 1 | 2 | ***123*** | 7 | 1 | 3 | ***124*** | 7 | 1 | 4 | ***125*** | 7 | 1 | 5 |
| ***126*** | 7 | 2 | 1 | ***127*** | 7 | 2 | 2 | ***128*** | 7 | 2 | 3 | ***129*** | 7 | 2 | 4 | ***130*** | 7 | 2 | 5 |
| ***131*** | 7 | 3 | 1 | ***132*** | 7 | 3 | 2 | ***133*** | 7 | 3 | 3 | ***134*** | 7 | 3 | 4 | ***135*** | 7 | 3 | 5 |
| ***136*** | 7 | 4 | 1 | ***137*** | 7 | 4 | 2 | ***138*** | 7 | 4 | 3 | ***139*** | 7 | 4 | 4 | ***140*** | 7 | 4 | 5 |
| ***141*** | 8 | 1 | 1 | ***142*** | 8 | 1 | 2 | ***143*** | 8 | 1 | 3 | ***144*** | 8 | 1 | 4 | ***145*** | 8 | 1 | 5 |
| ***146*** | 8 | 2 | 1 | ***147*** | 8 | 2 | 2 | ***148*** | 8 | 2 | 3 | ***149*** | 8 | 2 | 4 | ***150*** | 8 | 2 | 5 |
| ***151*** | 8 | 3 | 1 | ***152*** | 8 | 3 | 2 | ***153*** | 8 | 3 | 3 | ***154*** | 8 | 3 | 4 | ***155*** | 8 | 3 | 5 |
| ***156*** | 8 | 4 | 1 | ***157*** | 8 | 4 | 2 | ***158*** | 8 | 4 | 3 | ***159*** | 8 | 4 | 4 | ***160*** | 8 | 4 | 5 |

Table 5.4 Identification of the measurement points (continued)

| | | | | | | | | | | | | | | | | | | | |
|---|---|---|---|---|---|---|---|---|---|---|---|---|---|---|---|---|---|---|---|
| ***161*** | 9 | 1 | 1 | ***162*** | 9 | 1 | 2 | ***163*** | 9 | 1 | 3 | ***164*** | 9 | 1 | 4 | ***165*** | 9 | 1 | 5 |
| ***166*** | 9 | 2 | 1 | ***167*** | 9 | 2 | 2 | ***168*** | 9 | 2 | 3 | ***169*** | 9 | 2 | 4 | ***170*** | 9 | 2 | 5 |
| ***171*** | 9 | 3 | 1 | ***172*** | 9 | 3 | 2 | ***173*** | 9 | 3 | 3 | ***174*** | 9 | 3 | 4 | ***175*** | 9 | 3 | 5 |
| ***176*** | 9 | 4 | 1 | ***177*** | 9 | 4 | 2 | ***178*** | 9 | 4 | 3 | ***179*** | 9 | 4 | 4 | ***180*** | 9 | 4 | 5 |
| ***181*** | 10 | 1 | 1 | ***182*** | 10 | 1 | 2 | ***183*** | 10 | 1 | 3 | ***184*** | 10 | 1 | 4 | ***185*** | 10 | 1 | 5 |
| ***186*** | 10 | 2 | 1 | ***187*** | 10 | 2 | 2 | ***188*** | 10 | 2 | 3 | ***189*** | 10 | 2 | 4 | ***190*** | 10 | 2 | 5 |
| ***191*** | 10 | 3 | 1 | ***192*** | 10 | 3 | 2 | ***193*** | 10 | 3 | 3 | ***194*** | 10 | 3 | 4 | ***195*** | 10 | 3 | 5 |
| ***196*** | 10 | 4 | 1 | ***197*** | 10 | 4 | 2 | ***198*** | 10 | 4 | 3 | ***199*** | 10 | 4 | 4 | ***200*** | 10 | 4 | 5 |
| ***201*** | 11 | 1 | 1 | ***202*** | 11 | 1 | 2 | ***203*** | 11 | 1 | 3 | ***204*** | 11 | 1 | 4 | ***205*** | 11 | 1 | 5 |
| ***206*** | 11 | 2 | 1 | ***207*** | 11 | 2 | 2 | ***208*** | 11 | 2 | 3 | ***209*** | 11 | 2 | 4 | ***210*** | 11 | 2 | 5 |
| ***211*** | 11 | 3 | 1 | ***212*** | 11 | 3 | 2 | ***213*** | 11 | 3 | 3 | ***214*** | 11 | 3 | 4 | ***215*** | 11 | 3 | 5 |
| ***216*** | 11 | 4 | 1 | ***217*** | 11 | 4 | 2 | ***218*** | 11 | 4 | 3 | ***219*** | 11 | 4 | 4 | ***220*** | 11 | 4 | 5 |

Experiments are performed for various hydraulic gradients (Δh/L).

### *5.3.1 First experiment; Δh/L=* 0.007

The water levels at upstream end and downstream end are 51 cm and 42.5 cm, respectively. Average groundwater flow velocity is 0.07 cm/sec and the value of the Reynolds number is 2.8. The water levels through the longitudinal section are shown in Figure 5.5.

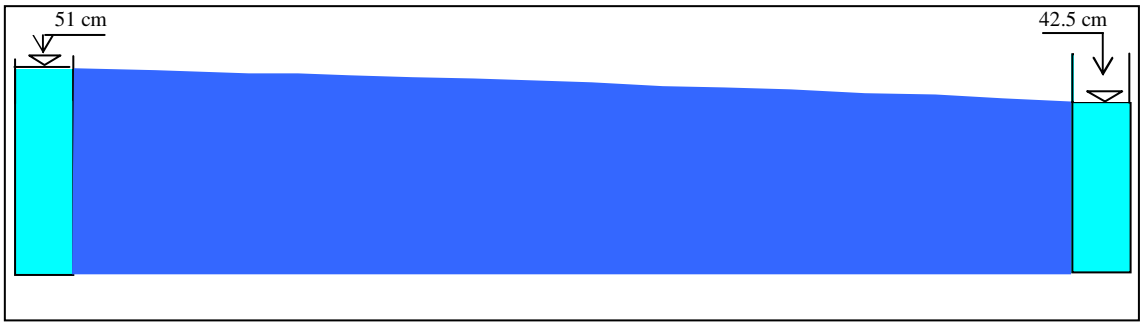


Figure 5.5 The water surface profile in the first experiment

The measured conductivity values are converted to concentration values by using the calibration curve given in Figure 5.3.

Figure 5.6, 5.7 and 5.8 illustrate the variation of the concentration in the form of breakthrough curves at some measurement points in vertical, longitudinal and transversal directions, respectively.

Concentration values are decreased through the vertical (z) direction as shown in Figure 5.6. This decrease is much more visible at sections located near the tracer box.

The concentrations at z/h=0.2 (z=10 cm from the top) and z/h=0.4 (z=21cm) are almost similar since the NaCl solution is given in the channel by means of the box 30 cm high. The concentrations at the measurement points located in front of the box (y/b=0.35) and at x/L=0.1 are approximately seven times greater than those located at the side of the channel (y/b=0.95). This difference decreases along the longitudinal direction. After the location x/L=0.54 concentrations are almost equal at points located in front of the box (y/b=0.35) and at the side of the channel (y/b=0.95) as shown in Figure 5.6. The observed concentrations are approximately similar through the vertical direction (z) at the end of the channel (x/L=1) (Figure 5.6).

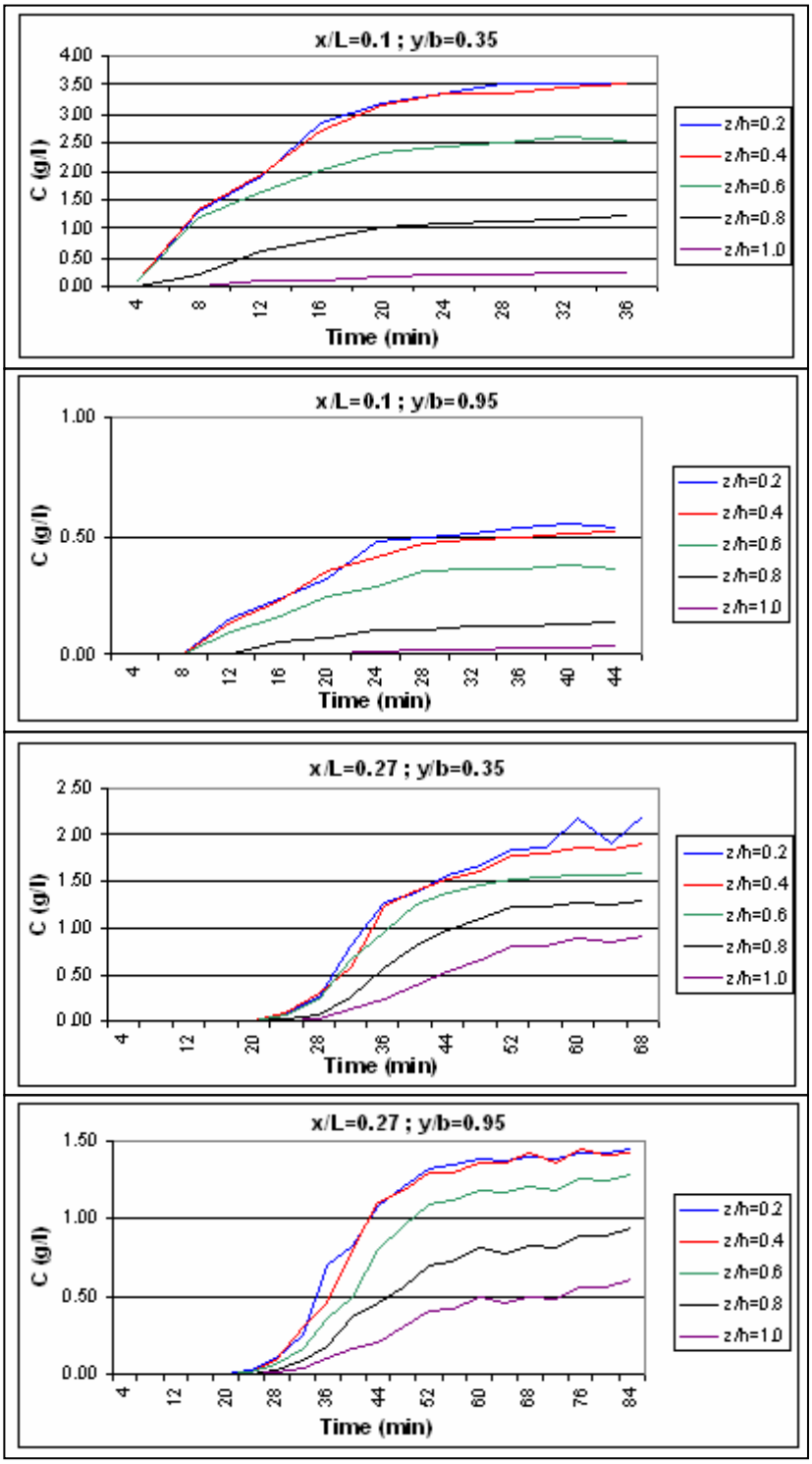


Figure 5.6 Measured concentration values in vertical direction during the first experiment

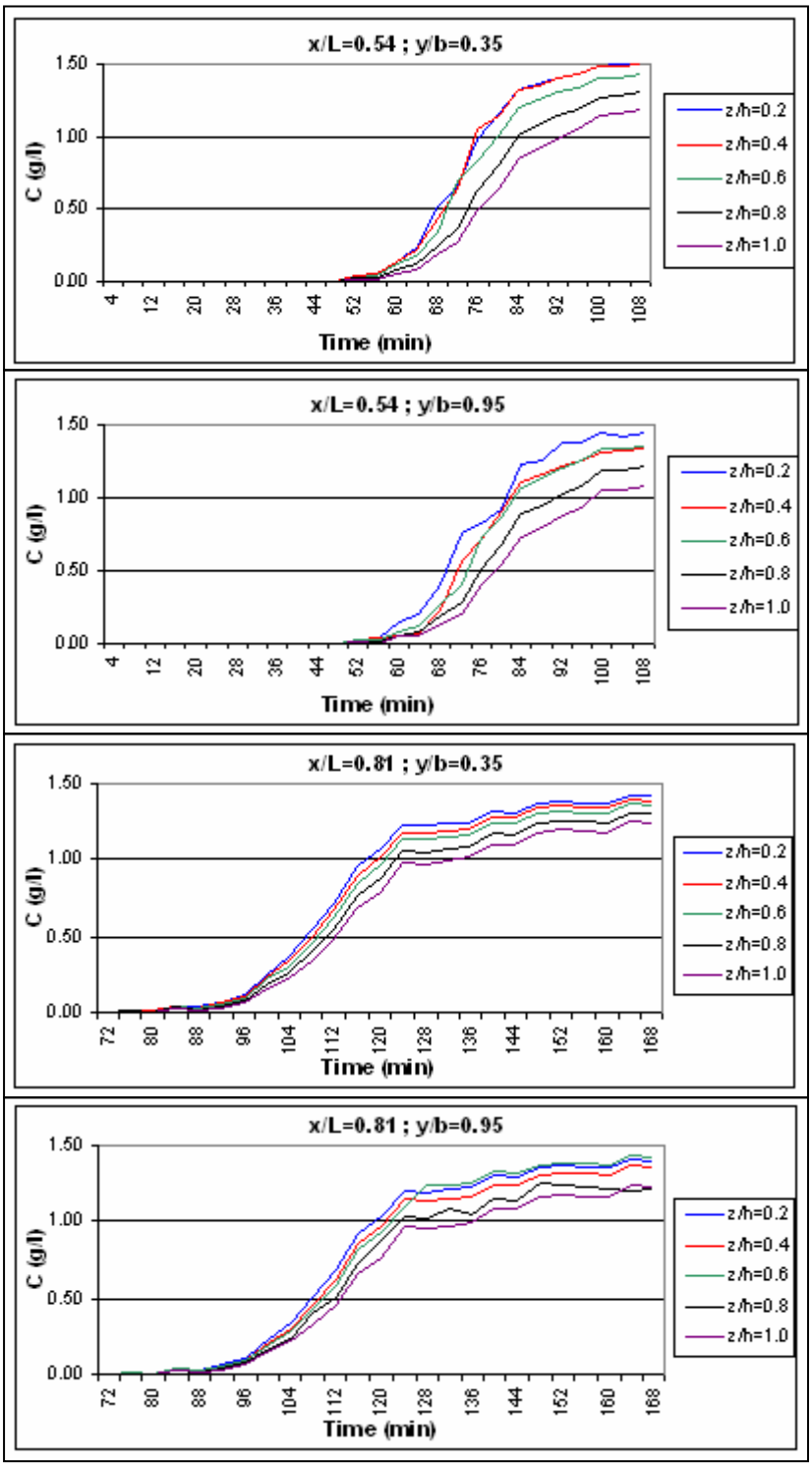


Figure 5.6 Measured concentration values in vertical direction during the first experiment (continued)

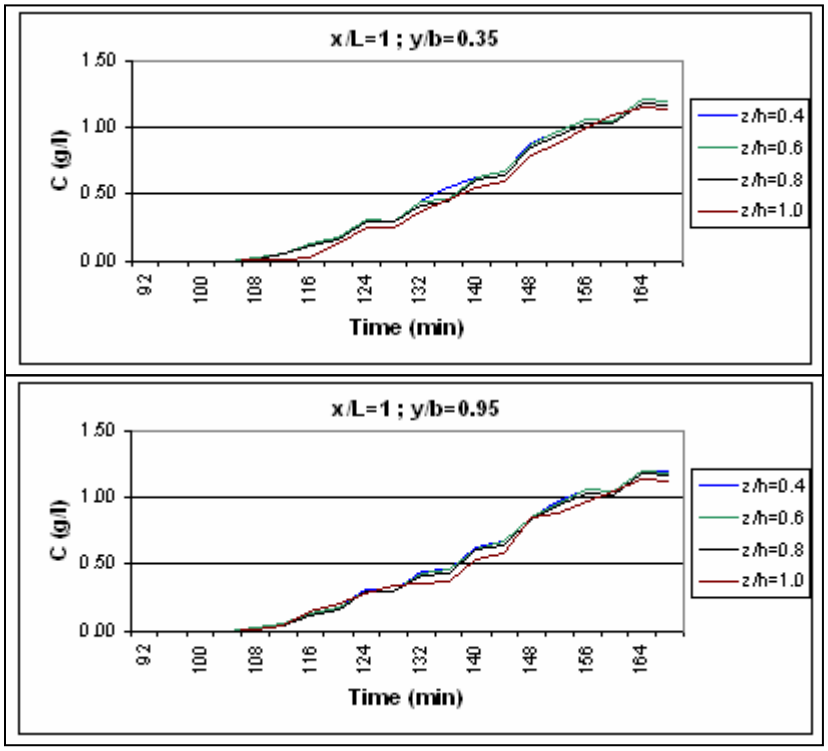


Figure 5.6 Measured concentration values in vertical direction during the first experiment (continued)

In longitudinal direction, maximum concentration values are observed at points close to and in front of the contamination area and, the concentrations decrease with distance as expected (Figure 5.7). The maximum concentrations are 3.7 g/l, 2.24 g/l, 1.56 g/l, 1.39 g/l and 1.21 g/l at x/L=0.1, x/L=0.27, x/L=0.54, x/L=0.81 and x/L=1, respectively.

The observed concentration values at points located at both sides of the channel walls (y/b=0.05 and y/b=0.95) are almost three times less than those located in front of the tracer box (y/b=0.35 and y/b=0.65). The main reasons of this decrease should be the geometry and location of the tracer box. At points x/L=0.1 and y/b=0.95 the observed concentrations are less compared to those of the other sections (Figure 5.7). Since NaCl solution moves with groundwater flow velocity it can not reach much at those points. The concentration values at x/L=0.1 and z/h=1 (close to the channel bottom) are the smallest because these locations are the least influenced zone.

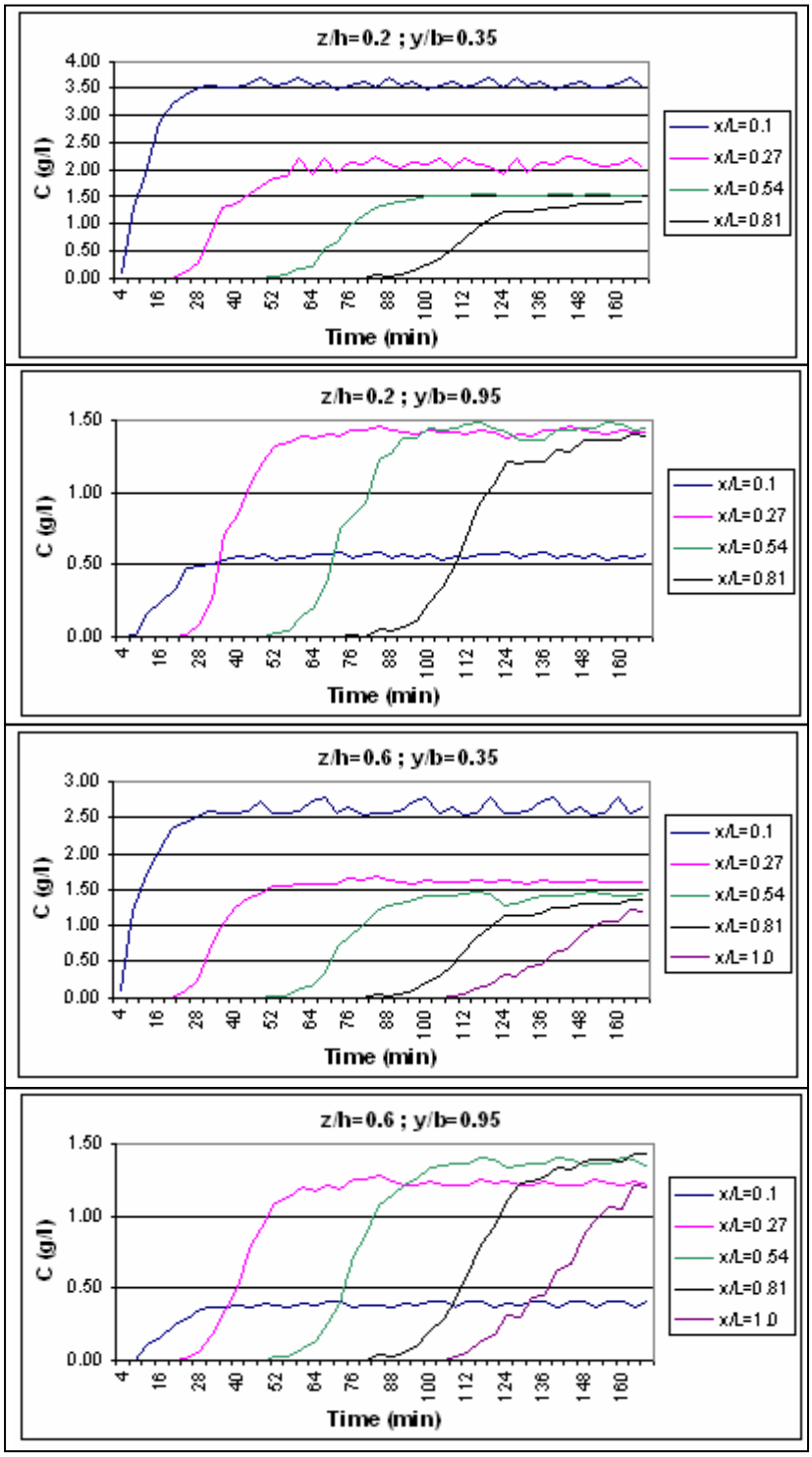


Figure 5.7 Measured concentration values in longitudinal direction during the first experiment

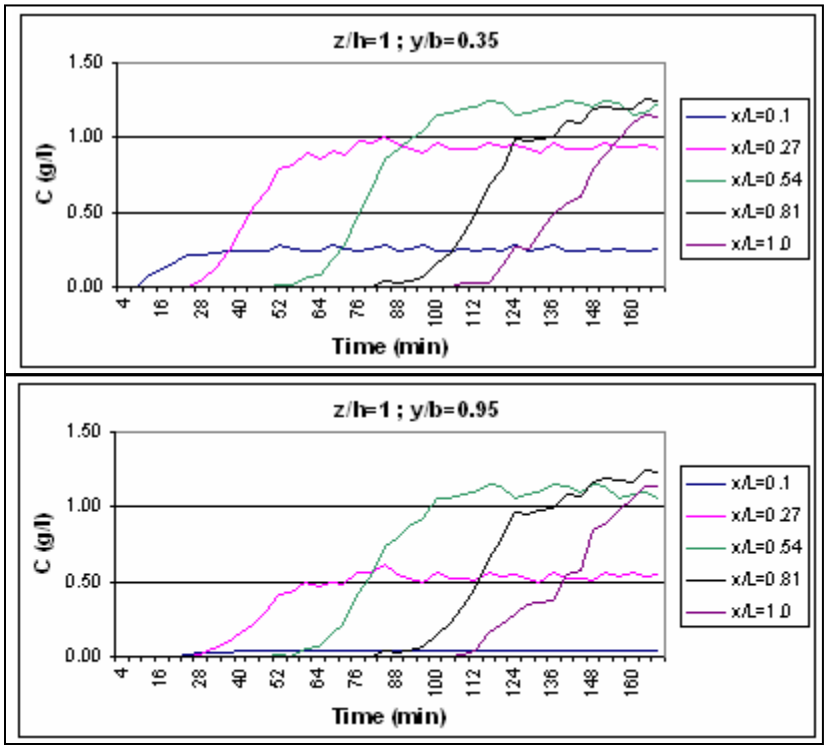


Figure 5.7 Measured concentration values in longitudinal direction during the first experiment (continued)

The breakthrough curves show that distribution of concentration is almost symmetric along the y direction as shown in Figure 5.8, since the porous medium is homogeneous, isotropic and flow is steady. The experimental results show that concentrations at y/b=0.05 and y/b=0.65 are almost equal to the concentrations at y/b=0.35 and y/b=0.95, respectively.

The maximum concentration in the channel is observed at points whose coordinates are x/L=0.1, z/h=0.2 and y/b=0.35 (or y/b=0.65). The contaminant arrived at downstream part of the channel approximately 6500 seconds after releasing the solution. It is revealed that, nearly 9800 seconds after the injection, concentrations remain constant at all of the measurement points.

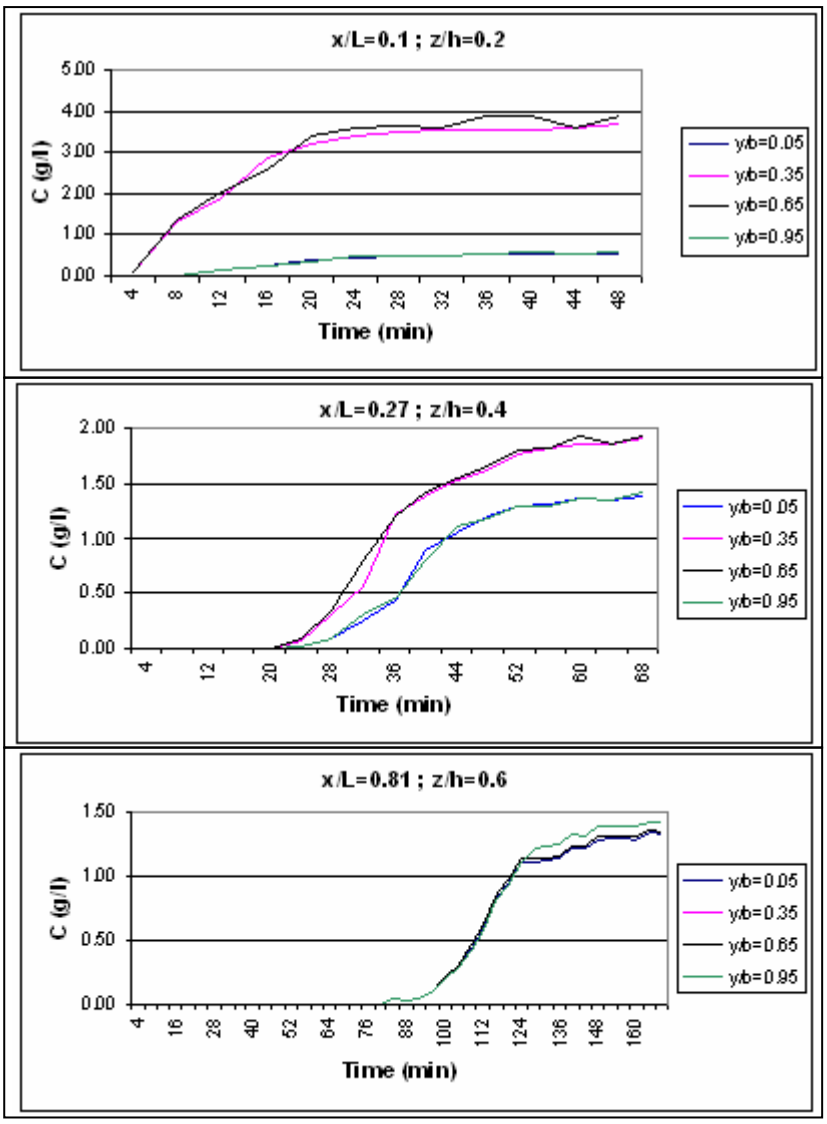


Figure 5.8 Measured concentration values in transversal direction during the first experiment

The maximum concentrations values and their arrival times to the measurement points are shown in Figure 5.9a and 5.9b, respectively for the vertical direction (z). The greatest maximum concentration values are observed at z/h=0.2 and they decrease downward. Maximum concentrations arrive almost at the same time along the z direction. Note that in such all figures the origins for axes are different and the digit 0 corresponds to the vertical axis.

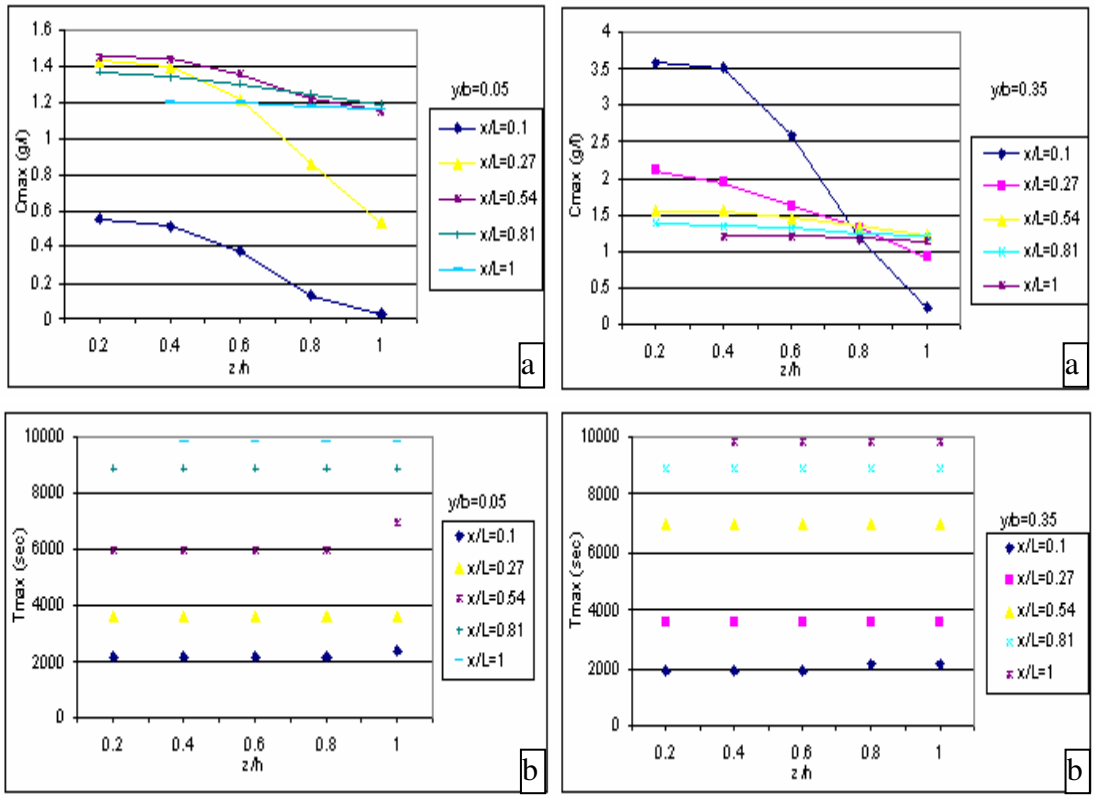


Figure 5.9 a) The maximum values of concentrations in vertical direction

b) The arrival times of the maximum concentrations in vertical direction

Figure 5.10a and 5.10b show the maximum concentrations values and their arrival times to the measurement points for the transversal direction (y). The greatest maximum concentration values are observed at y/b=0.35 and y/b=0.65 which are located in front of the tracer box. Maximum concentrations arrive almost at the same time along the y direction.

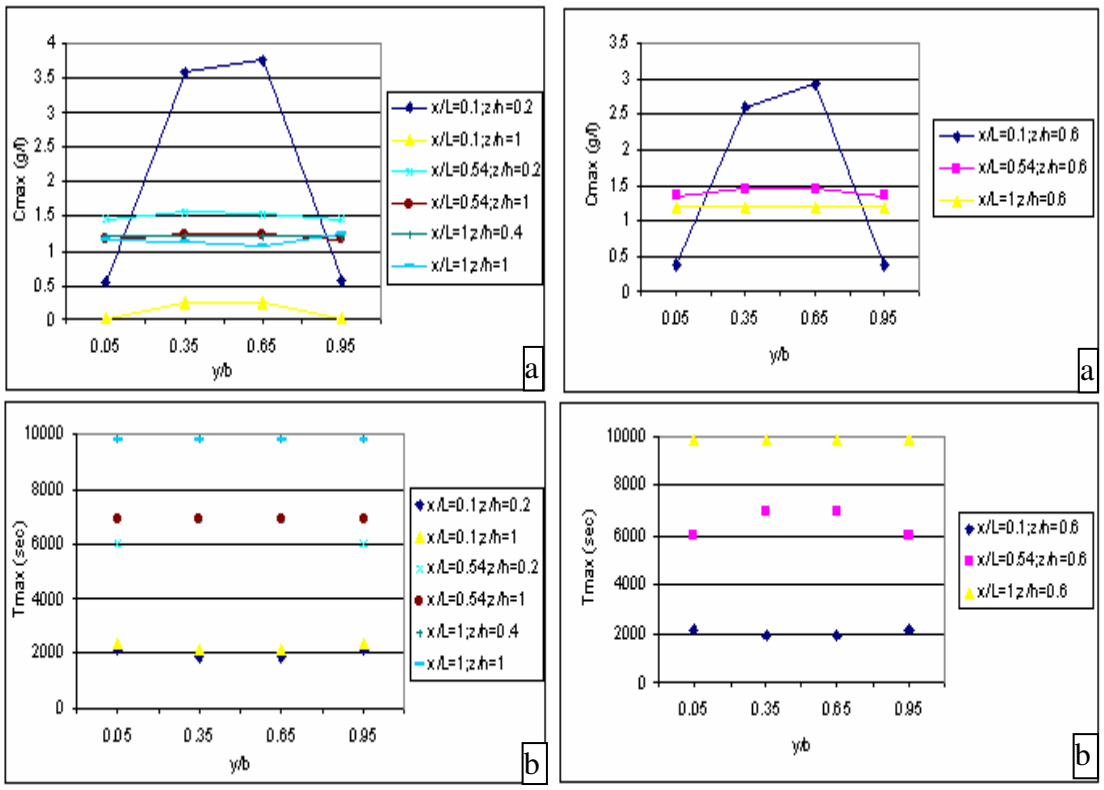


Figure 5.10 a) The maximum values of concentrations in transversal direction

b) The arrival times of the maximum concentrations in transversal direction

The maximum concentrations values and their arrival times to the measurement points are give in Figure 5.11a and 5.11b for the longitudinal direction (x). Although the maximum concentration values decrease through the x direction at points located in front of the tracer box, they increase through the x direction at points located near the channel wall. Maximum concentrations arrived approximately 2000 seconds after giving the solution at points x/L=0.1, while the arrival time is 9800 seconds for points x/L=1, as shown in Figure 5.11b.

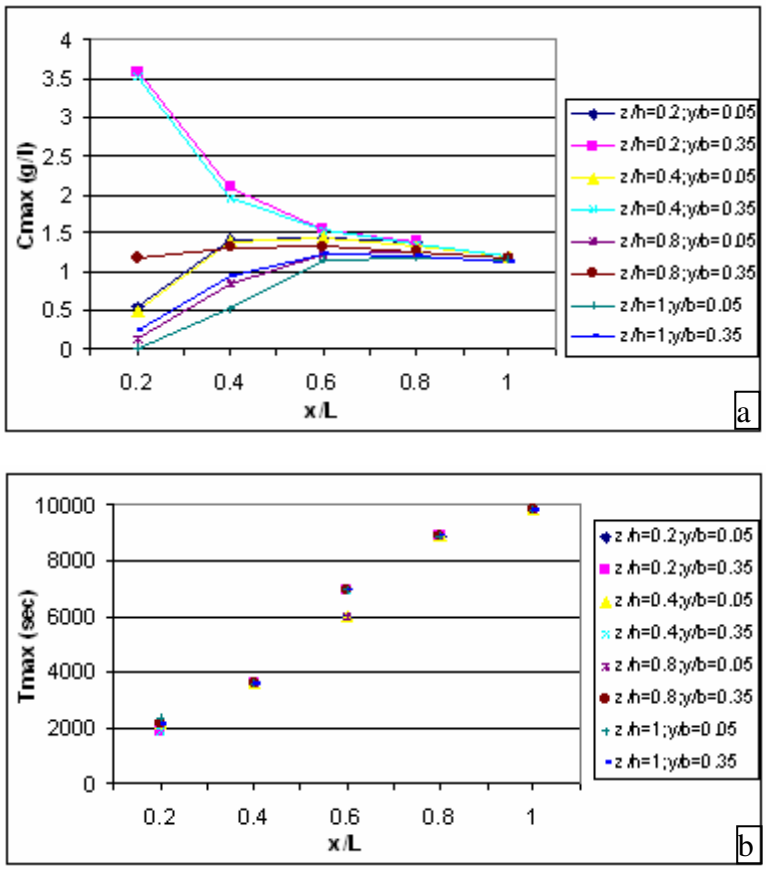


Figure 5.11 a) The maximum values of concentrations in longitudinal direction

b) The arrival times of the maximum concentrations in longitudinal direction

The relative concentrations in terms of dimensionless distance for the longitudinal direction at certain times are given in Figure 5.12.

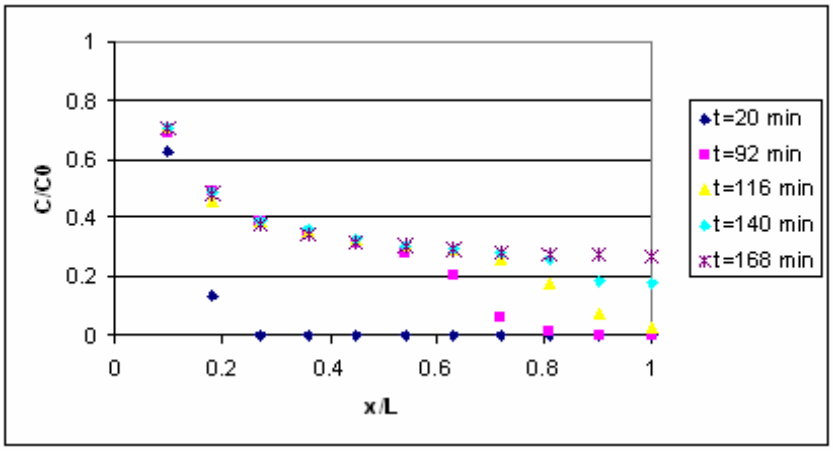


Figure 5.12 Relative concentrations versus dimensionless distance for the first experiment

### *5.3.2 Second experiment; Δh/L=* 0.025

The water levels are 50.3 cm and 20.2 cm at upstream end and downstream end, respectively, during the second experiment. Average groundwater flow velocity is 0.25 cm/sec and the value of the Reynolds number is 10.

Figure 5.13, 5.14 and 5.15 show the variation of the concentration at some measurement points in vertical, longitudinal and transversal directions, respectively.

All interpretations done for the first experiment are valid for the second experiment. The only difference between two experiments is the hydraulic gradient and its effects are observed only at arrival times of the maximum concentrations.

In longitudinal direction maximum concentration values are observed at points close to and in front of the tracer box and, the concentrations decrease with distance as

expected (Figure 5.14). The maximum concentrations are 3.2 g/l, 1.72 g/l, 1.46 g/l, 1.38 g/l and 1.37 g/l at x/L=0.1, x/L=0.27, x/L=0.54, x/L=0.81 and x/L=1, respectively.

The contaminant arrived at downstream part of the channel approximately 1680 seconds after giving the solution. It is revealed that nearly 2880 seconds after the injection, concentrations remain constant at all of the measurement points.

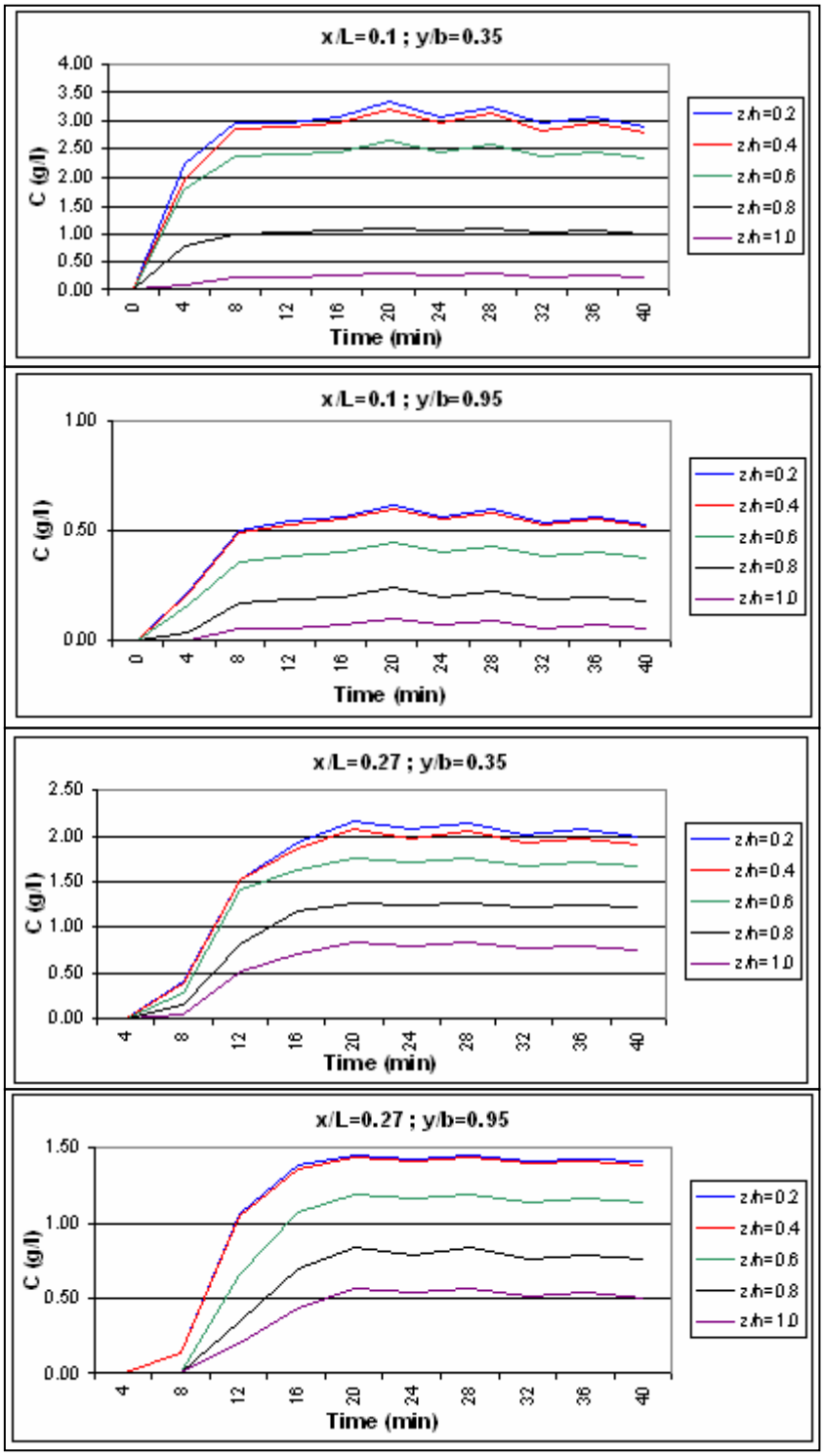


Figure 5.13 Measured concentration values in vertical direction during the second experiment

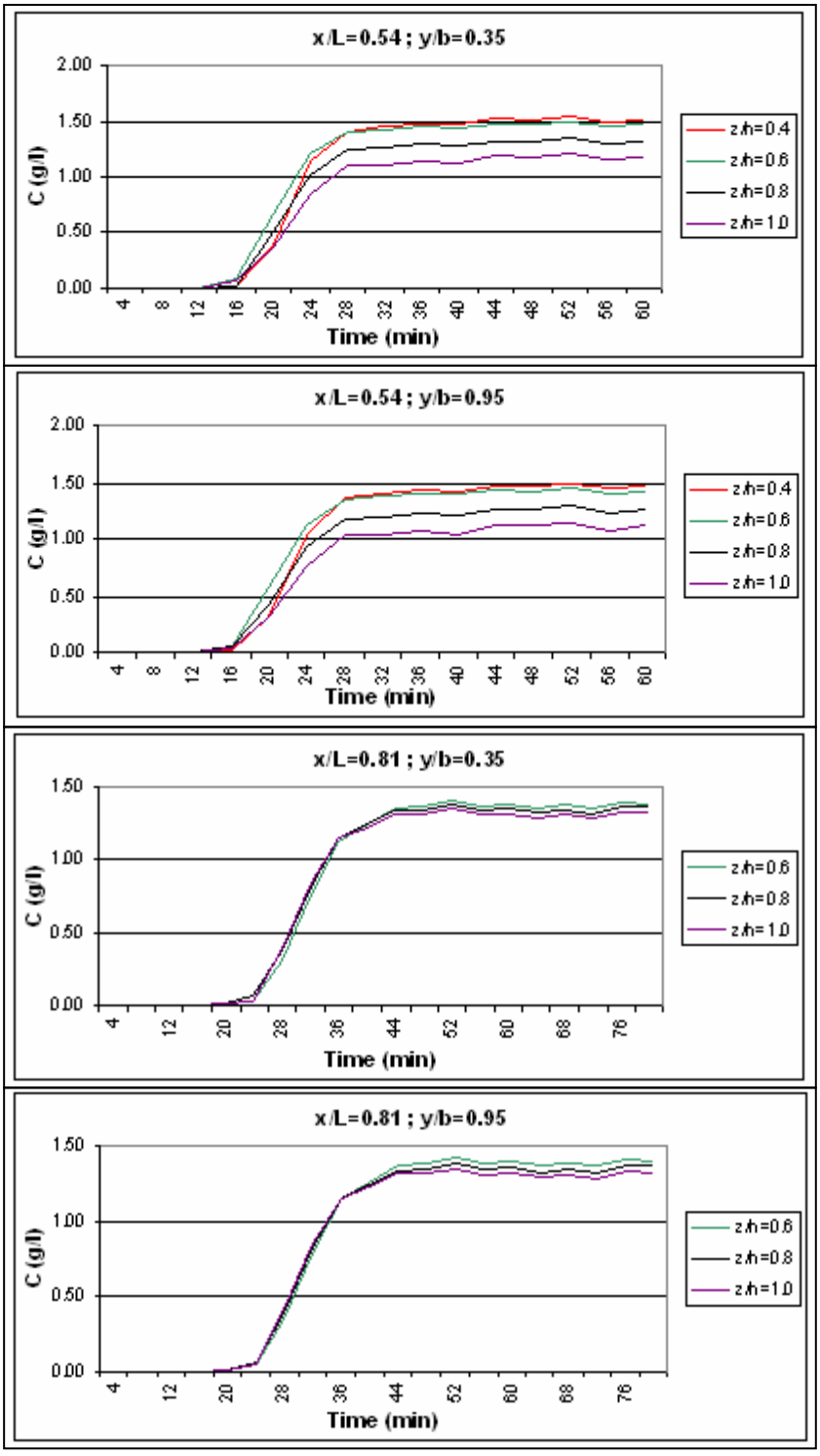


Figure 5.13 Measured concentration values in vertical direction during the second experiment (continued)

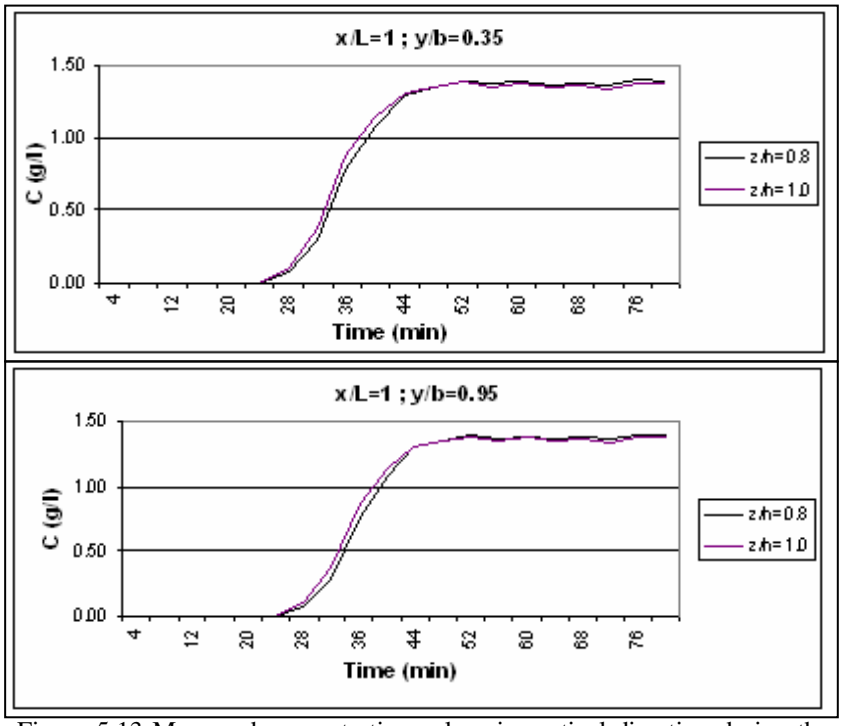


Figure 5.13 Measured concentration values in vertical direction during the second experiment (continued)

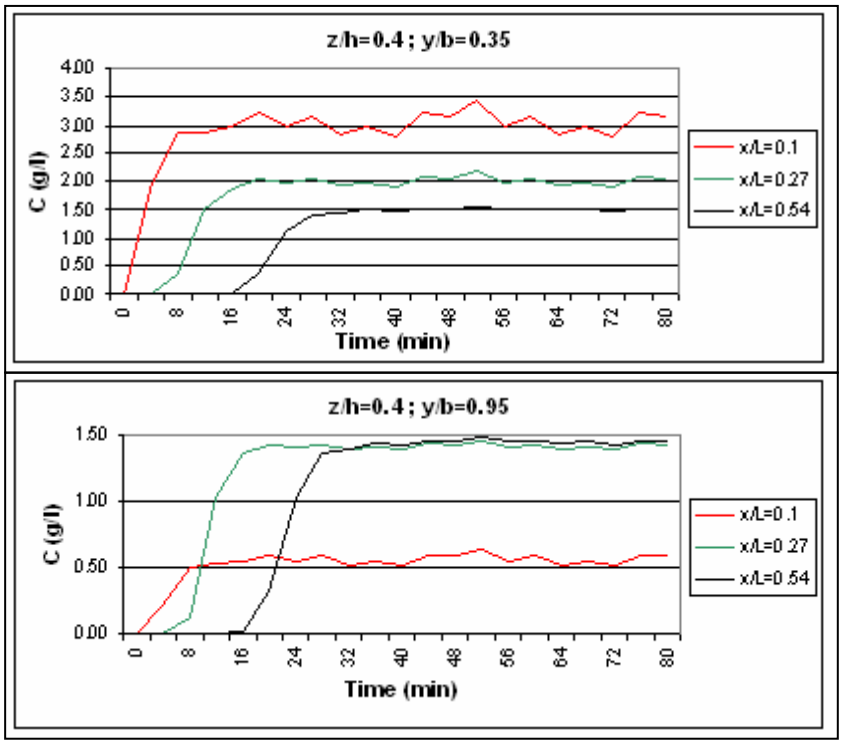


Figure 5.14 Measured concentration values in longitudinal direction during the second experiment

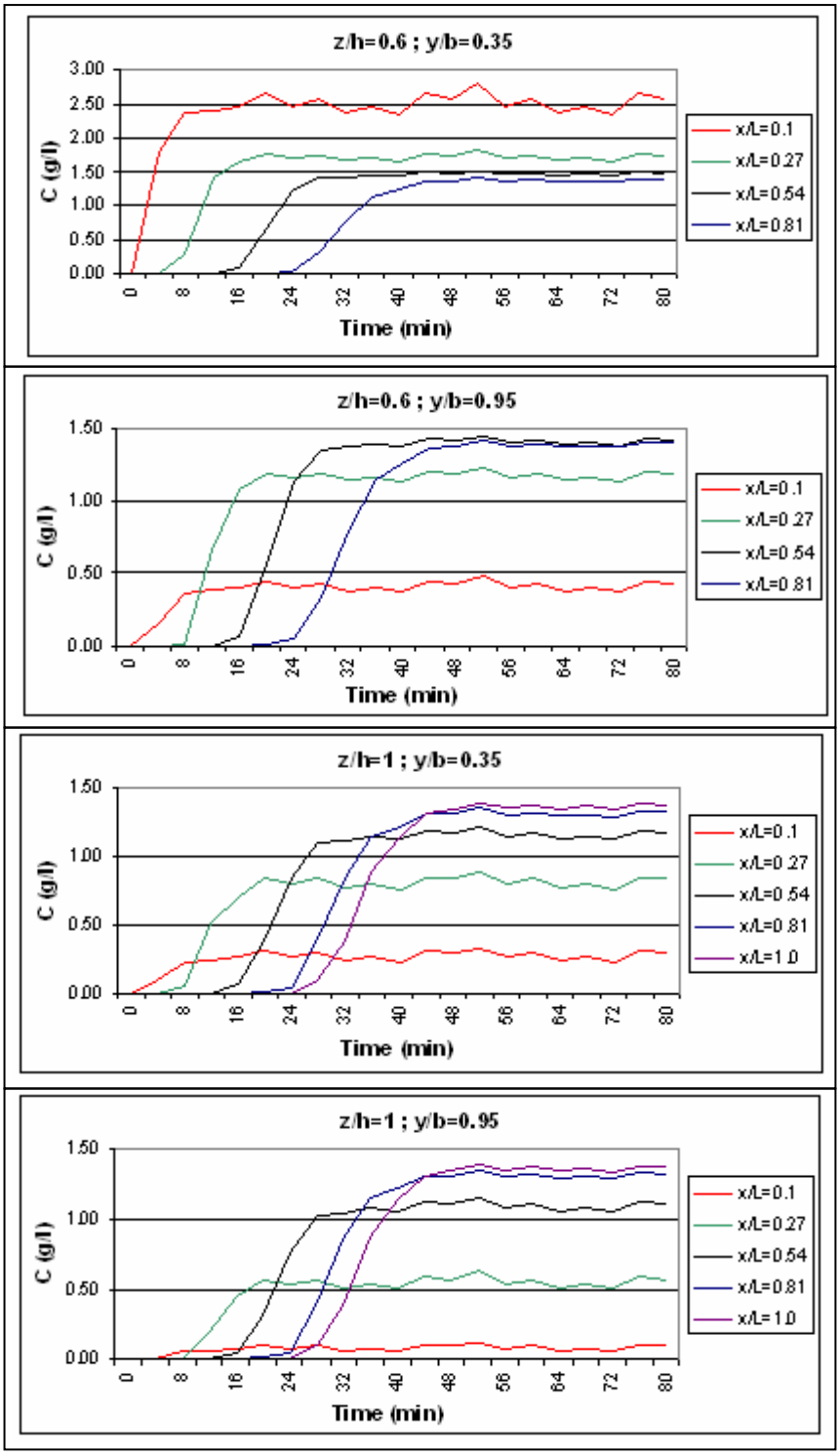


Figure 5.14 Measured concentration values in longitudinal direction during the second experiment (continued)

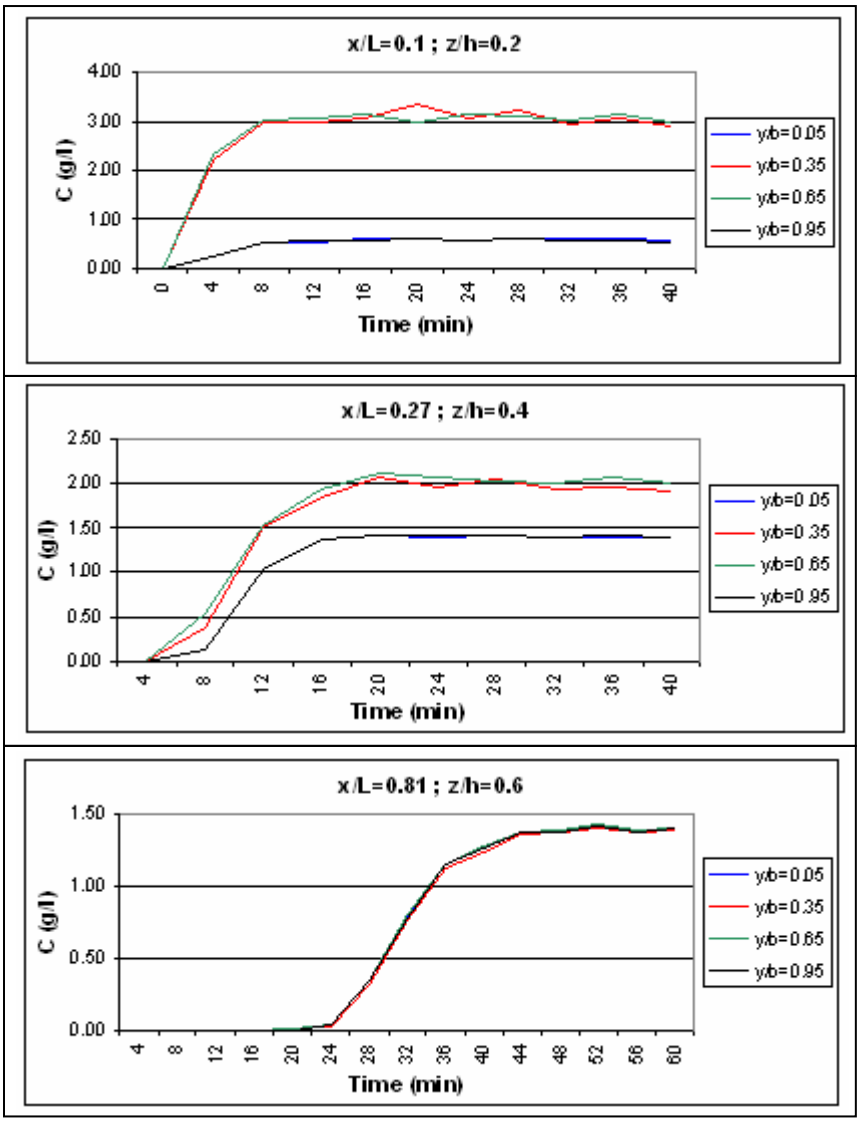


Figure 5.15 Measured concentration values in transversal direction during the second experiment

The maximum concentrations values and their arrival times to the measurement points are shown in Figure 5.16a and 5.16 b, respectively for the vertical direction (z). The greatest maximum concentration values are observed at z/h=0.2 and they decrease downward. Maximum concentrations arrive almost at the same time along the z direction.

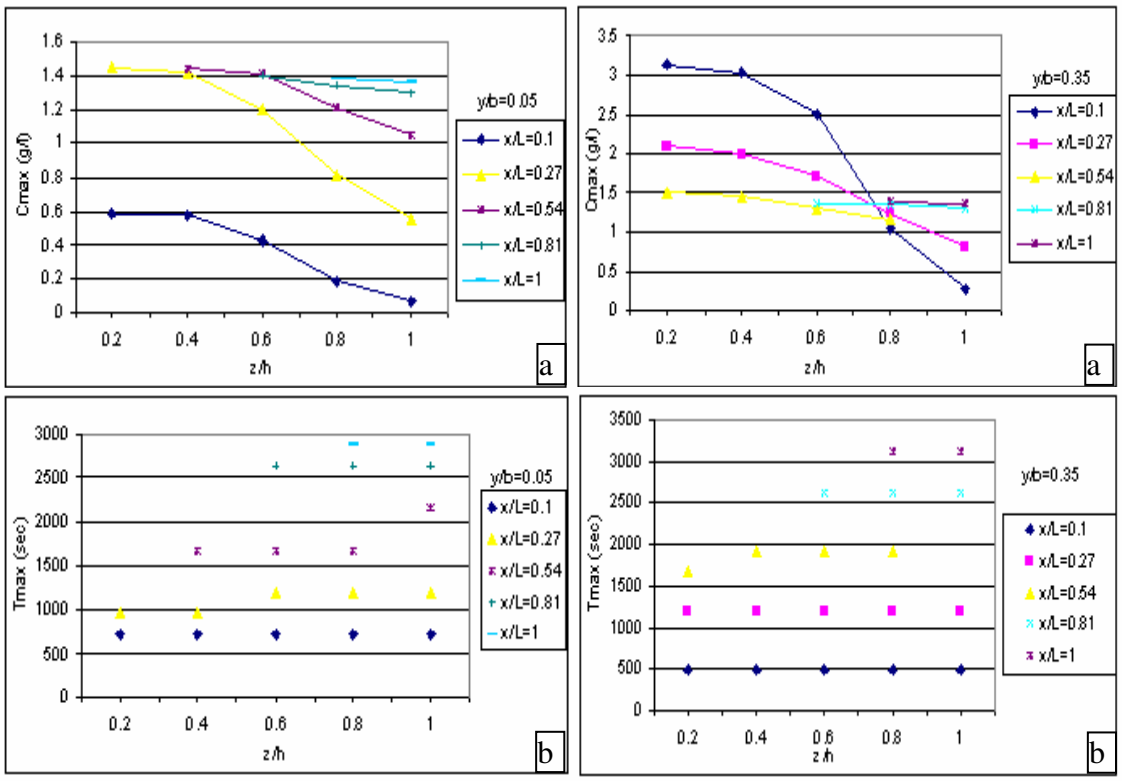


Figure 5.16 a) The maximum values of concentrations in vertical direction

b) The arrival times of the maximum concentrations in vertical direction

Figure 5.17a and 5.17b show the maximum concentrations values and their arrival times to the measurement points for the transversal direction (y). The greatest maximum concentration values are observed at y/b=0.35 and y/b=0.65 which are located in front of the tracer box.

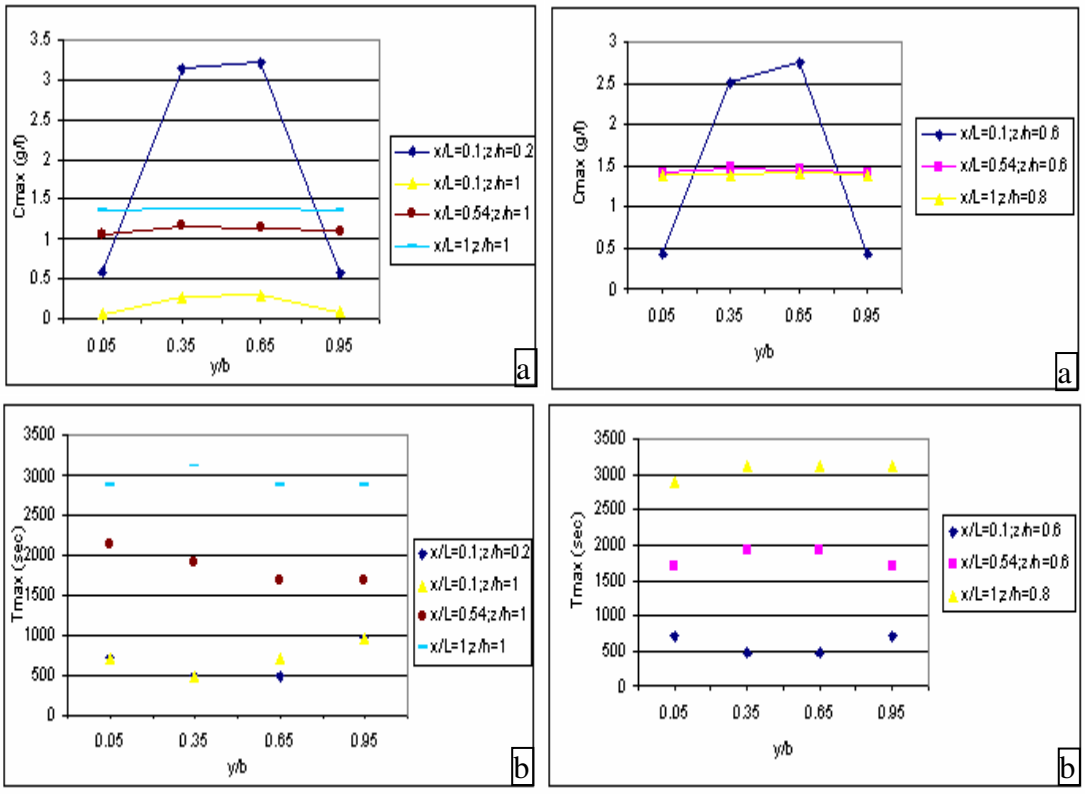


Figure 5.17 a) The maximum values of concentrations in transversal direction

b) The arrival times of the maximum concentrations in transversal direction

The maximum concentrations values and their arrival times to the measurement points are give in Figure 5.18a and 5.18b for the longitudinal direction (x). Although the maximum concentration values decrease through the x direction at points located in front of the tracer box, they increase through the x direction at points located near the channel wall. Maximum concentrations arrived approximately 600 seconds after giving the solution at points x/L=0.1, while the arrival time is 3000 seconds for points x/L=1, as shown in Figure 5.18b.

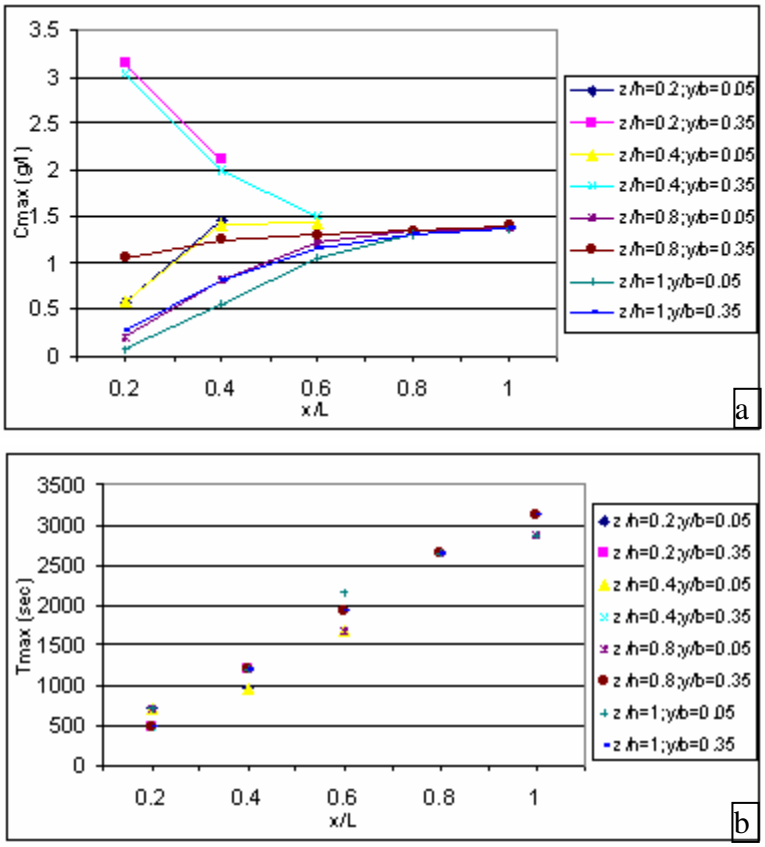


Figure 5.18 a) The maximum values of concentrations in longitudinal direction

b) The arrival times of the maximum concentrations in longitudinal direction

The relative concentrations in terms of dimensionless distance for the longitudinal direction at certain times are given in Figure 5.19.

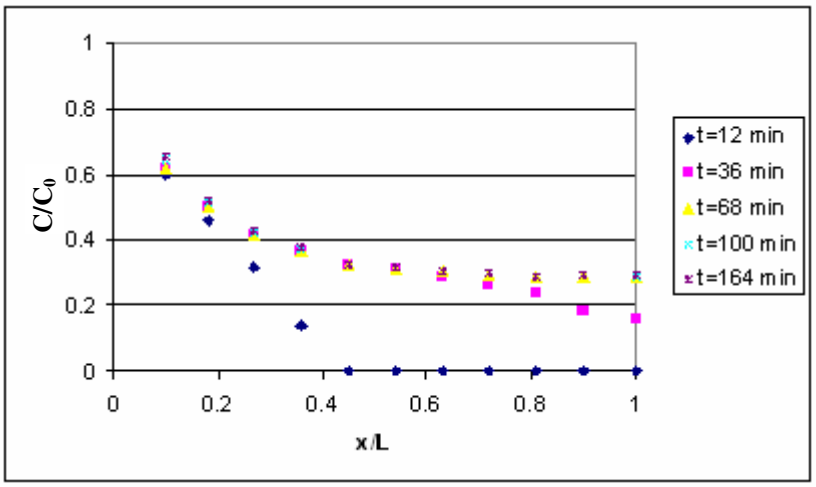


Figure 5.19 Relative concentrations versus dimensionless distance for the second experiment

### *5.3.3 Third experiment; Δh/L=* 0.038

The water levels are 51.5 cm and 6 cm at upstream end and downstream end, respectively during the third experiment. The values of mean velocity and Reynolds number are 0.38 cm/sec and 15, respectively. Although the Reynolds number exceeds the value of 10, experimental results are evaluated and interpreted.

Figure 5.20, 5.21 and 5.22 show the variation of the concentration at some measurement points in vertical, longitudinal and transversal directions, respectively.

The hydraulic gradient is higher than that of precedent experiments, thus the propagation of the concentration is faster when compared to the other two experiments.

The contaminant arrived at downstream part of the channel approximately 1000 seconds after giving the solution. It is revealed that, nearly 2000 seconds after the injection concentrations remain constant at all of the measurement points.

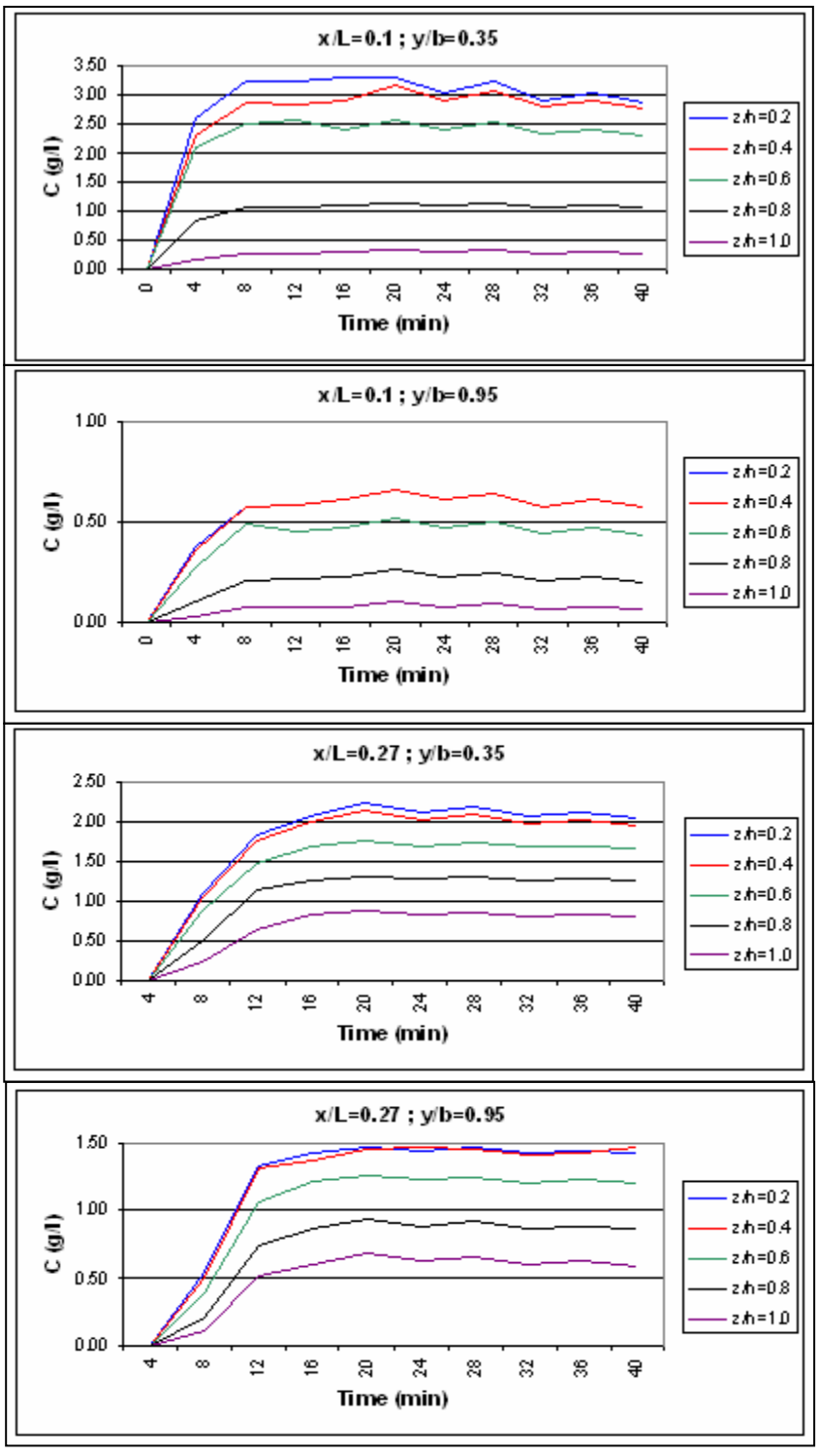


Figure 5.20 Measured concentration values in vertical direction during the third experiment

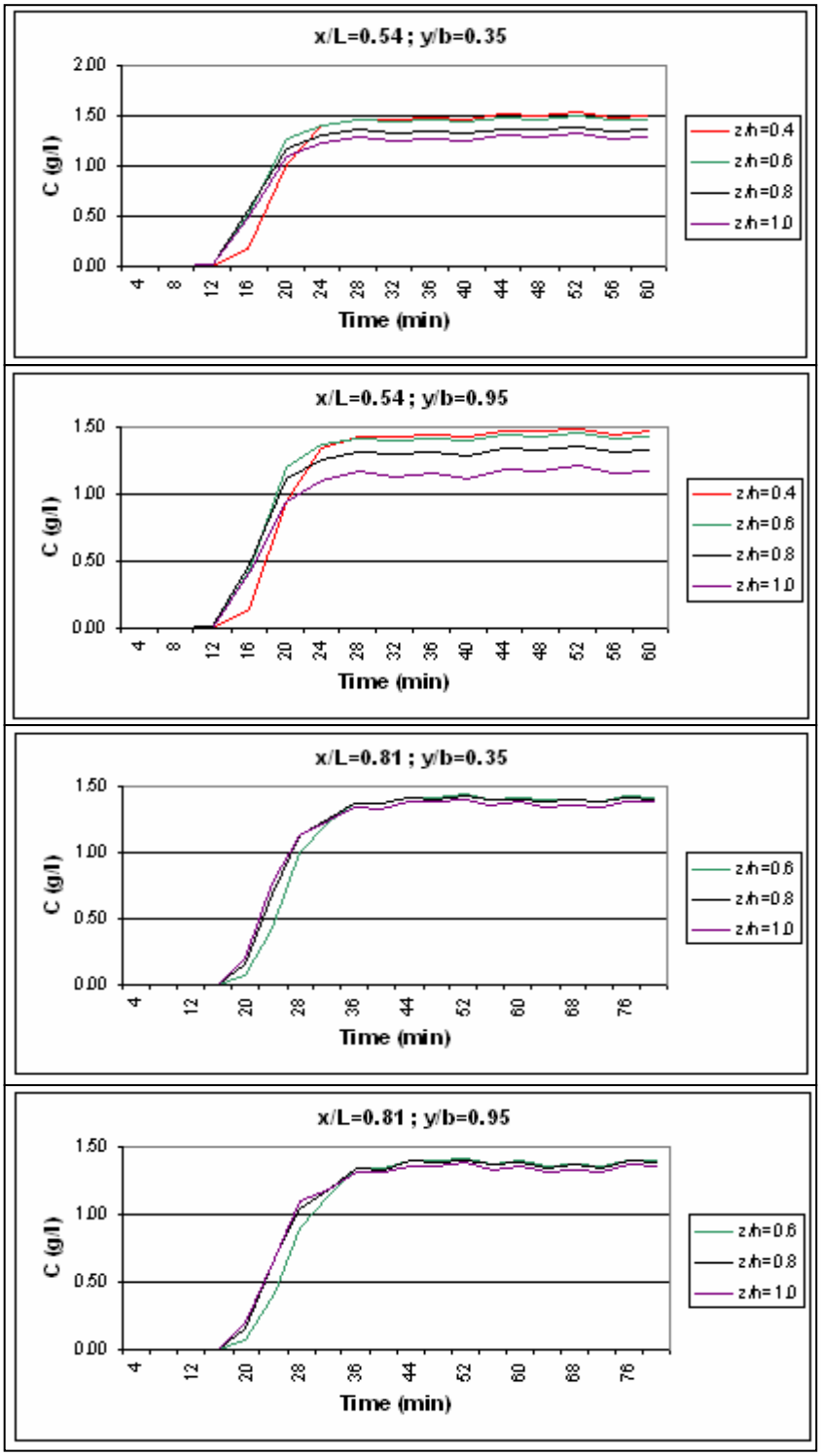


Figure 5.20 Measured concentration values in vertical direction during the third experiment (continued)

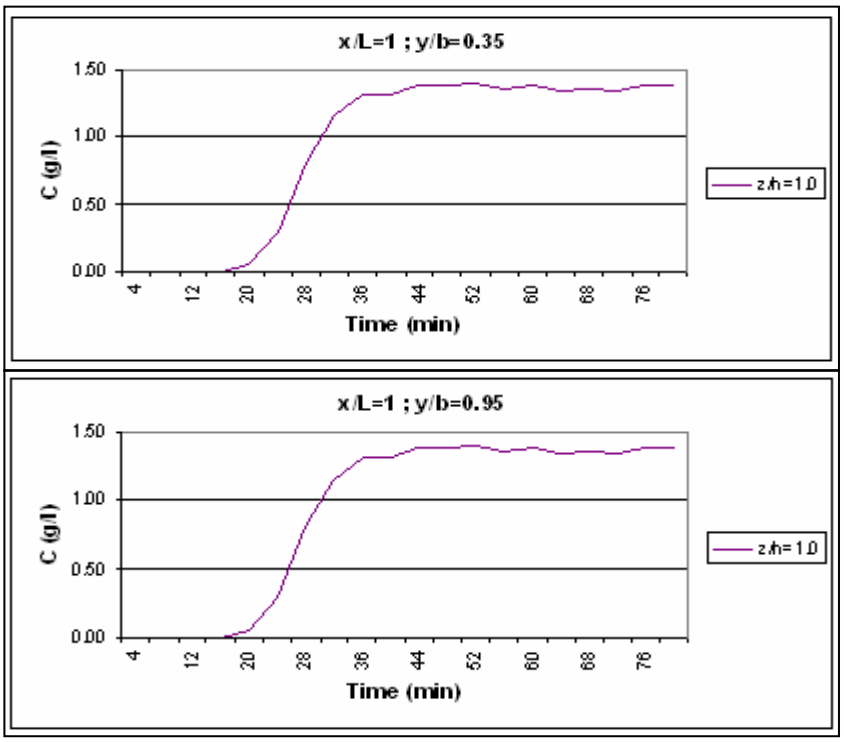


Figure 5.20 Measured concentration values in vertical direction during the third experiment (continued)

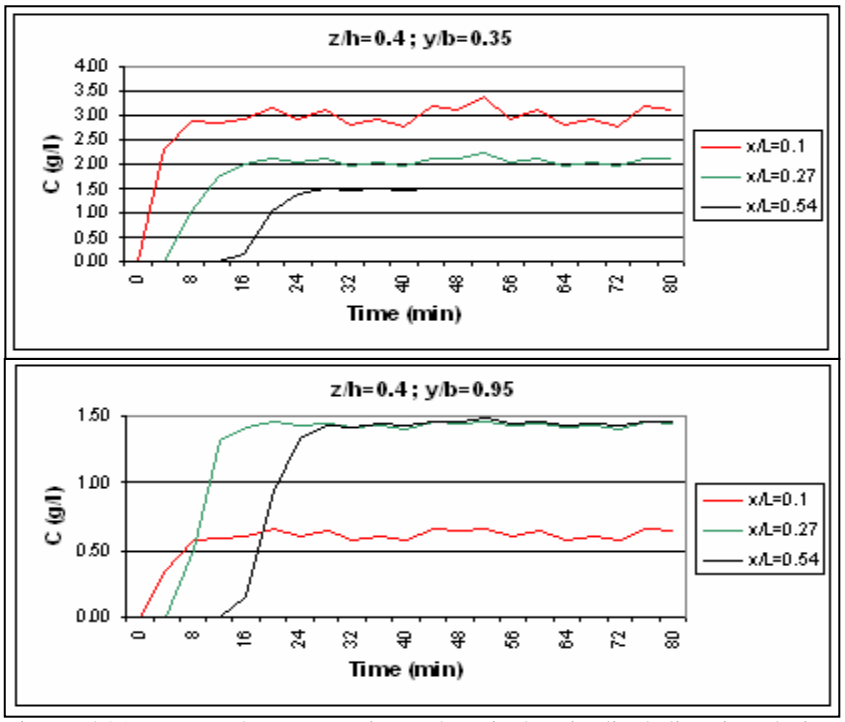


Figure 5.21 Measured concentration values in longitudinal direction during the third experiment

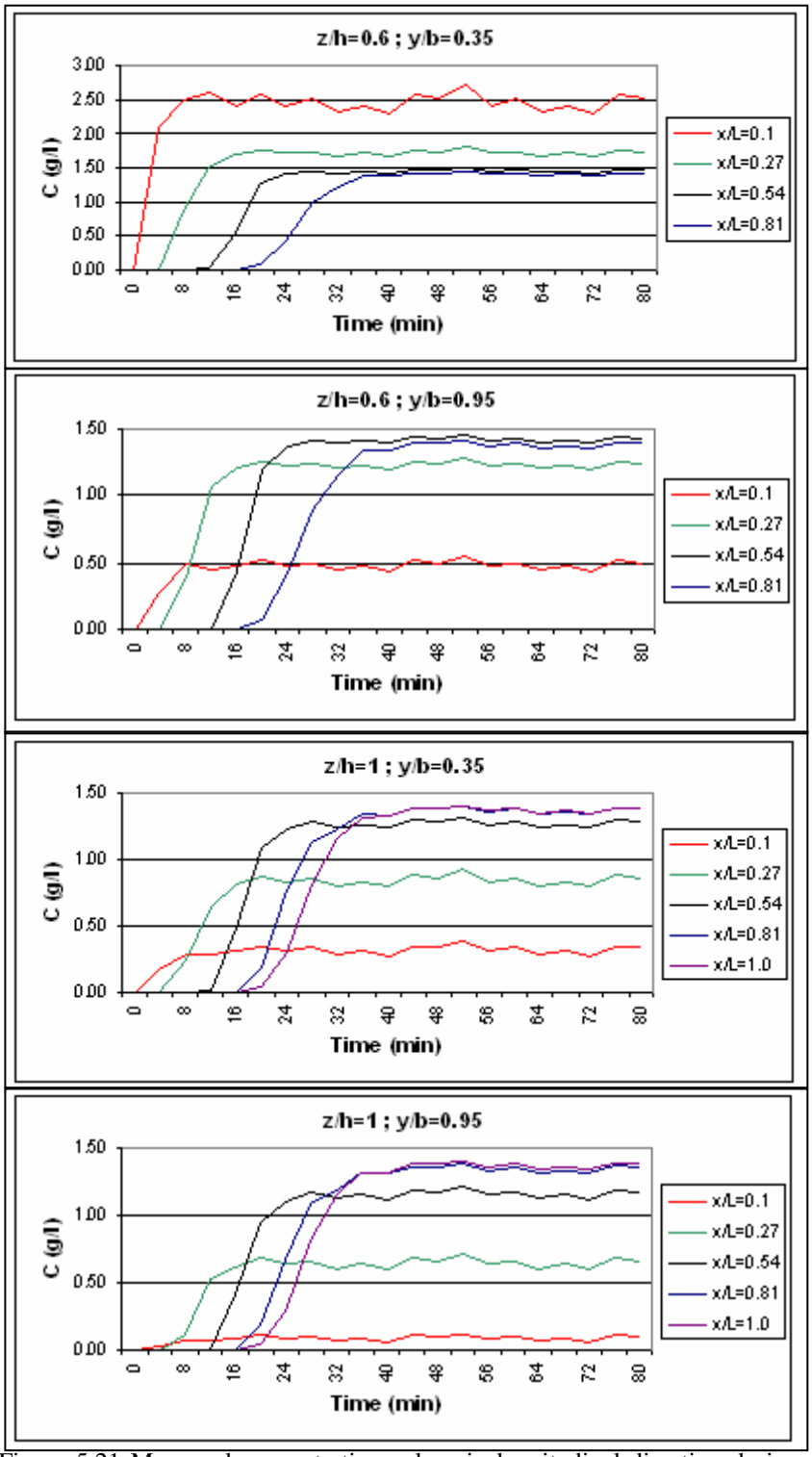


Figure 5.21 Measured concentration values in longitudinal direction during the third experiment (continued)

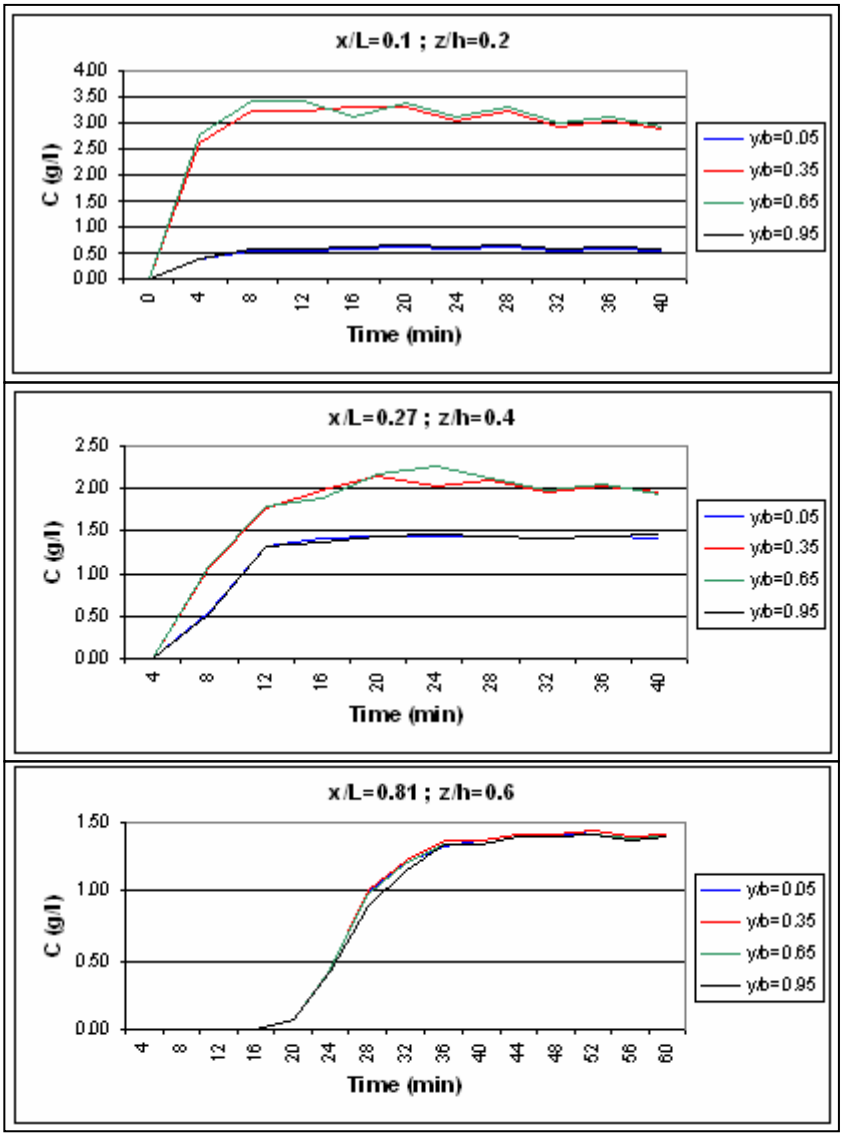


Figure 5.22 Measured concentration values in transversal direction during the third experiment

The relative concentrations in terms of dimensionless distance for the longitudinal direction at certain times are given in Figure 5.23.

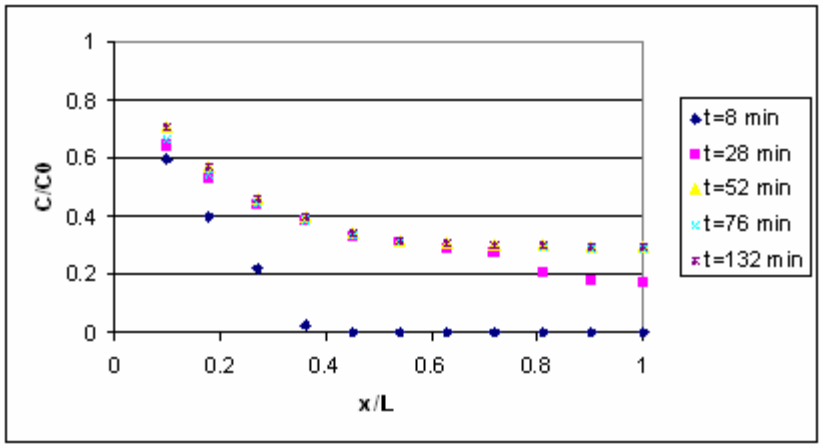


Figure 5.23 Relative concentrations versus dimensionless distance for the third experiment

According the results of the three experiments, the variation of the arrival times of the maximum concentrations with average hydraulic gradient through the channel is given in Figure 5.24. The arrival times of the maximum concentrations increase with hydraulic gradient as expected. The variation of the maximum concentrations with hydraulic gradient through the channel is given in Table 5.5.

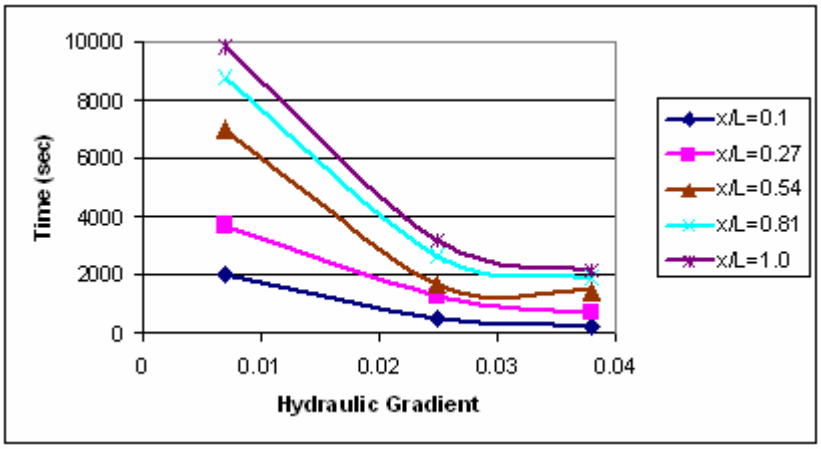


Figure 5.24 The variation of the arrival times of the maximum concentrations with hydraulic gradient

Table 5.5 The variation of the maximum concentrations with hydraulic gradient through the channel

| Average Hyd. Gradient | x/L=0.1 | x/L=0.27 | x/L=0.54 | x/L=0.81 | x/L=1 |
|---|---|---|---|---|---|
| Δh/L=0.007 | 3.7 g/l | 2.2 g/l | 1.5 g/l | 1.4 g/l | 1.25 g/l |
| Δh/L=0.025 | 3.2 g/l | 2.2 g/l | 1.45 g/l | 1.35 g/l | 1.3 g/l |
| Δh/L=0.038 | 3.25 g/l | 2.2 g/l | 1.5 g/l | 1.4 g/l | 1.35 g/l |

## 5.4 Contaminant transport experiments in heterogeneous porous medium

Heterogeneous porous medium is prepared by using three different granular materials. The properties of the materials, the locations of the measurement points and related photos are shown in Figure 5.25a and b, respectively.

The measured conductivity values are converted to concentration values by using the calibration curve given in Figure 5.3. The volume of the contaminant supply tank is 2 $m^3$, its net volume is 1.24 $m^3$. Since the flow rate is 0.1 lt/sec the time elapsed for emptying the tank is 3.5 hours and, the experimental results are evaluated for 12480 seconds.

The hydraulic conductivities of layer 1 and that of layer 2 are determined by experiments performed as explained in section 5.1.

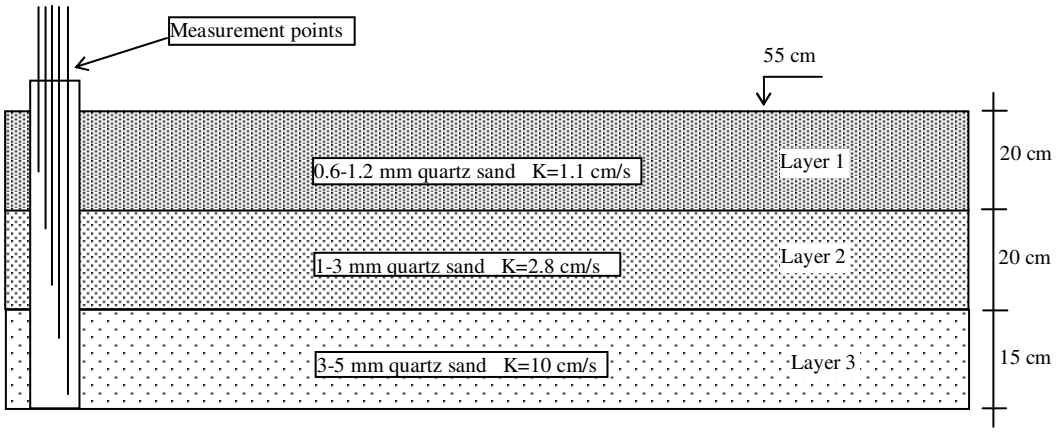


Figure 5.25a The sketch of heterogeneous porous medium

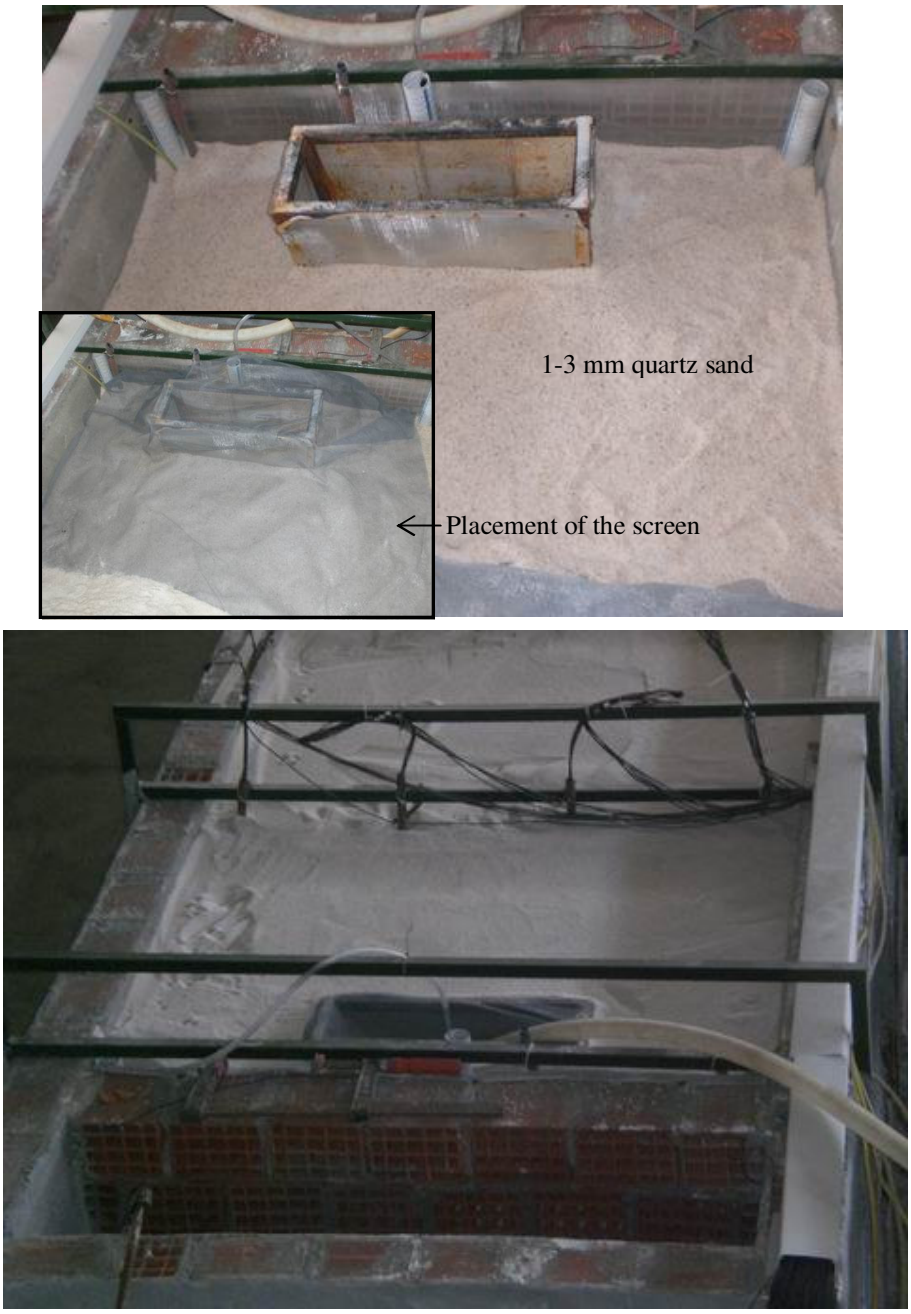


Figure 5.25b Preparation of the heterogeneous porous medium

### *5.4.1 First experiment; Δh/L=* **0.00375**

The water levels are kept constant as 51.5 cm and 47 cm at upstream end and downstream end, respectively during the experiment. Average groundwater flow velocities are 0.0041 cm/sec, 0.0105 cm/sec and 0.0375 cm/sec for the first, second and third layer, respectively. Reynolds numbers are 0.0369, 0.21 and 1.5 for the first, second and third layer, respectively.

Figure 5.26, 5.27 and 5.28 show the variation of the concentration at some measurement points in vertical, longitudinal and transversal directions, respectively.

Since hydraulic gradient is small, NaCl solution is displaced on 3.5 m in the first layer which has a small hydraulic conductivity.

The concentration values in the first layer (z/h=0.2) are observed quite small except at the measurement point located in front of the tracer box (x/L=0.1; y/b=0.35 or y/b=0.65). The tracer (NaCl solution) is not observed at measurement point located near the channel wall in the first layer (Figure 5.26). NaCl solution can not arrive at the downstream end of the channel due to the small hydraulic gradient.

The maximum concentration in the channel is observed at points x/L=0.1, z/h=0.2 and y/b=0.35 (or y/b=0.65). The contaminant arrived at first measurement point 2640 seconds after giving the NaCl solution in the first layer while the arrival time in the second and third layer are 720 and 1440 seconds, respectively. This situation can be explained by the geometry of the tracer box which has a height of 30 cm. NaCl is displaced 3.5 m, 9 m and 11 m in the first, second and third layer, respectively, 12480 seconds after giving the solution.

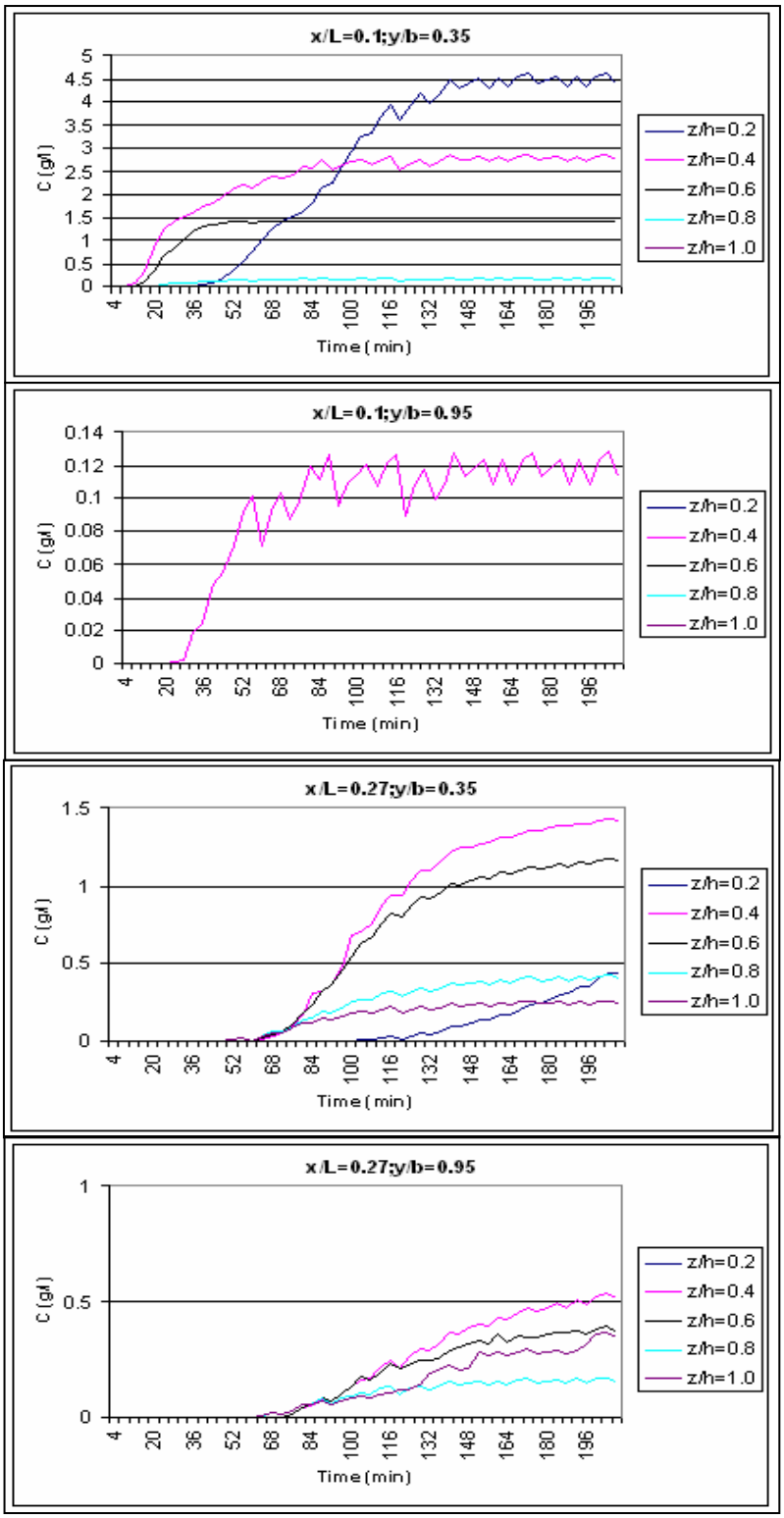


Figure 5.26 Measured concentration values in vertical direction during the first experiment in heterogeneous medium

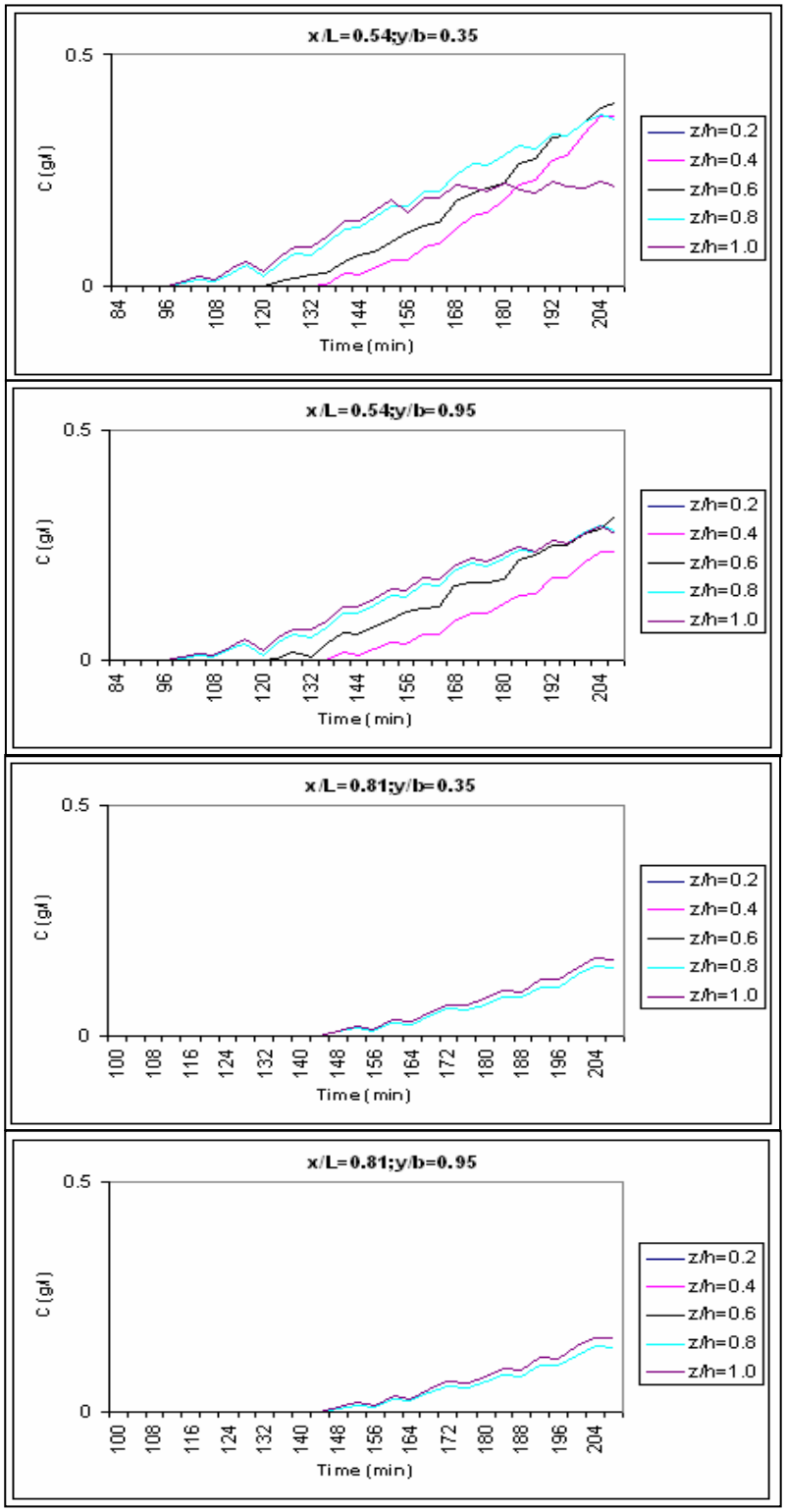


Figure 5.26 Measured concentration values in vertical direction during the first experiment in heterogeneous medium (continued)

In longitudinal direction concentration values decrease with distance as expected (Figure 5.27).

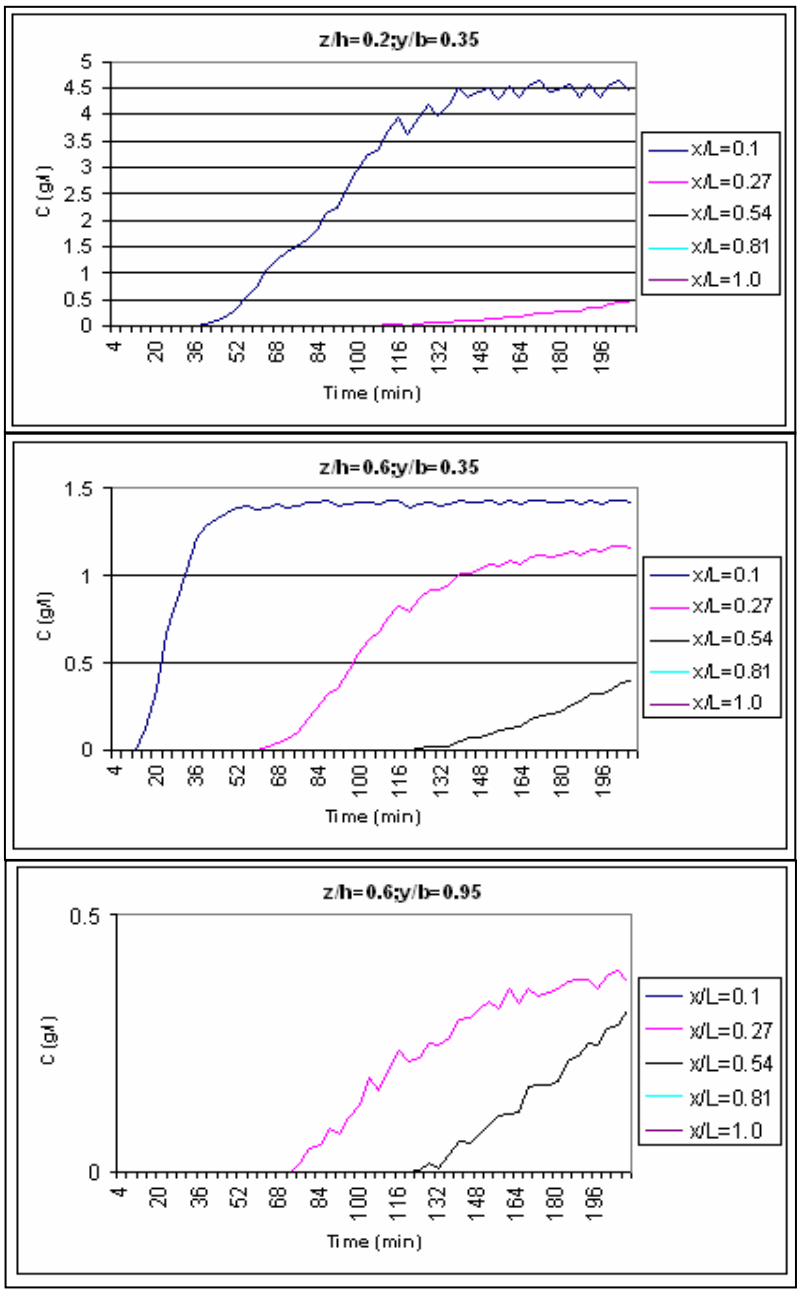


Figure 5.27 Measured concentration values in longitudinal direction during first experiment in heterogeneous medium

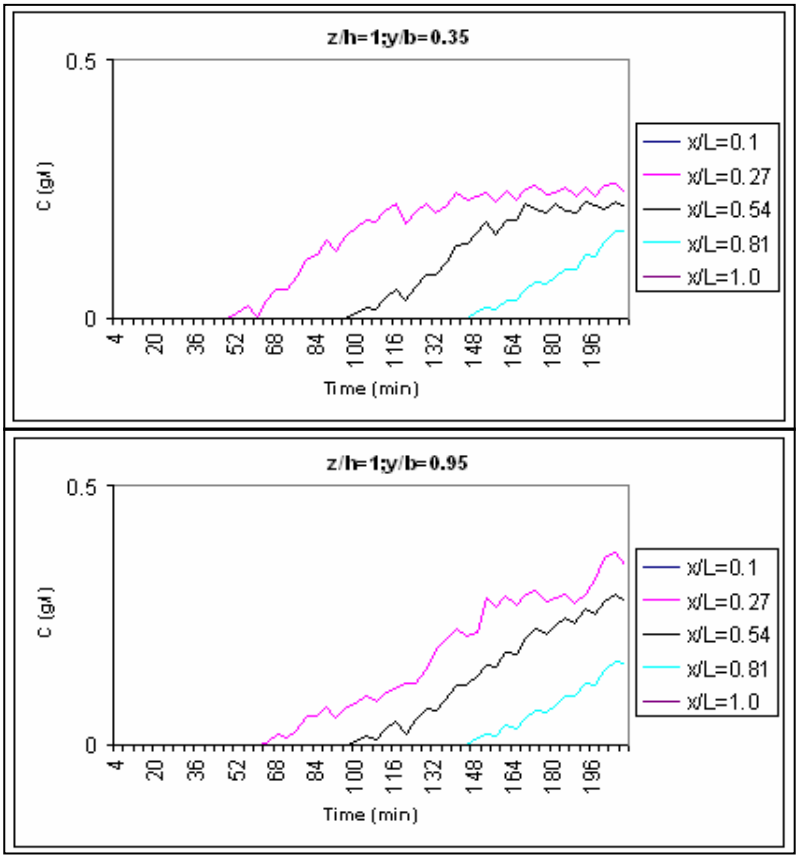


Figure 5.27 Measured concentration values in longitudinal direction during first experiment in heterogeneous medium (continued)

The experimental results show that concentrations at y/b=0.05 and y/b=0.65 are almost equal to the concentrations at y/b=0.35 and y/b=0.95, respectively (Figure 5.28).

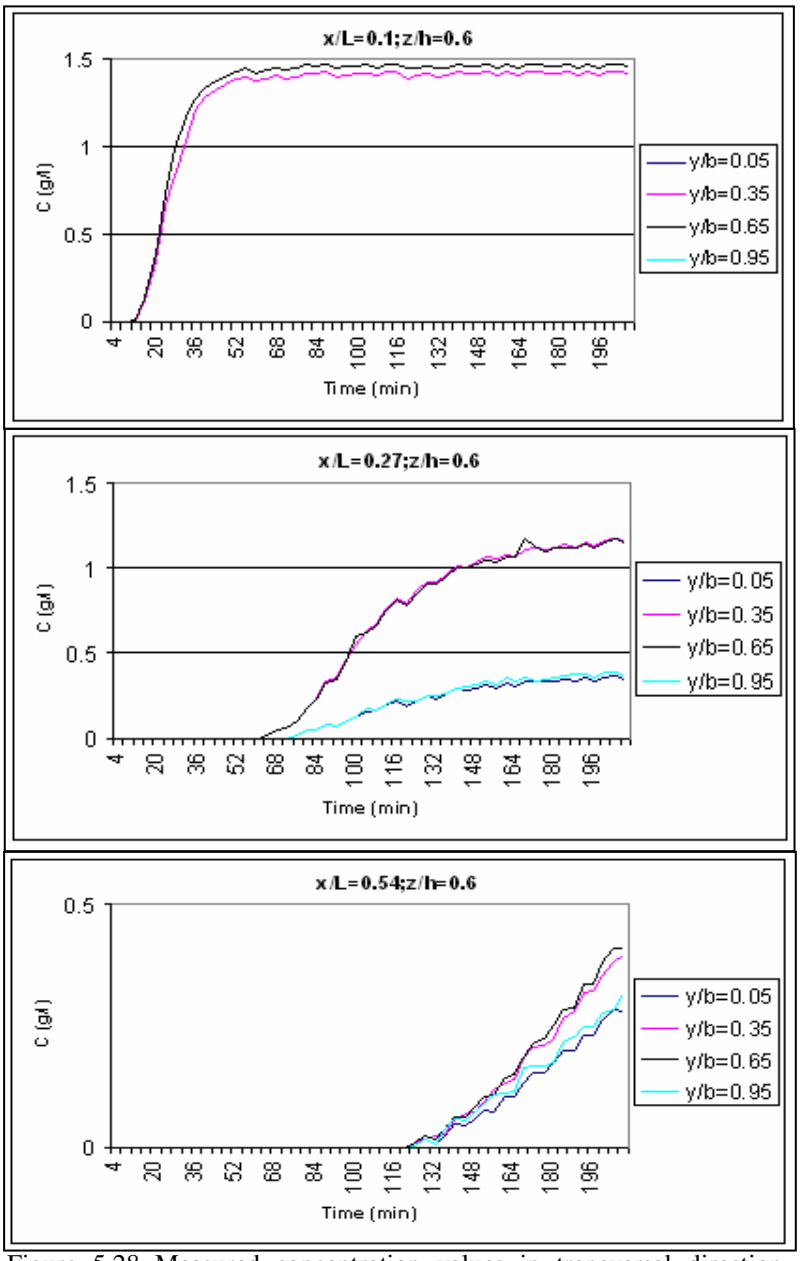


Figure 5.28 Measured concentration values in transversal direction during the first experiment in heterogeneous medium

### *5.4.2 Second experiment; Δh/L=* **0.026**

Hydraulic gradient is increased in the second experiment for better observation of concentration distribution in the channel. The water levels are kept constant as 51 cm and 19.5 cm at upstream end and downstream end, respectively during the experiment. Average groundwater flow velocities are 0.0286 cm/sec, 0.073 cm/sec and 0.26 cm/sec for the first, second and third layer, respectively. Reynolds numbers are 0.257, 1.46 and 10.4 for the first, second and third layer, respectively.

Figure 5.29, 5.30 and 5.31 show the variation of the concentration at some measurement points in vertical, longitudinal and transversal directions, respectively.

The interpretations done for the first experiments are valid for the second experiments. The only difference between two experiments is hydraulic gradient and consequently the groundwater velocity.

The contaminant arrived at first measurement point 720 seconds after giving the NaCl solution in the first layer, while the arrival time in the second and third layer are 240 and 480 seconds, respectively. NaCl is displaced 6.5 m, 11 m and 12 m in the first, second and third layer, respectively, 12480 seconds after giving the solution.

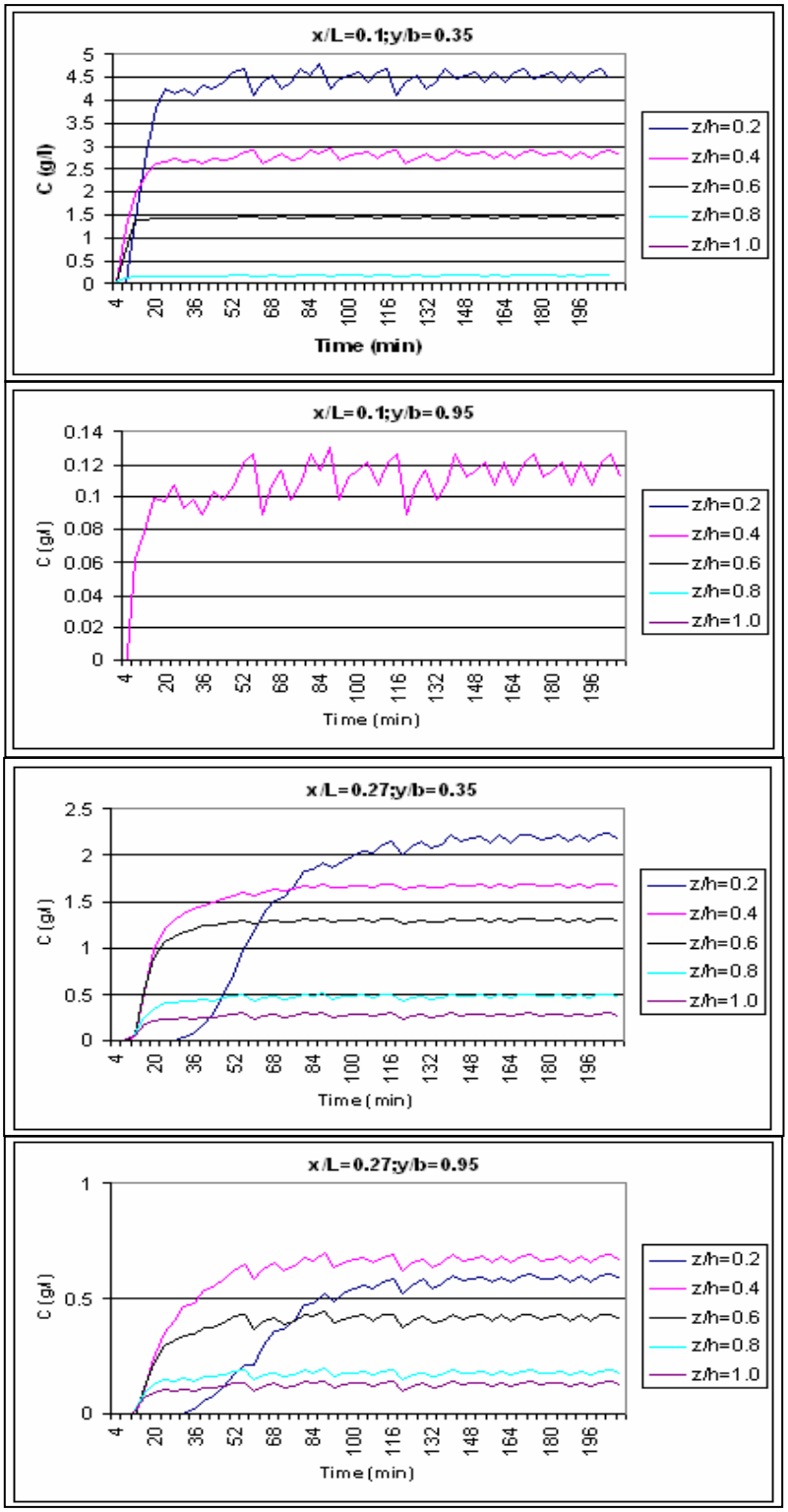


Figure 5.29 Measured concentration values in vertical direction during the second experiment in heterogeneous medium

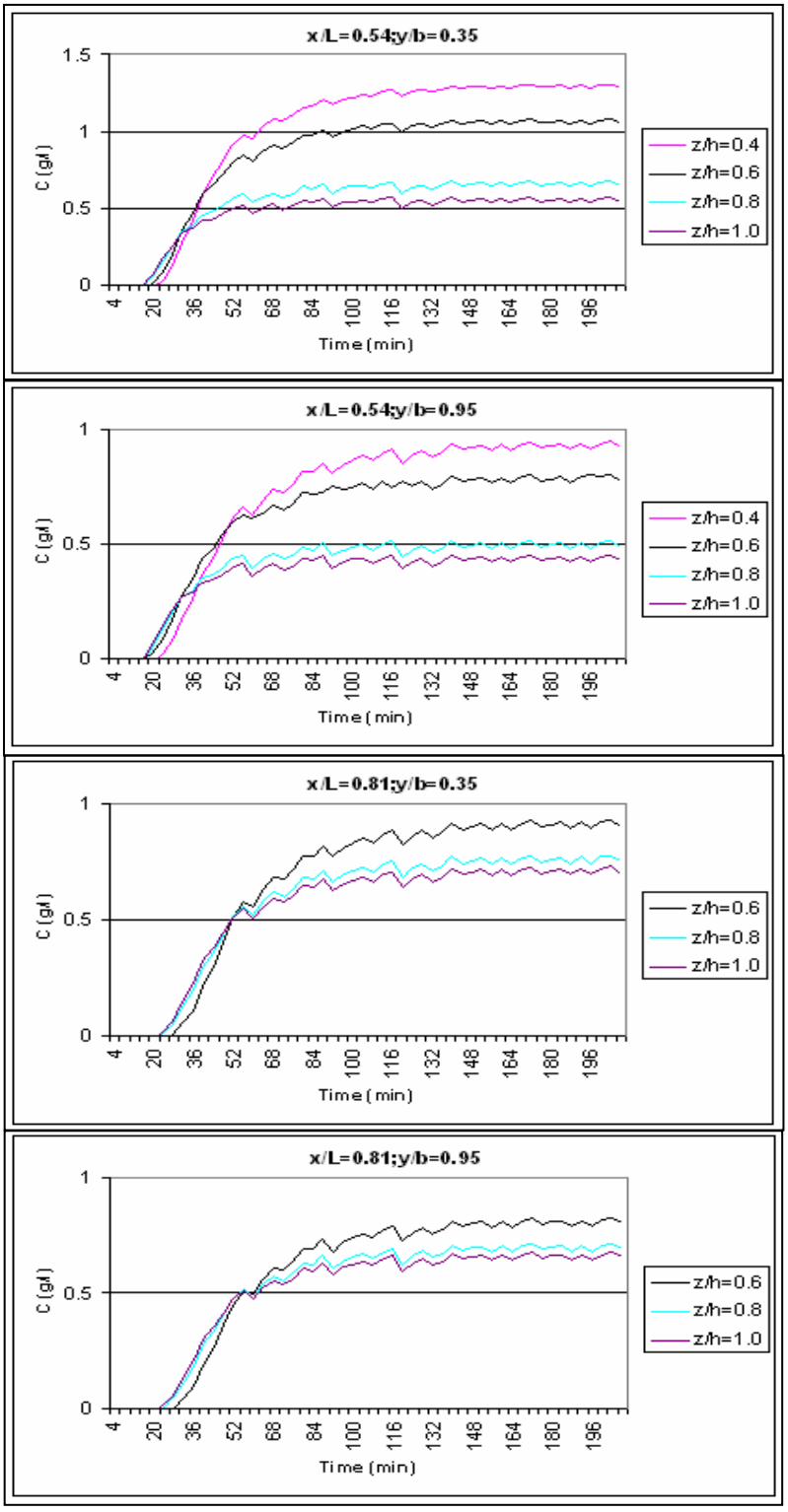


Figure 5.29 Measured concentration values in vertical direction during the second experiment in heterogeneous medium (continued)

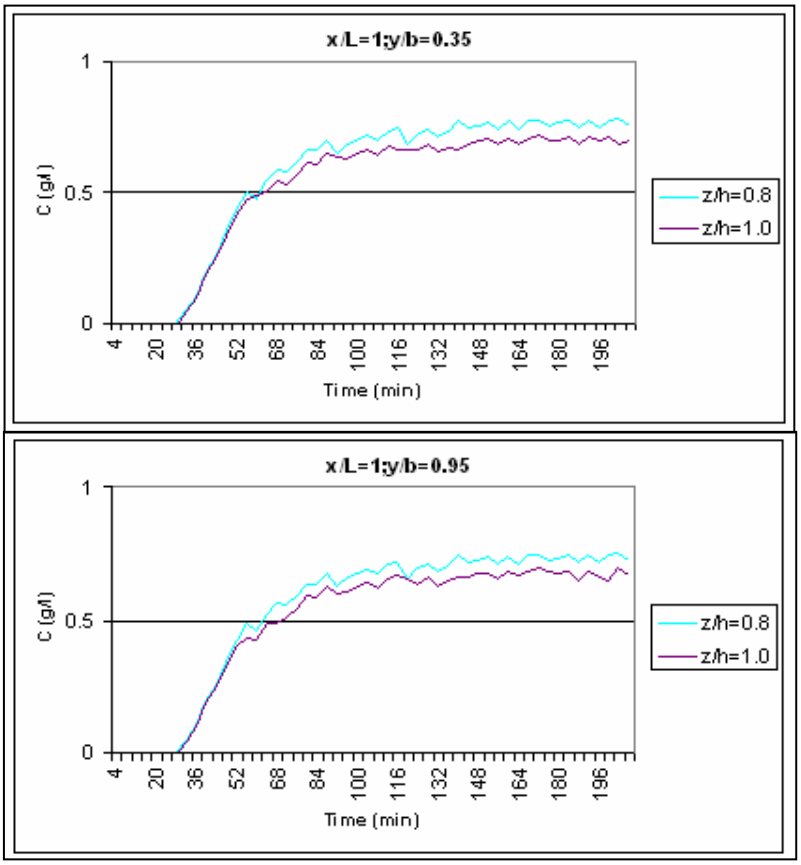


Figure 5.29 Measured concentration values in vertical direction during the second experiment in heterogeneous medium (continued)

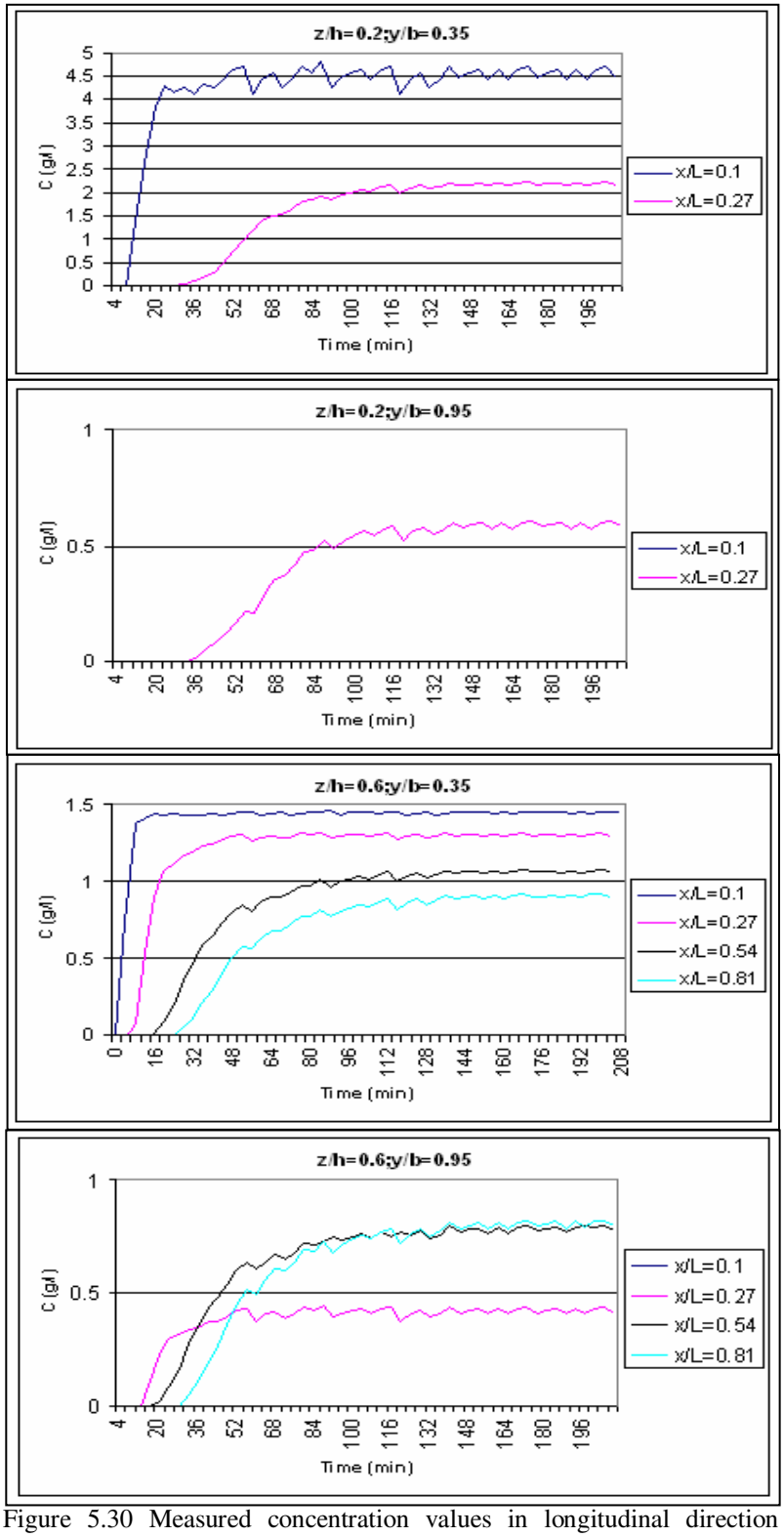


Figure 5.30 Measured concentration values in longitudinal direction during the second experiment in heterogeneous medium

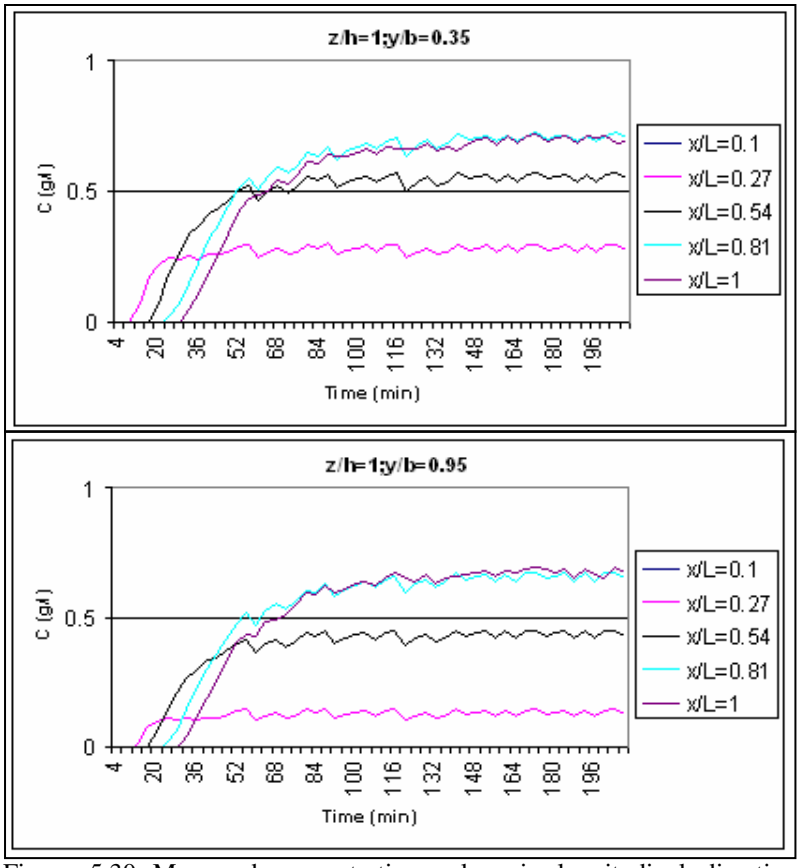


Figure 5.30 Measured concentration values in longitudinal direction during the second experiment in heterogeneous medium (continued)

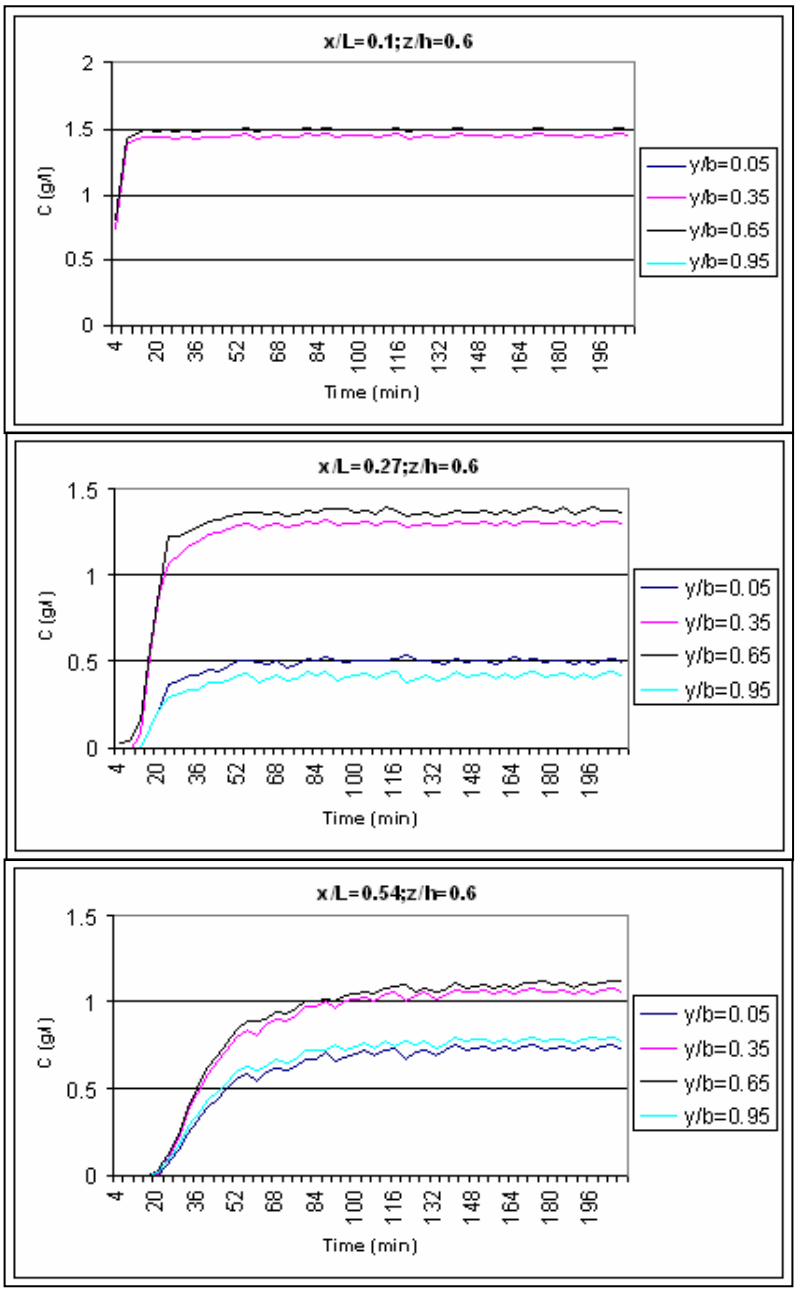


Figure 5.31 Measured concentration values in transversal direction during the second experiment in heterogeneous medium

### *5.4.3 Third experiment; Δh/L=* **0.0136**

In this experiment, it is intended to obtain the contaminant transport in the two lower layers only. During the third experiment, the water levels are kept constant at upstream end and downstream end of the channel as 35.5 cm and 19.2 cm, respectively. Thus the concentration distribution could be observed only in the layers 2 and 3. This will be helpful to determine the dispersivity values of the granular materials placed in these layers. Average groundwater flow velocities are 0.038 cm/sec and 0.136 cm/sec for the second and third layer, respectively. Reynolds numbers are 0.76 and 5.44 for the second and third layer, respectively.

Figure 5.32, 5.33 and 5.34 show the variation of the concentration at some measurement points in vertical, longitudinal and transversal directions, respectively.

NaCl moves 10 m and 12 m in the second and third layer, respectively, 12480 seconds after giving the solution.

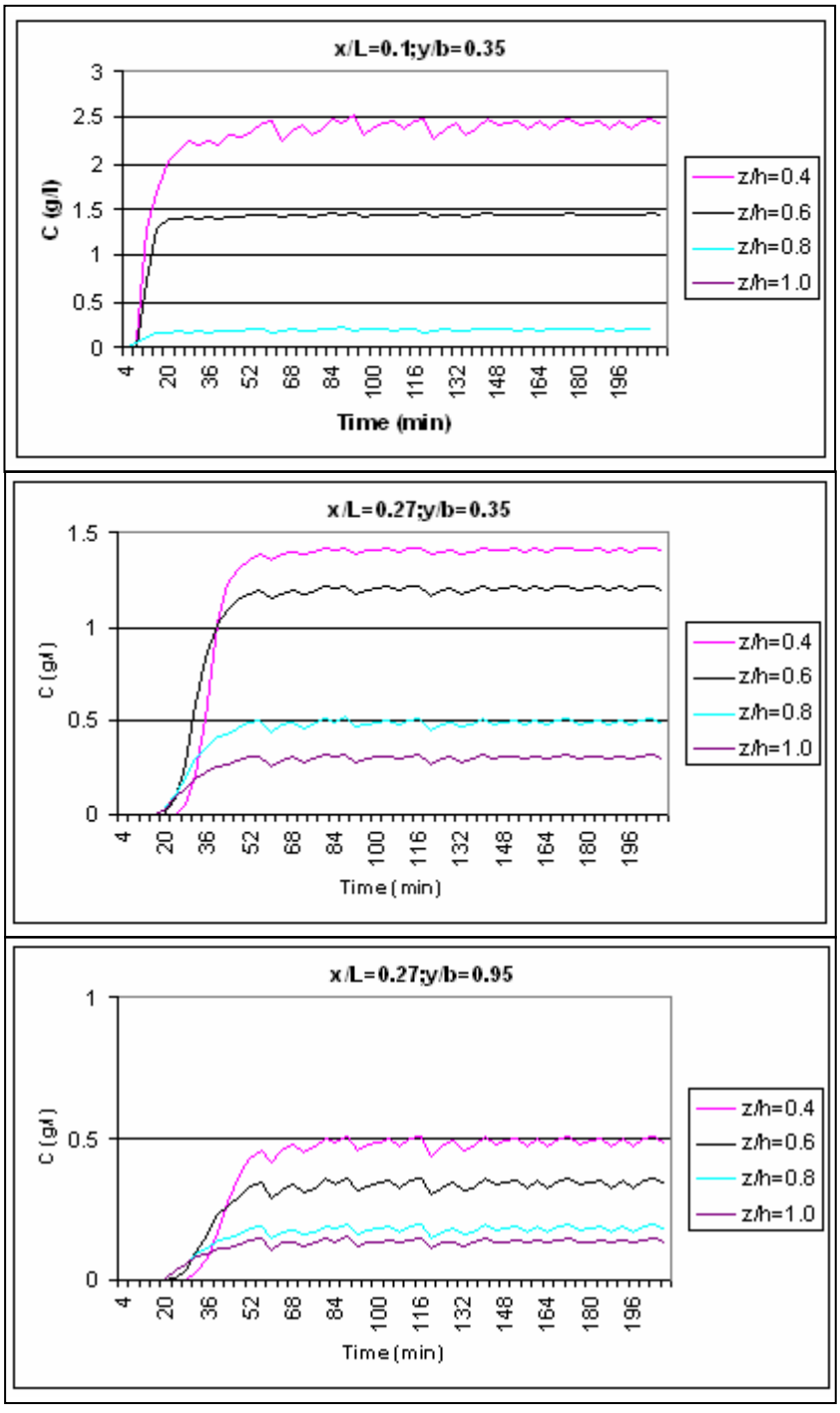


Figure 5.32 Measured concentration values in vertical direction during the third experiment in heterogeneous medium

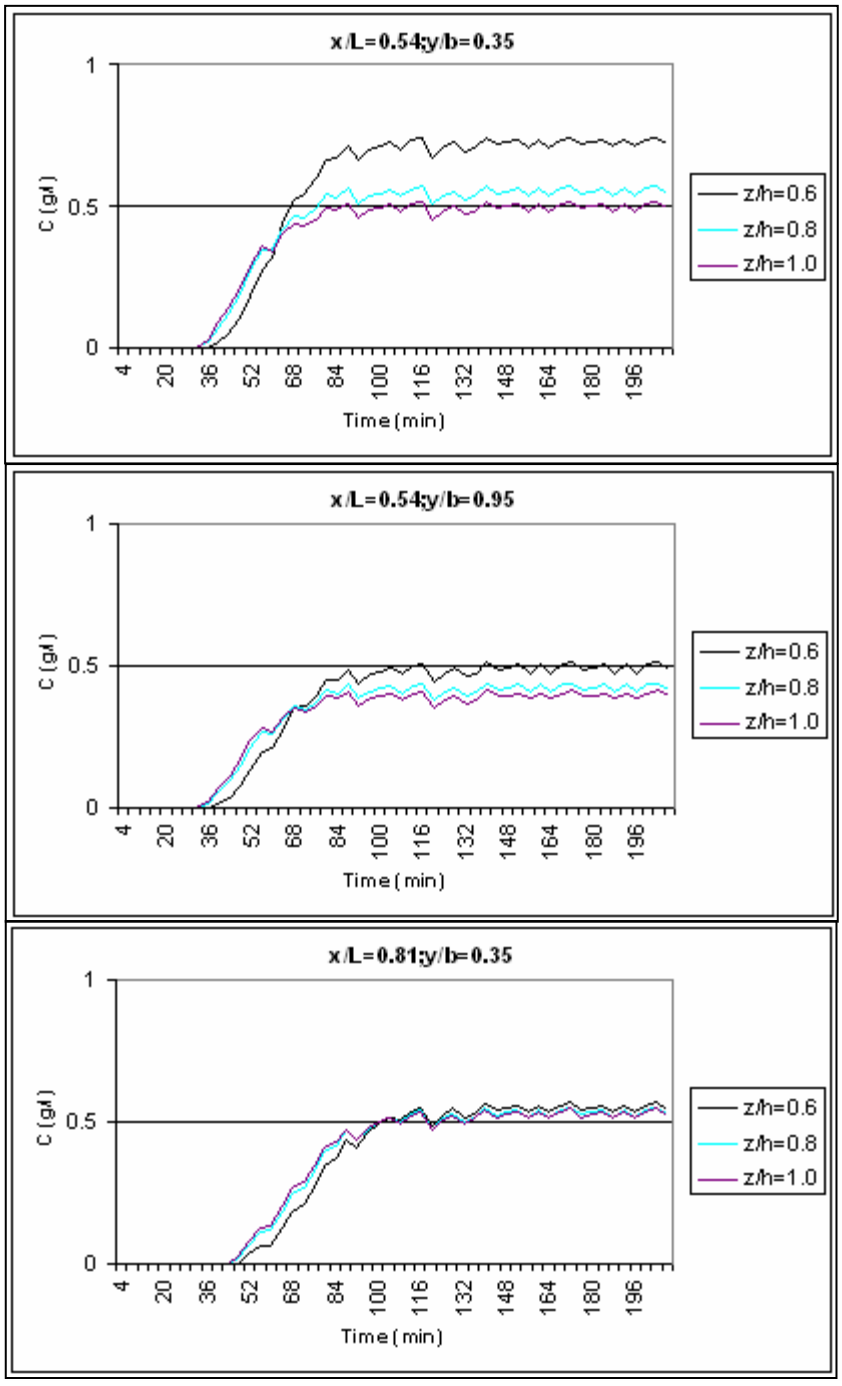


Figure 5.32 Measured concentration values in vertical direction during the third experiment in heterogeneous medium (continued)

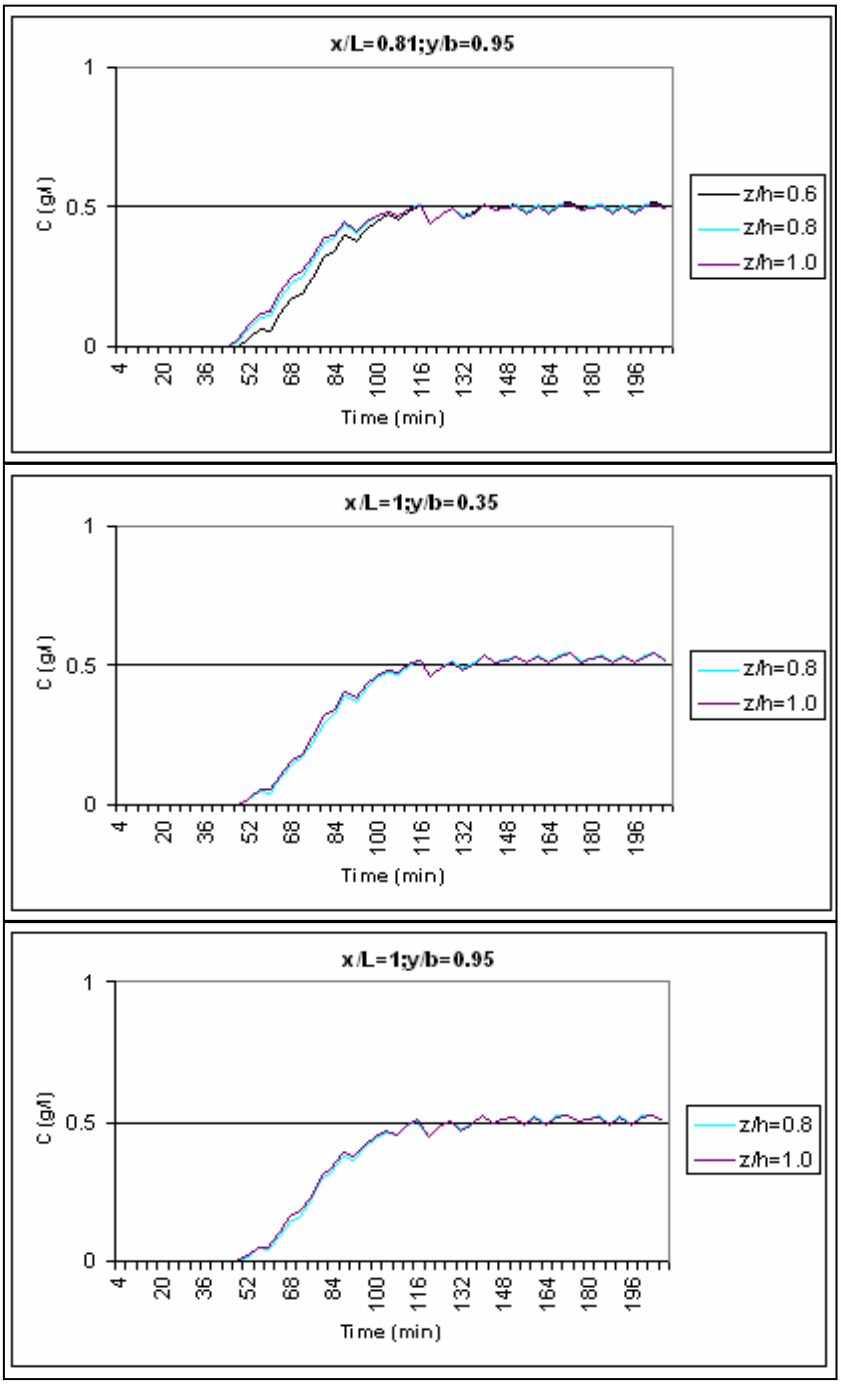


Figure 5.32 Measured concentration values in vertical direction during the third experiment in heterogeneous medium (continued)

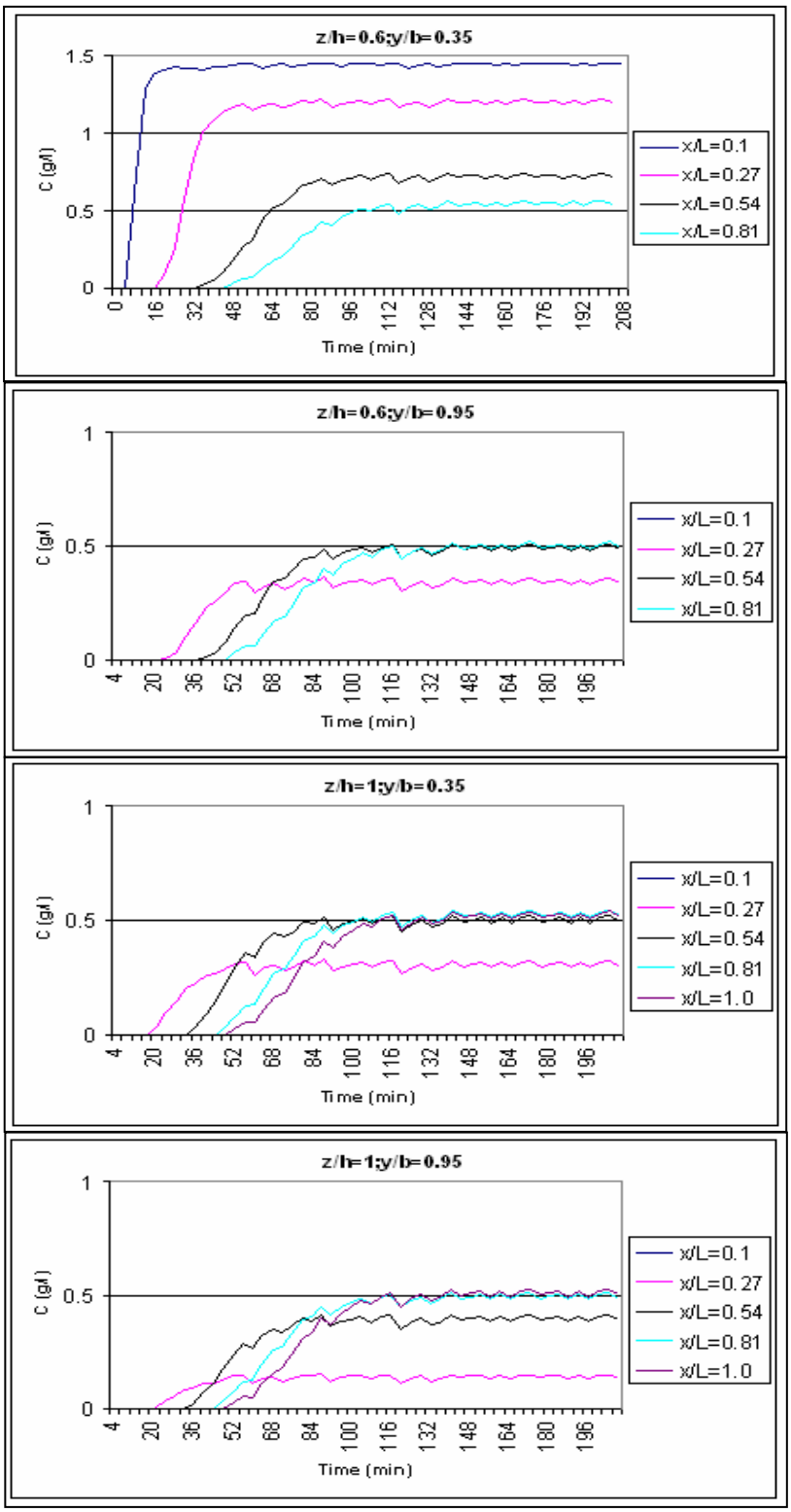


Figure 5.33 Measured concentration values in longitudinal direction during the third experiment in heterogeneous medium

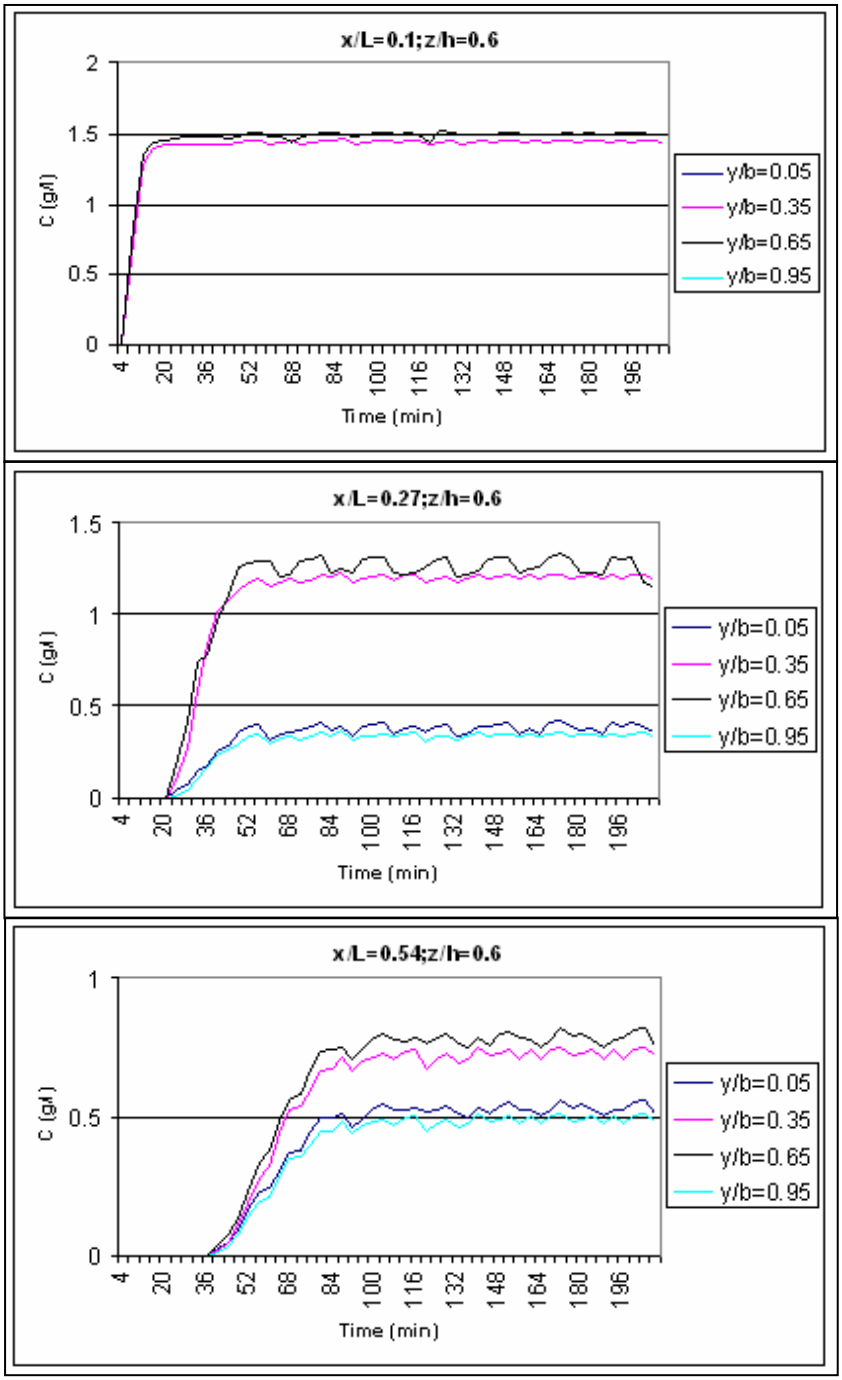


Figure 5.34 Measured concentration values in transversal direction during the third second experiment in heterogeneous medium

# CHAPTER SIX
# DETERMINATION OF DISPERSIVITIES

To estimate dispersivity values from experimental data the best approach is to plot theoretical and observed breakthrough curves for various values of dispersivity and determine the values which give the best over-all fit (Charbeneau, 2000).

In this study MODFLOW which is a modular three-dimensional finite difference flow code developed by U.S. Geological survey (McDonald and Harbaugh, 1988) is used to simulate groundwater flow.

## 6.1 Dispersivity values of homogeneous porous medium

The three-dimensional groundwater flow model has been established as grid of 10 rows, 100 columns and 5 layers. Since the water level is constant at upstream and downstream end, the upstream and downstream boundary conditions are described as specific head boundary conditions and aquifer is specified as unconfined. The hydraulic conductivity values are taken as 10 cm/sec in three directions since the medium is homogeneous and isotropic. Mass Transport 3 Dimensional (Zheng and Wang, 1999, MT3DMS code) which is a three-dimensional solute transport simulation model incorporating finite differences solution option is used to solve the three dimensional advective-dispersive transport equation. Diffusion is neglected due to the sufficiently high values of velocity, as this is the case in practice. The estimated dispersivity values are modified until an acceptable compatibility between the observed and calculated concentrations at measurement points is reached.

After the calculation performed by using the first experiment data, the best match is obtained for $\alpha_x$=12 cm, $\alpha_y / \alpha_x$= 0.2 and $\alpha_z / \alpha_x$= 0.05. These ratios are compatible with those given in the literature. The observed concentrations and those calculated by using the formentioned dispersivity values are given in Figure 6.1 for some

measurement points. Plan and cross-sectional view of plume distributions in terms of time are given in Figure 6.2 and Figure 6.3, respectively.

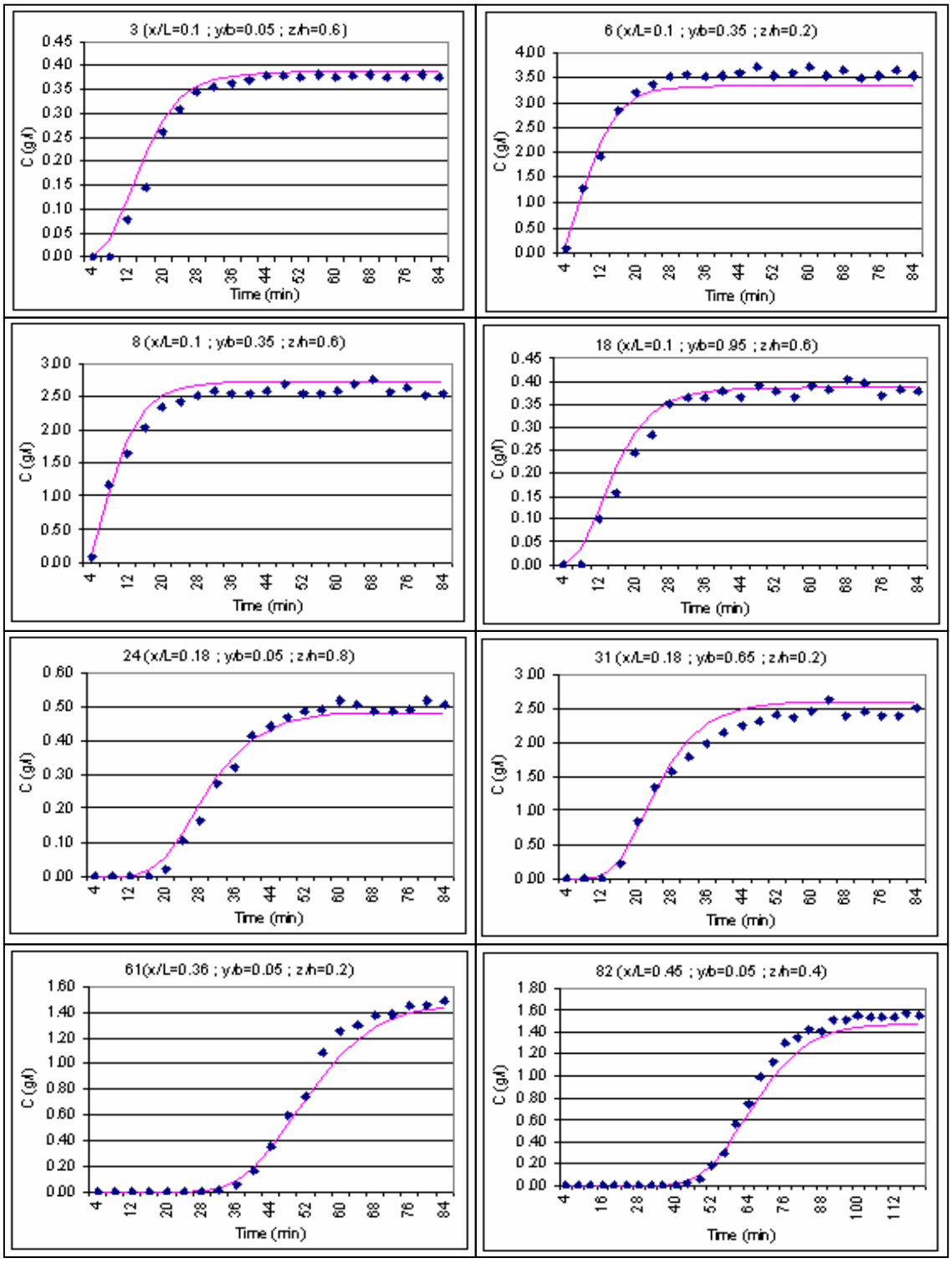


Figure 6.1 The observed (dots) and calculated (lines) concentrations of the first experiment in homogeneous medium

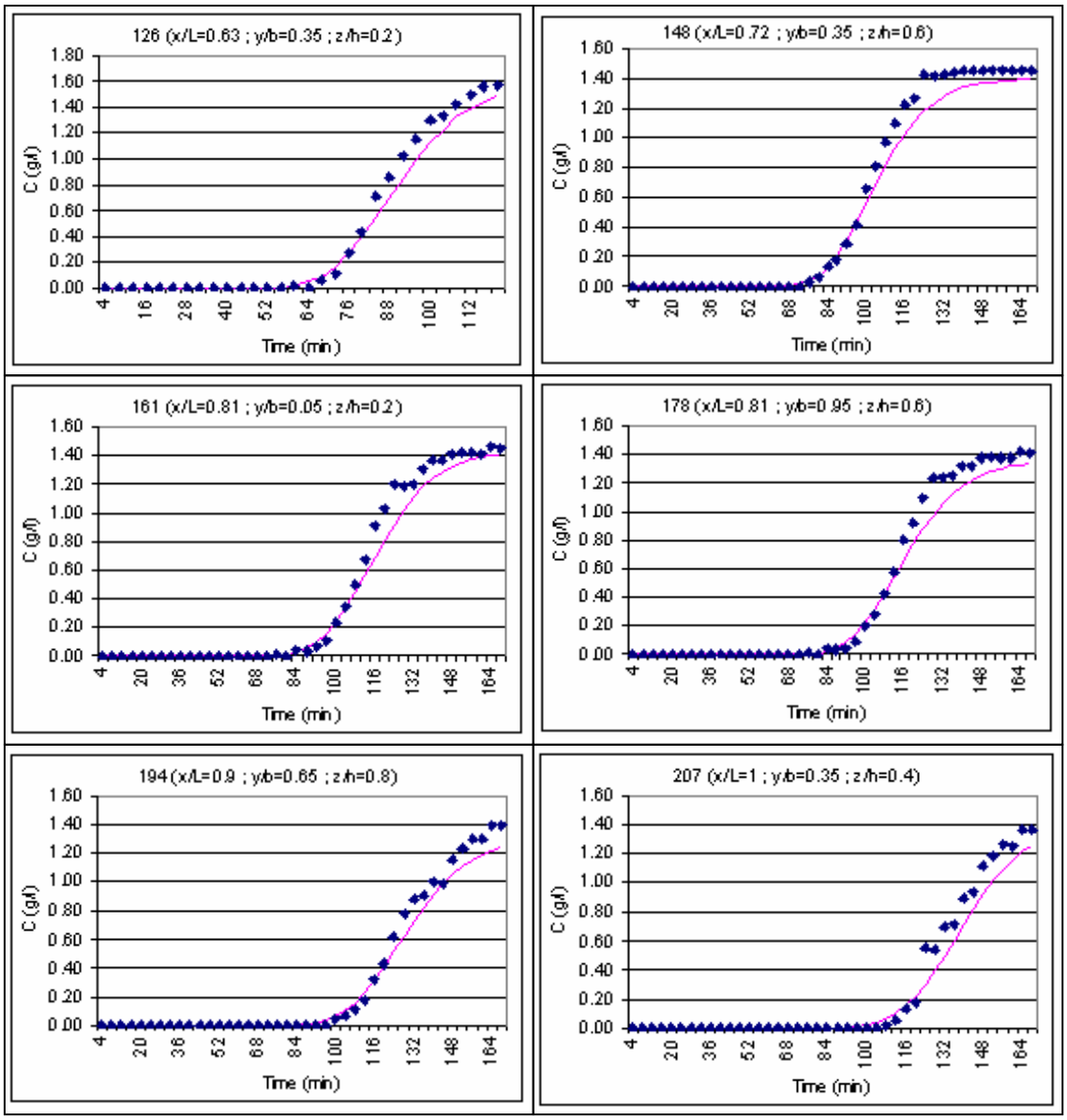


Figure 6.1 The observed (dots) and calculated (lines) concentrations of the first experiment in homogeneous medium (continued)

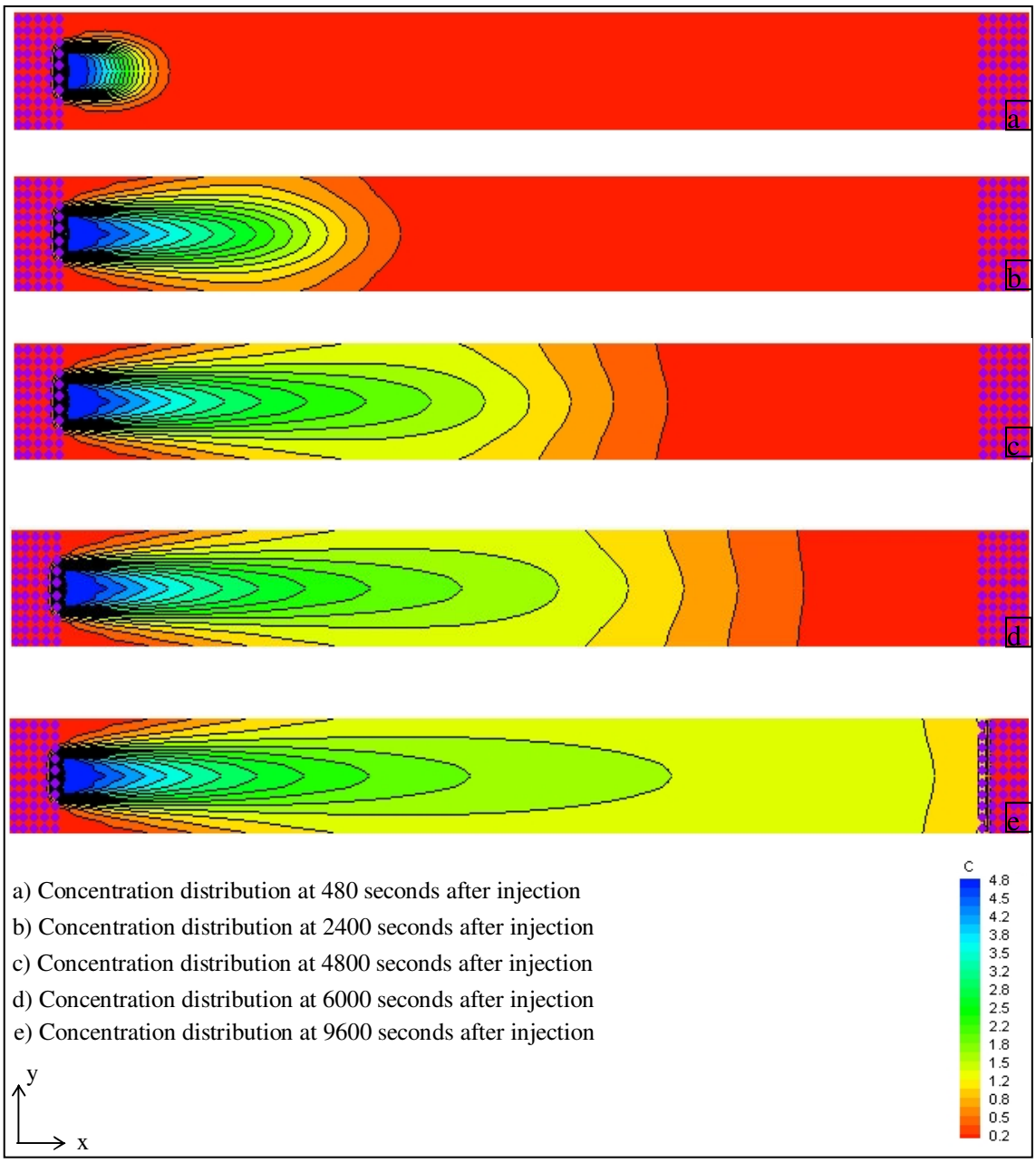


Figure 6.2 Plan view of the plume distribution versus time in homogeneous medium (first experiment)

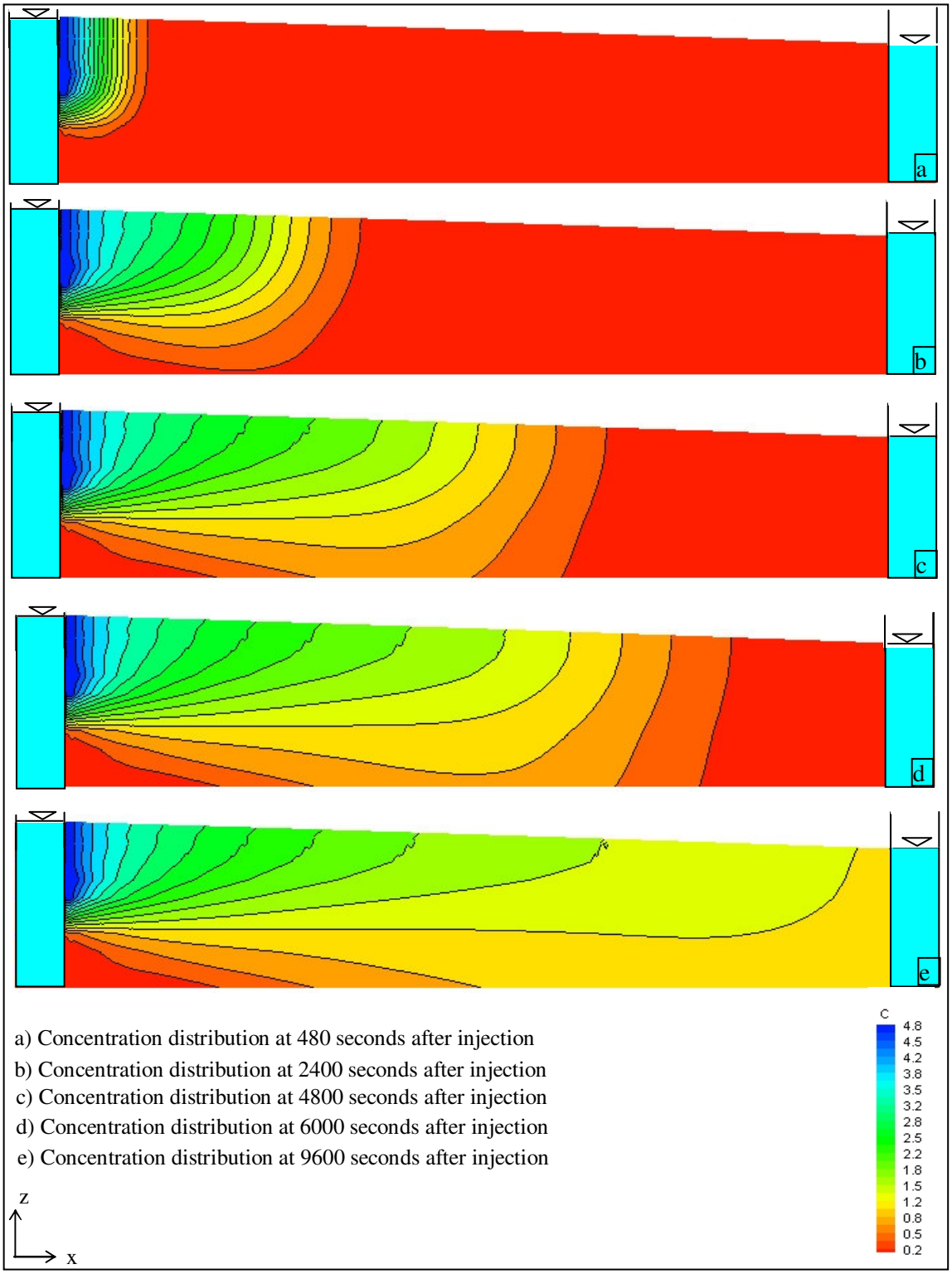


Figure 6.3 Longitudinal-sectional view of the plume distribution versus time in homogeneous medium (first experiment)

When the second experiment's data is used, the best match is obtained for $\alpha_x$=12.3 cm, $\alpha_y / \alpha_x$ = 0.22 and $\alpha_z / \alpha_x$ = 0.05. The observed concentrations and those calculated by using the formentioned dispersivity values are given in Figure 6.4 for some measurement points. Plan and cross-sectional view of plume distributions in terms of time are given in Figure 6.5 and Figure 6.6, respectively.

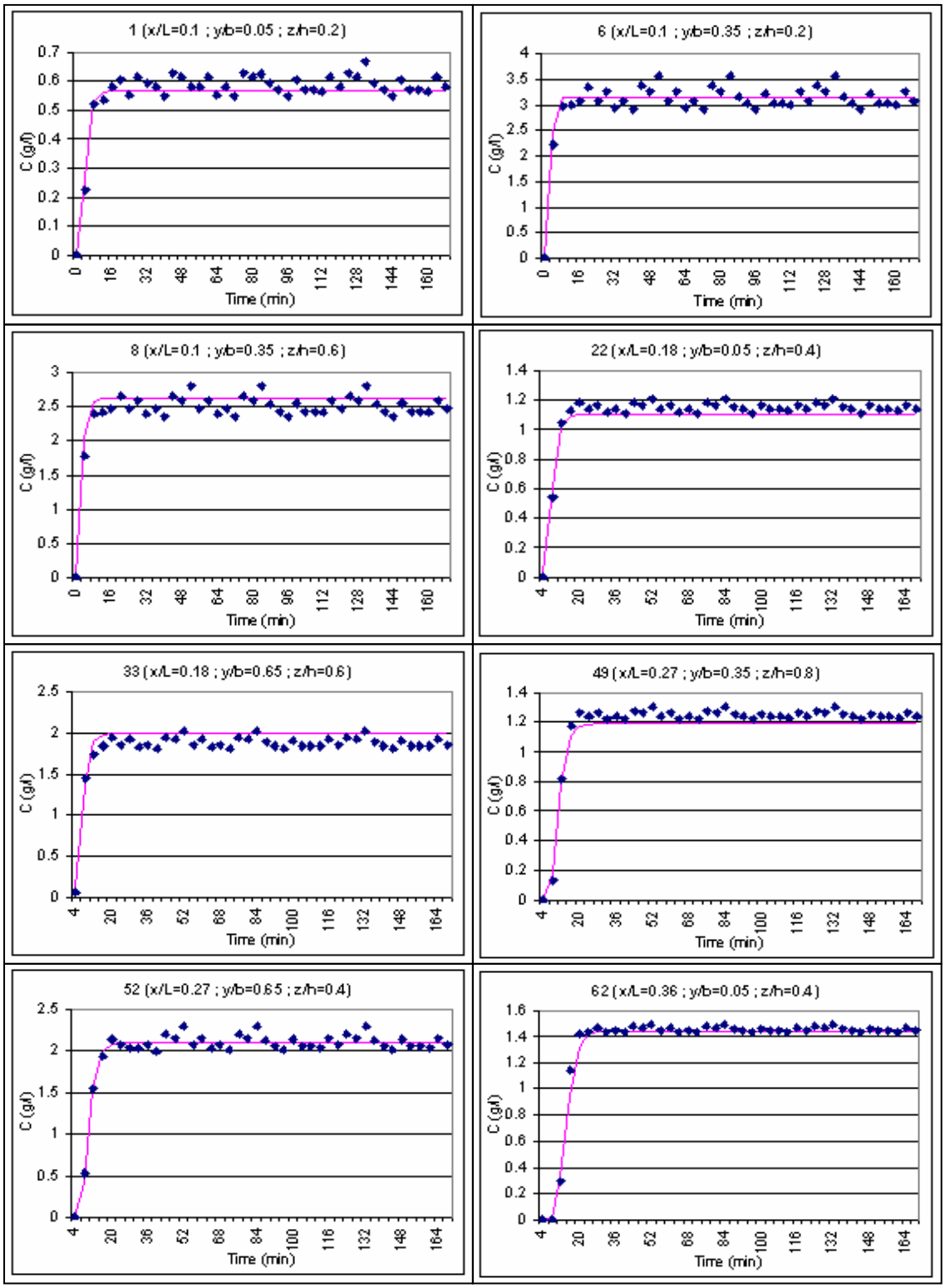


Figure 6.4 The observed (dots) and calculated (lines) concentrations of the second experiment in homogeneous medium

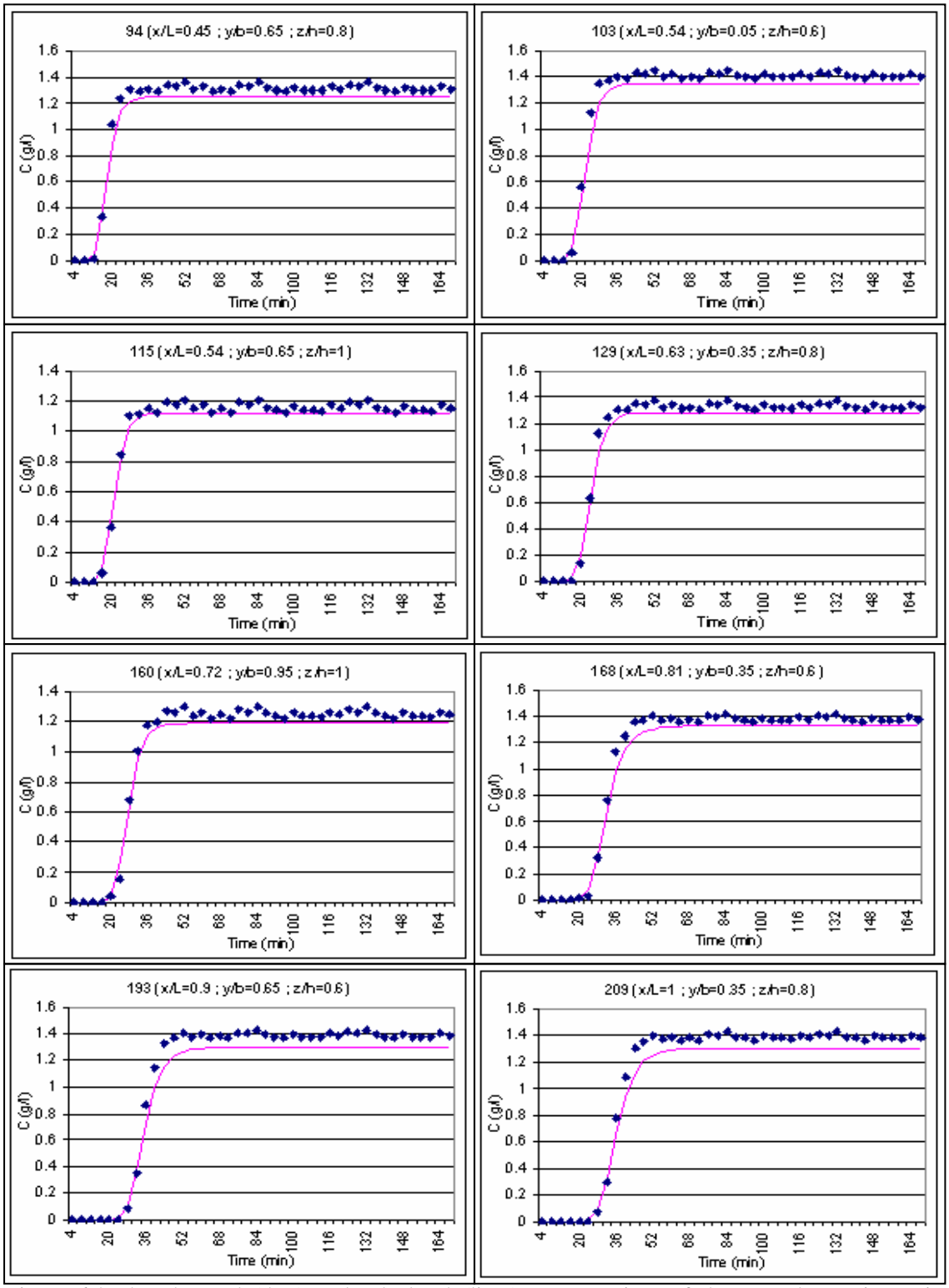


Figure 6.4 The observed (dots) and calculated (lines) concentrations of the second experiment in homogeneous medium (continued)

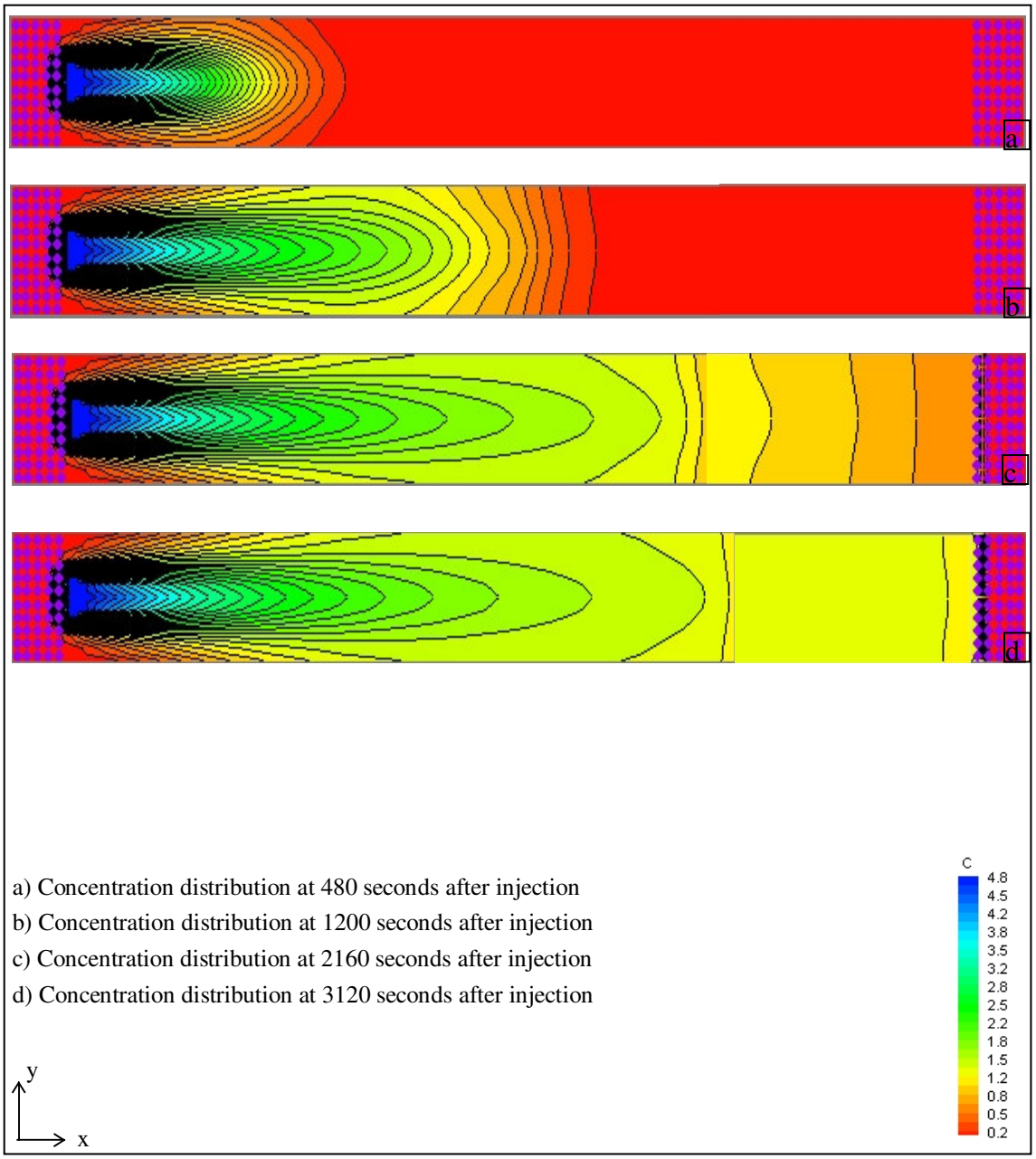


Figure 6.5 Plan view of the plume distribution versus time in homogeneous medium (second experiment)

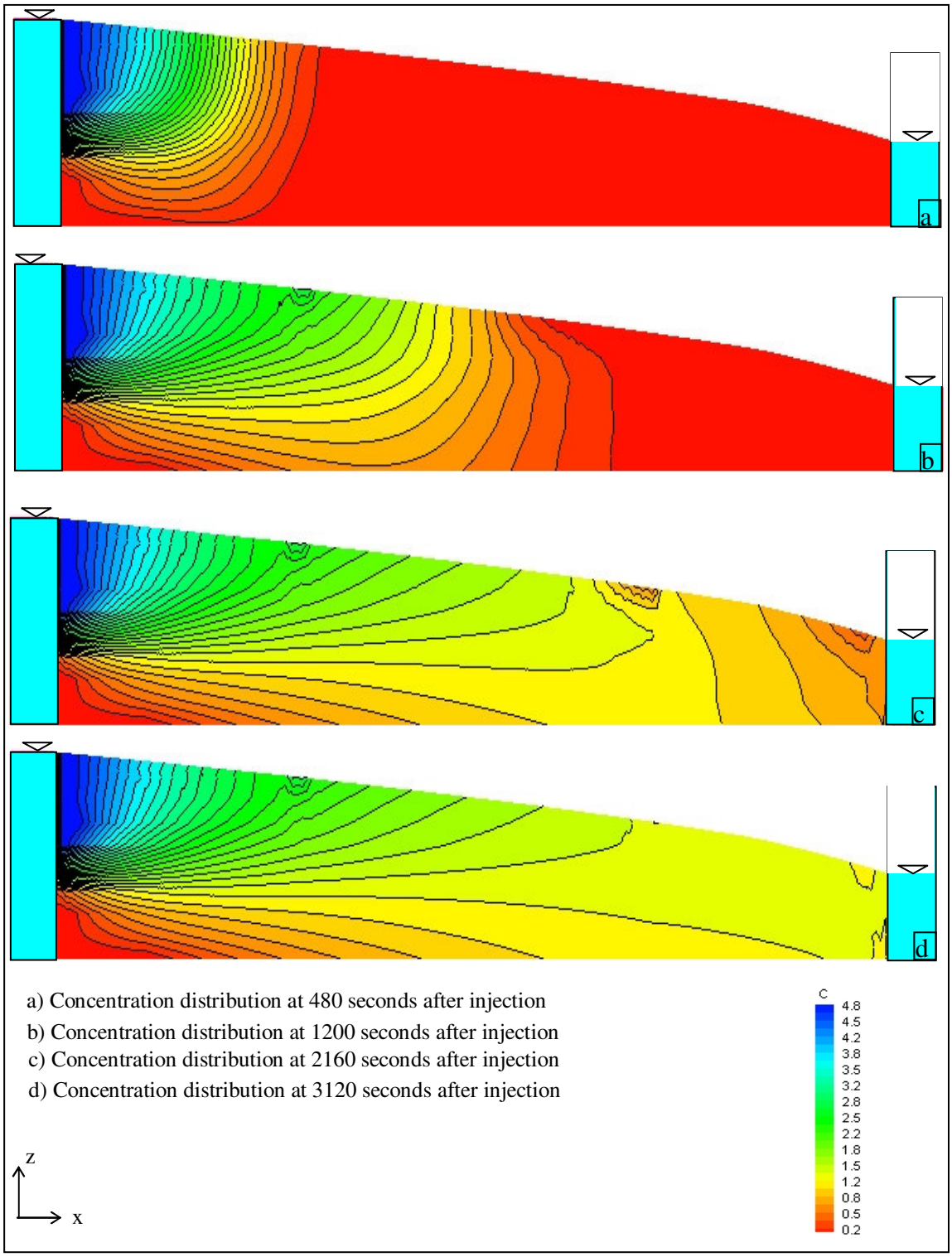


Figure 6.6 Longitudinal-sectional view of the plume distribution versus time in homogeneous medium (second experiment)

As the present study is an inverse problem, the experimental concentration values concerning the first two experiments are used to obtain dispersivities from relevant equations by using trial and error method, and then these dispersivity values are used to calculate concentration values with conditions corresponding to the third experiment. These theoretical concentration values are compared with experimental ones for the sake of verification.

The average values of dispersivities ($\alpha_x$=12.2 cm, $\alpha_y / \alpha_x$ = 0.21 and $\alpha_z / \alpha_x$ = 0.05) obtained from first two experiments are used into the mass transport model to calculate concentrations corresponding to the third experiment. The observed and calculated concentrations are given in Figure 6.7 for some measurement points. Plan and cross-sectional view of plume distributions in terms of time are given in Figure 6.8 and Figure 6.9, respectively.

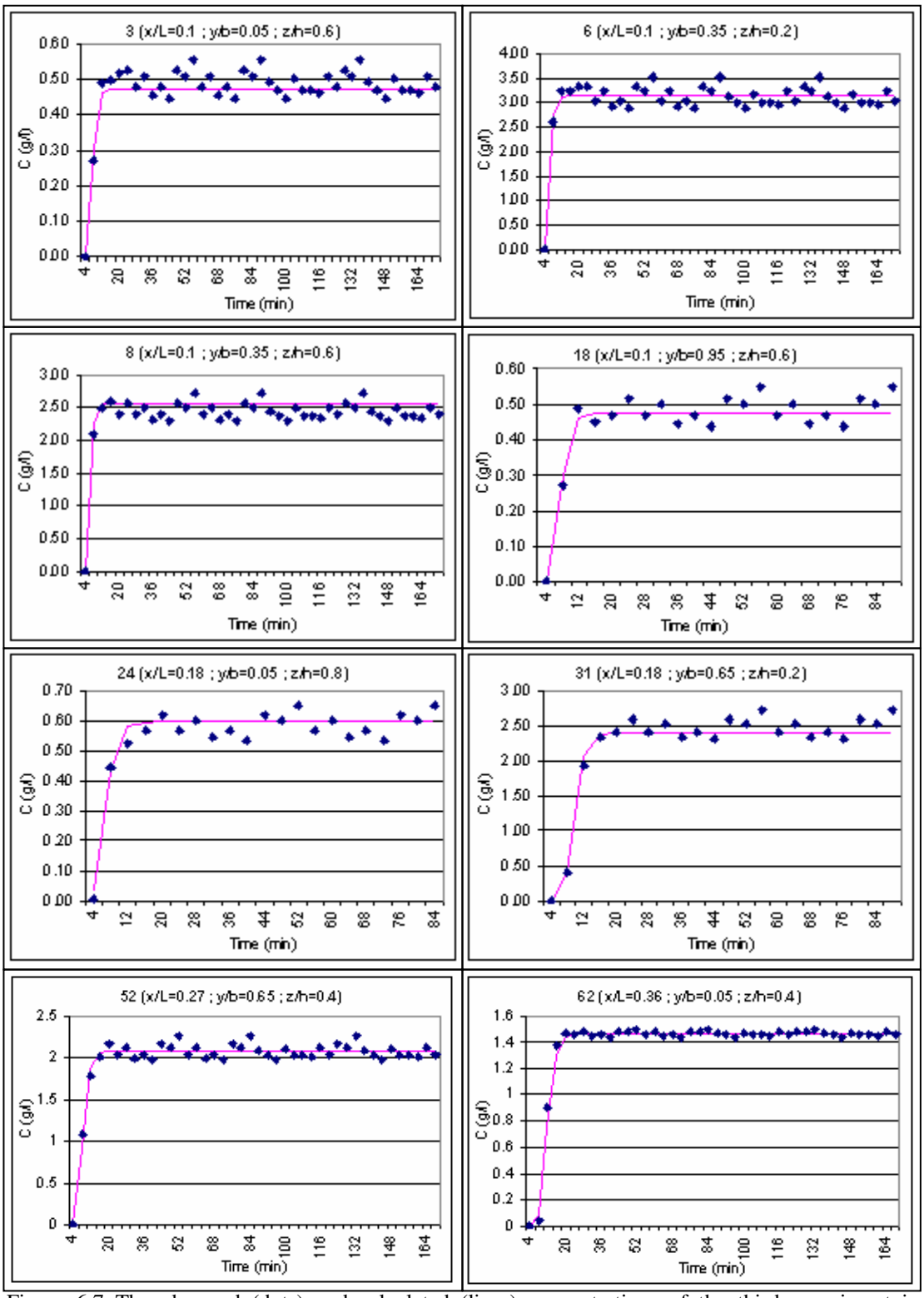


Figure 6.7 The observed (dots) and calculated (lines) concentrations of the third experiment in homogeneous medium

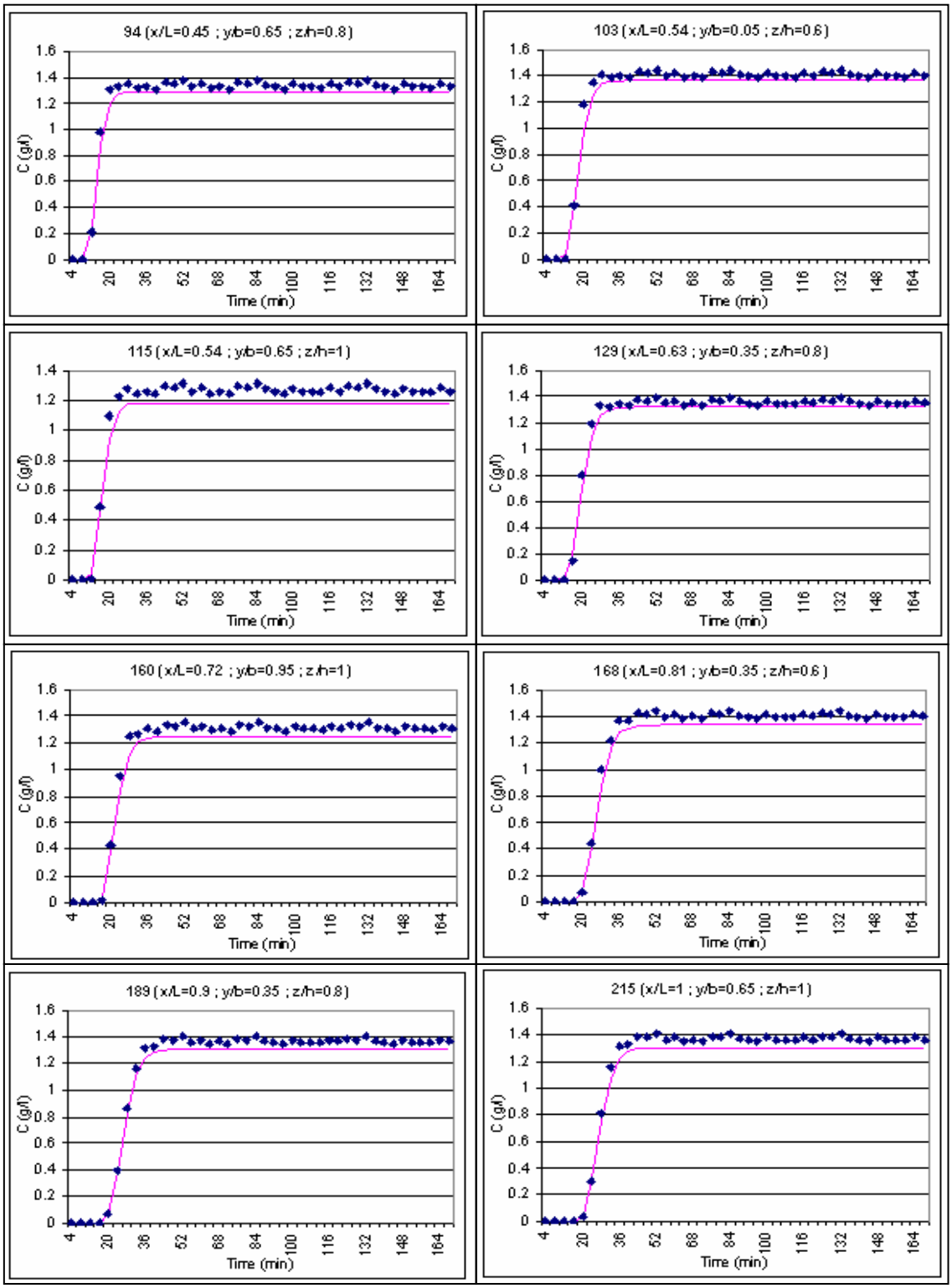


Figure 6.7 The observed (dots) and calculated (lines) concentrations of the third experiment in homogeneous medium (continued)

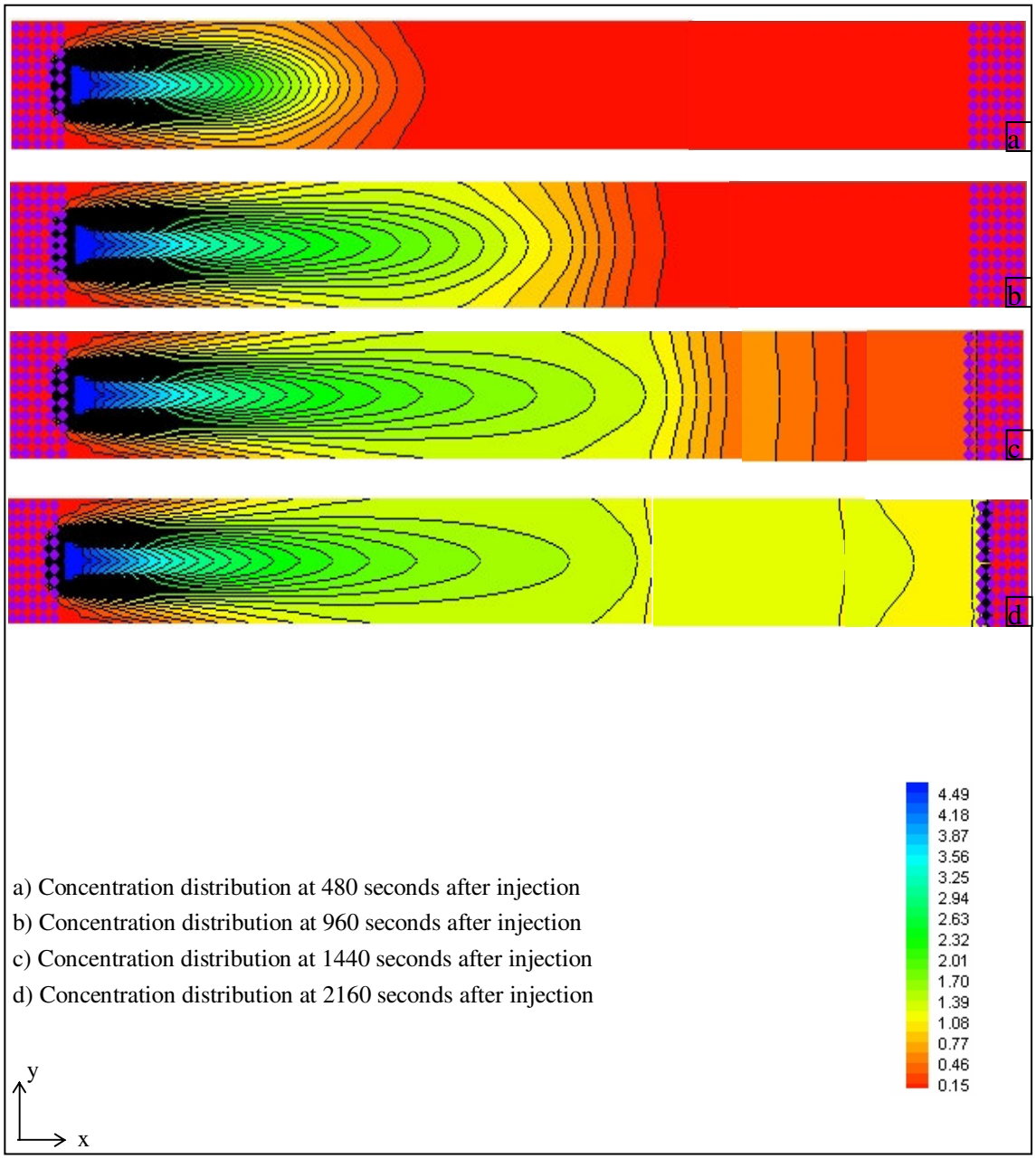


Figure 6.8 Plan view of the plume distribution versus time in homogeneous medium (third experiment)

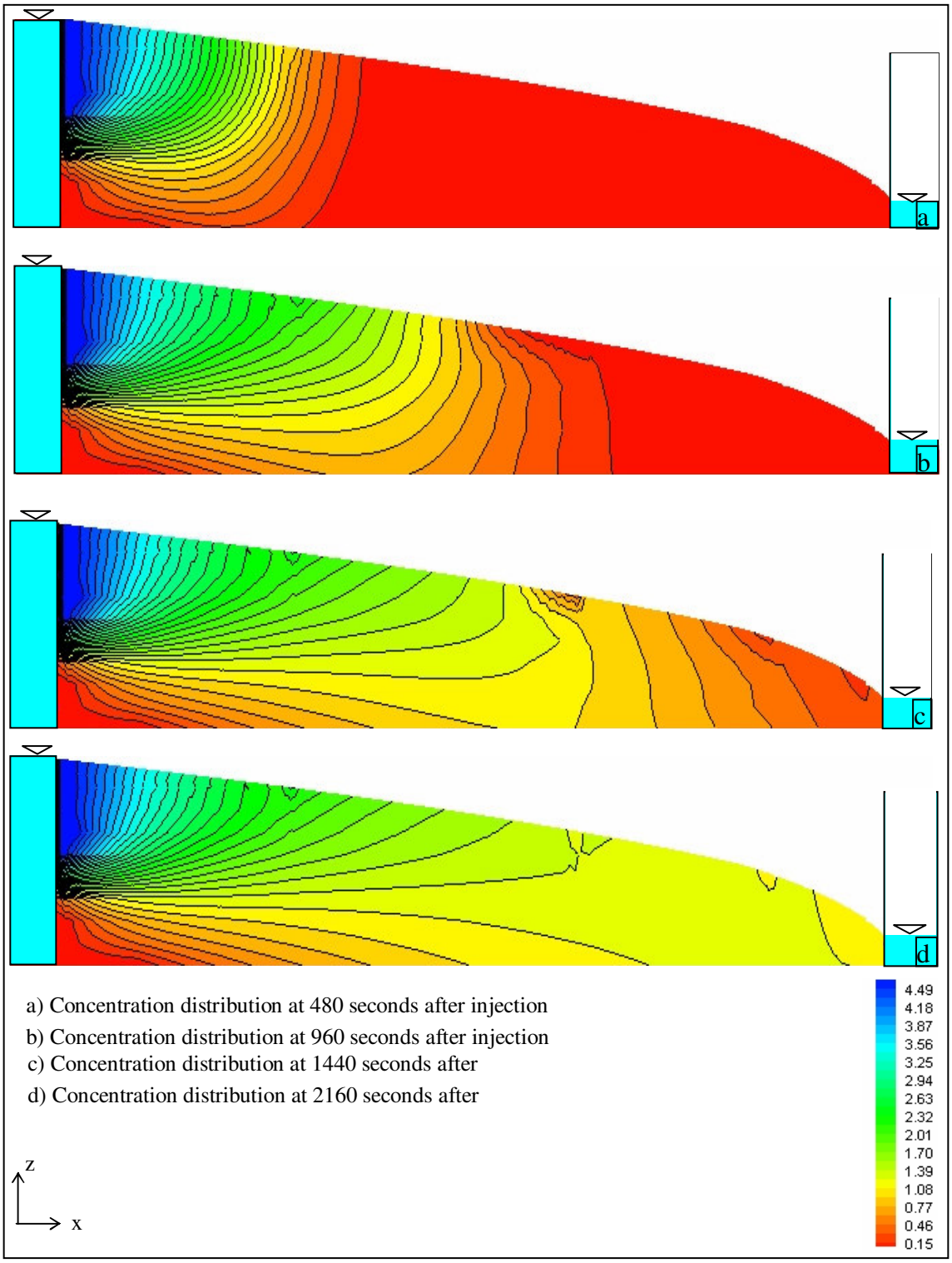


Figure 6.9 Longitudinal-sectional view of the plume distribution versus time in homogeneous medium (third experiment)

## 6.2 Dispersivity values of heterogeneous porous medium

The three-dimensional groundwater flow model has been established as grid of 10 rows, 100 columns and 11 layers for heterogeneous porous medium. Since the water level is constant at upstream and downstream end, the upstream and downstream boundary conditions are described as specific head boundary conditions and aquifer is specified as unconfined. The hydraulic conductivity values are taken as 1.1 cm/sec, 2.8 cm/sec and 10 cm/sec for 0.6-1.2 mm, 1-3 mm and 3-5 mm quartz sand, respectively, as shown in Figure 5.21. Mass Transport 3 Dimensional (Zheng and Wang, 1999, MT3DMS code) is used to solve the three dimensional advective-dispersive transport equation, neglecting the diffusion. The estimated dispersivity values are modified until an acceptable compatibility between the observed and calculated concentrations at measurement points is reached.

The dispersivity values of 3-5 mm quartz sand, determined from the experiment in homogeneous porous medium are incorporated into the mass transport model as $\alpha_x$=12.2 cm, $\alpha_y / \alpha_x$ = 0.21 and $\alpha_z / \alpha_x$ = 0.05. The dispersivity values of the 1-3 mm quartz sand are determined by using the observed concentrations obtained from the third experiment in heterogeneous medium of two layers. The best match is obtained for $\alpha_x$=5.5 cm, $\alpha_y / \alpha_x$ = 0.25 and $\alpha_z / \alpha_x$ = 0.07. The observed concentrations and those calculated by using the formentioned dispersivity values are given in Figure 6.10 for some measurement points. Plan and cross-sectional view of plume distributions in terms of time are given in Figure 6.11 and Figure 6.12, respectively.

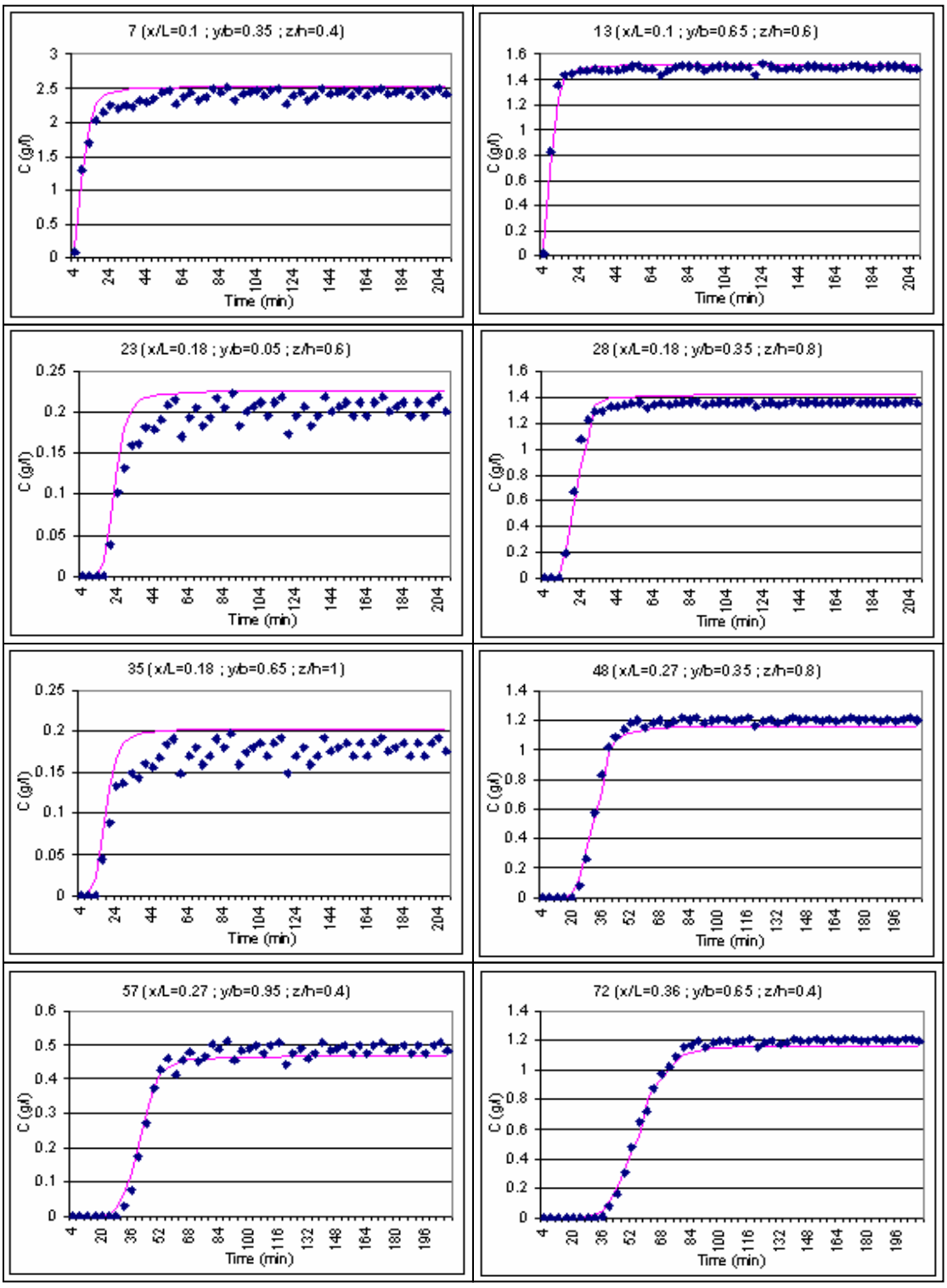


Figure 6.10 The observed (dots) and calculated (lines) concentrations of the third experiment in heterogeneous medium of two layers

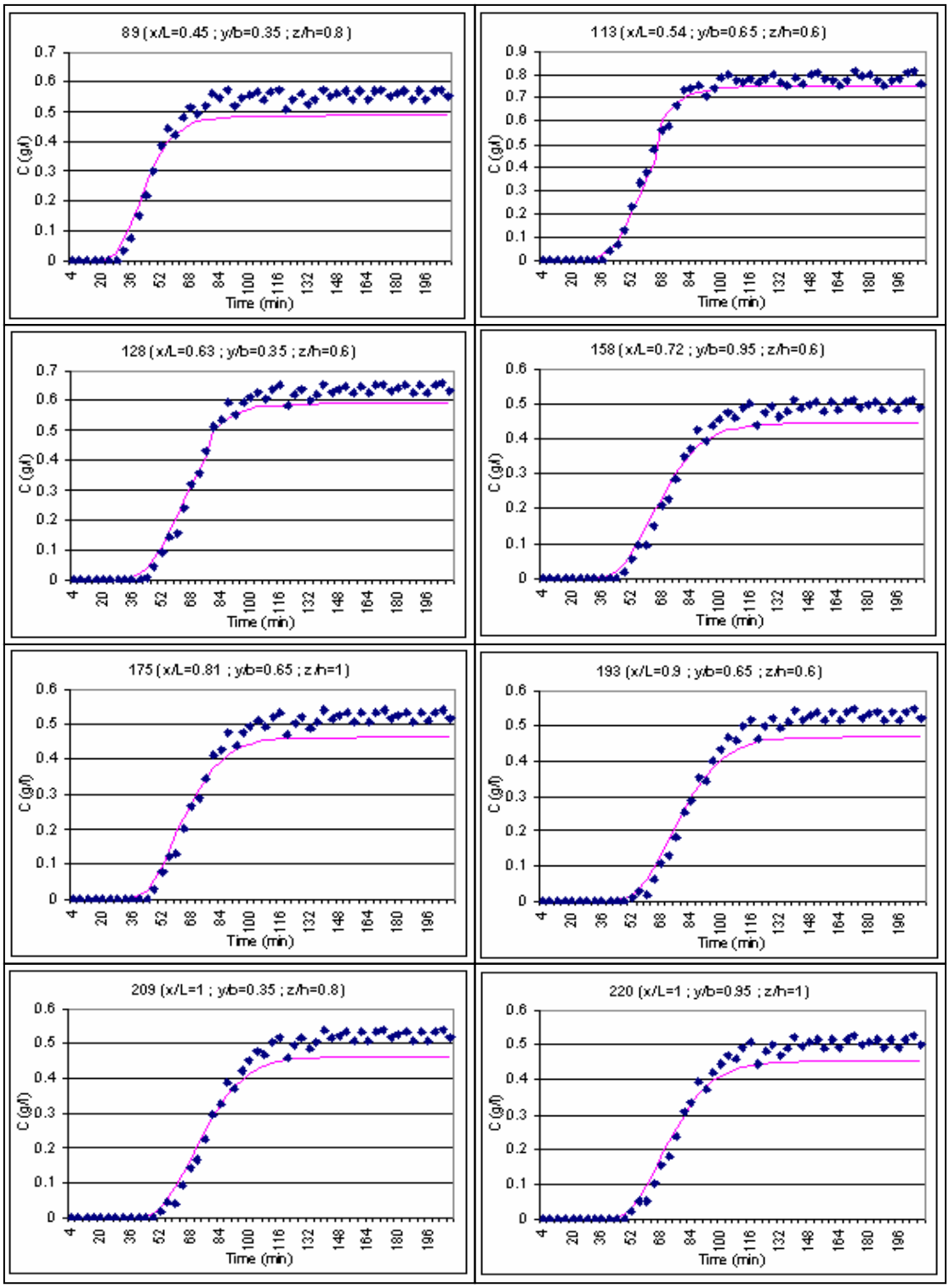


Figure 6.10 The observed (dots) and calculated (lines) concentrations of the third experiment in heterogeneous medium of two layers (continued)

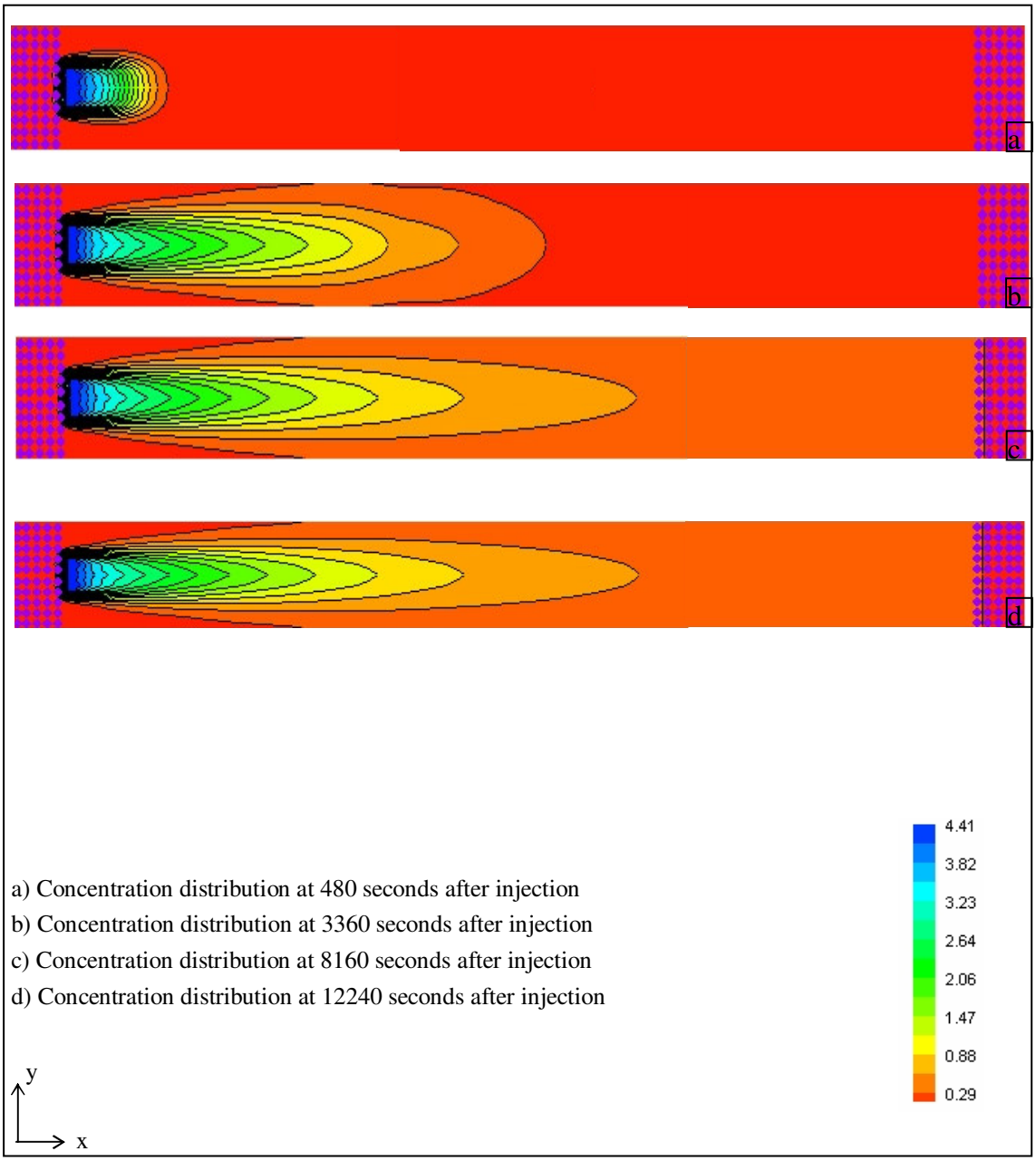


Figure 6.11 Plan view of the plume distribution versus time in heterogeneous medium of two layers (third experiment)

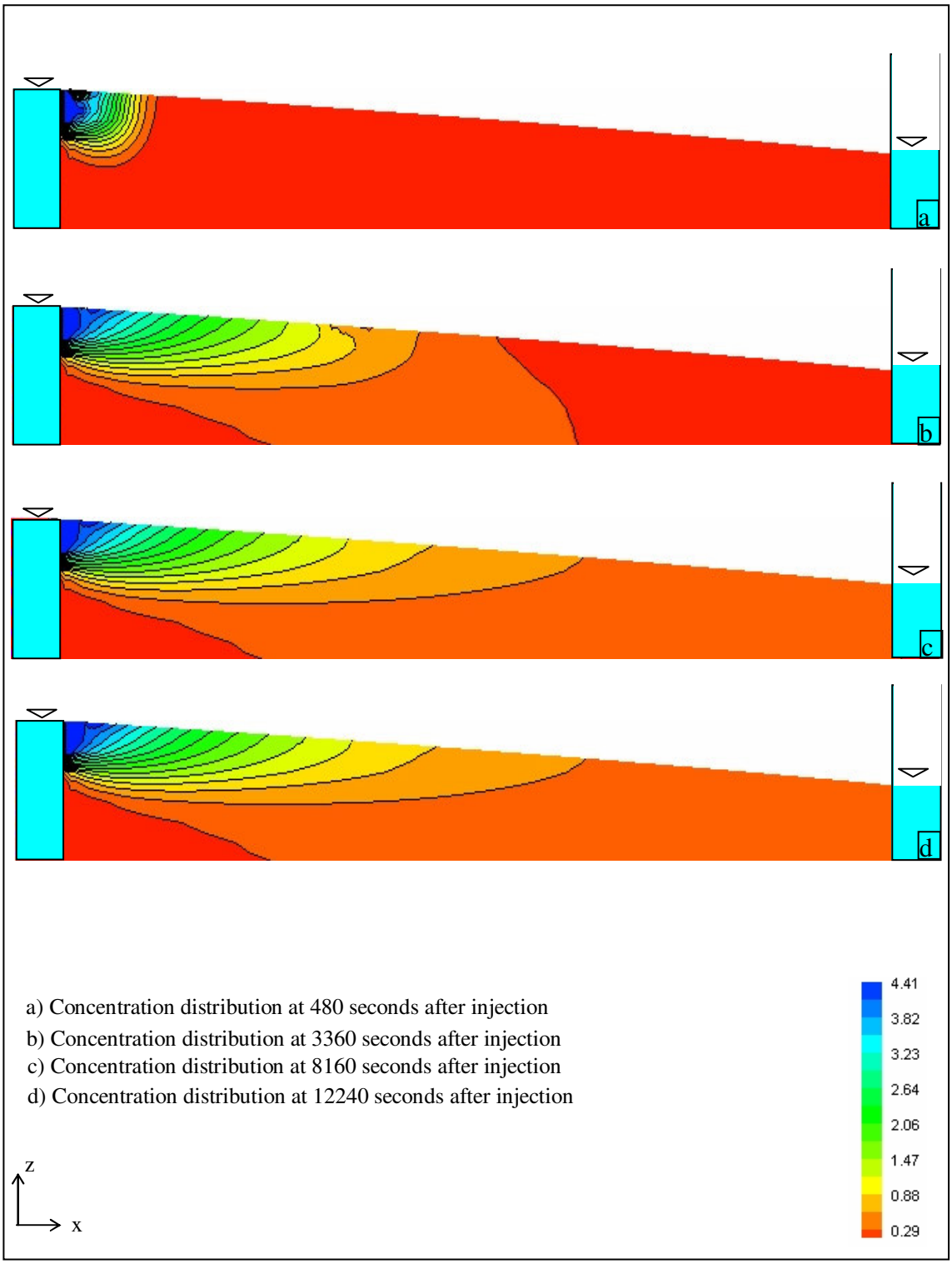


Figure 6.12 Longitudinal-sectional view of the plume distribution versus time in heterogeneous medium of two layers (third experiment)

The dispersivity values determined for the 3-5 mm and 1-3 mm quartz sand ( $\alpha_x$=12.2 cm, $\alpha_y / \alpha_x$ = 0.21, $\alpha_z / \alpha_x$ = 0.05 and $\alpha_x$=5.5 cm, $\alpha_y / \alpha_x$ = 0.25, $\alpha_z / \alpha_x$ = 0.07) are incorporated into the mass transport model. By using the observed concentration values obtained from the second experiment in heterogeneous medium of three layers, the dispersivity values of the 0.6-1.2 mm quartz sand are determined. The best match is obtained for $\alpha_x$ = 3 cm, $\alpha_y / \alpha_x$ = 0.18 and $\alpha_z / \alpha_x$ = 0.055 The observed concentrations and those calculated by using the formentioned dispersivity values are given in Figure 6.13 for some measurement points. Plan and cross-sectional view of plume distributions in terms of time are given in Figure 6.14 and Figure 6.15, respectively.

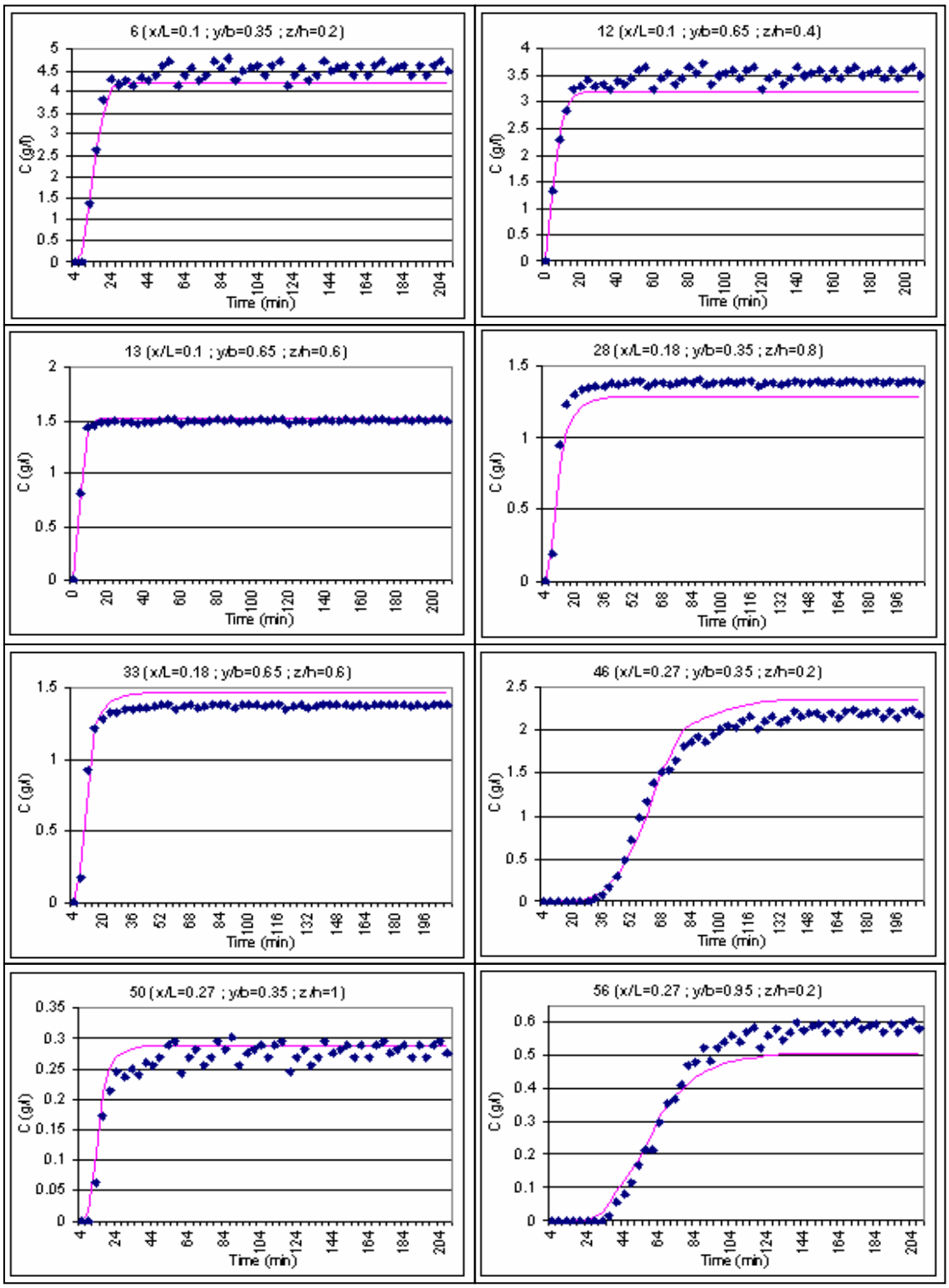


Figure 6.13 The observed (dots) and calculated (lines) concentrations of the second experiment in heterogeneous medium of three layers

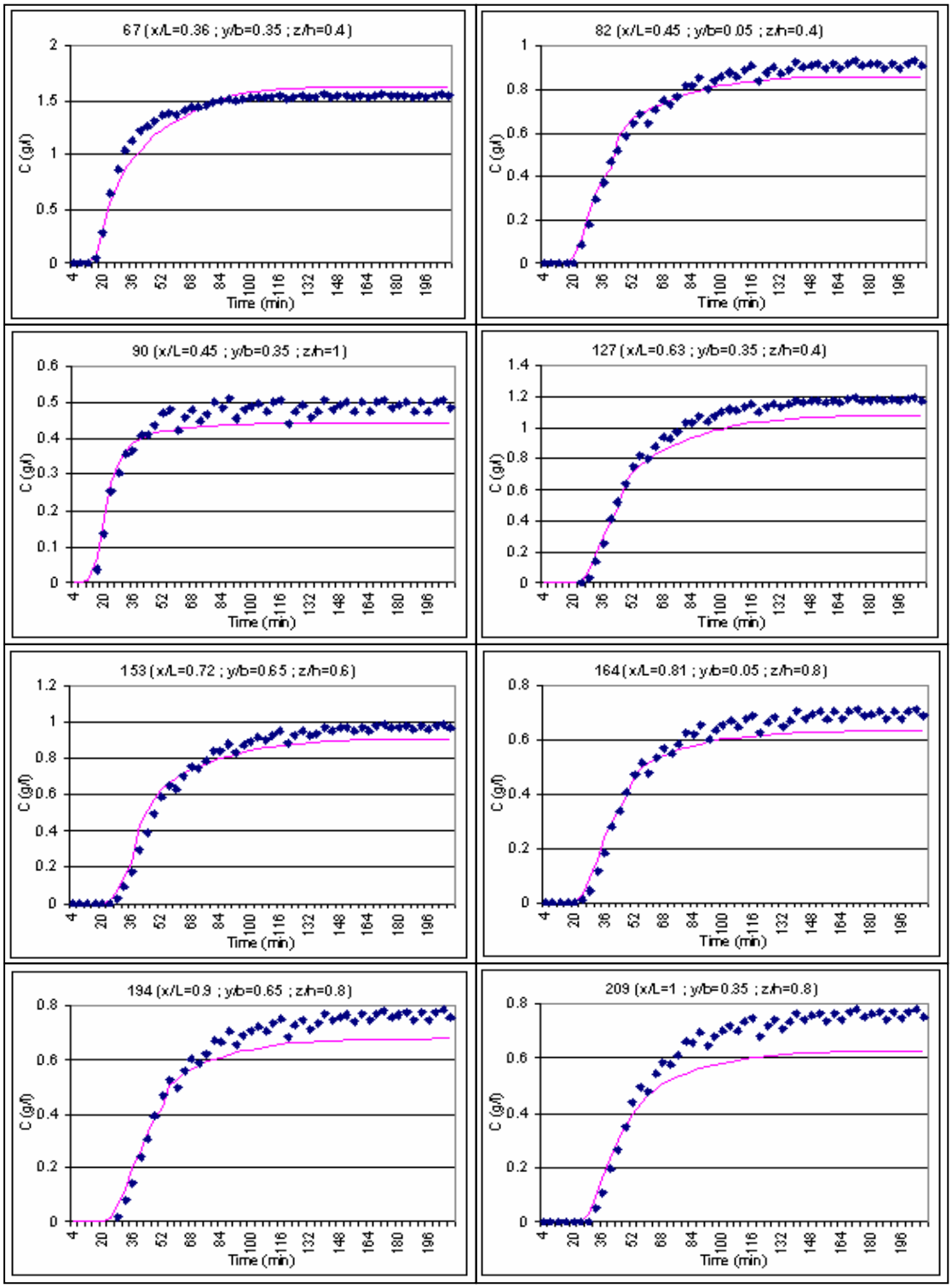


Figure 6.13 The observed (dots) and calculated (lines) concentrations of the second experiment in heterogeneous medium of three layers (continued)

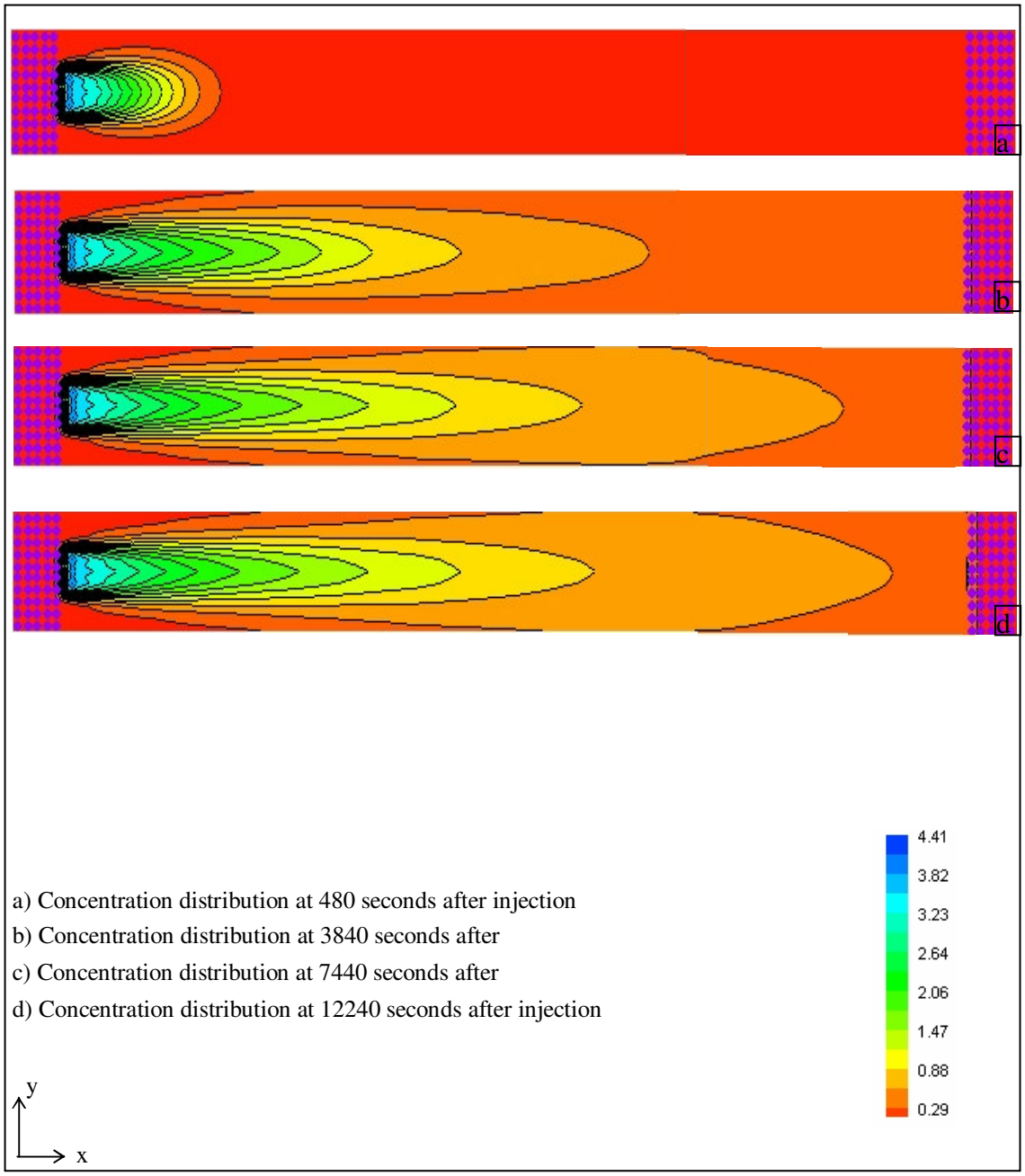


Figure 6.14 Plan view of the plume distribution versus time in heterogeneous medium of three layers (second experiment)

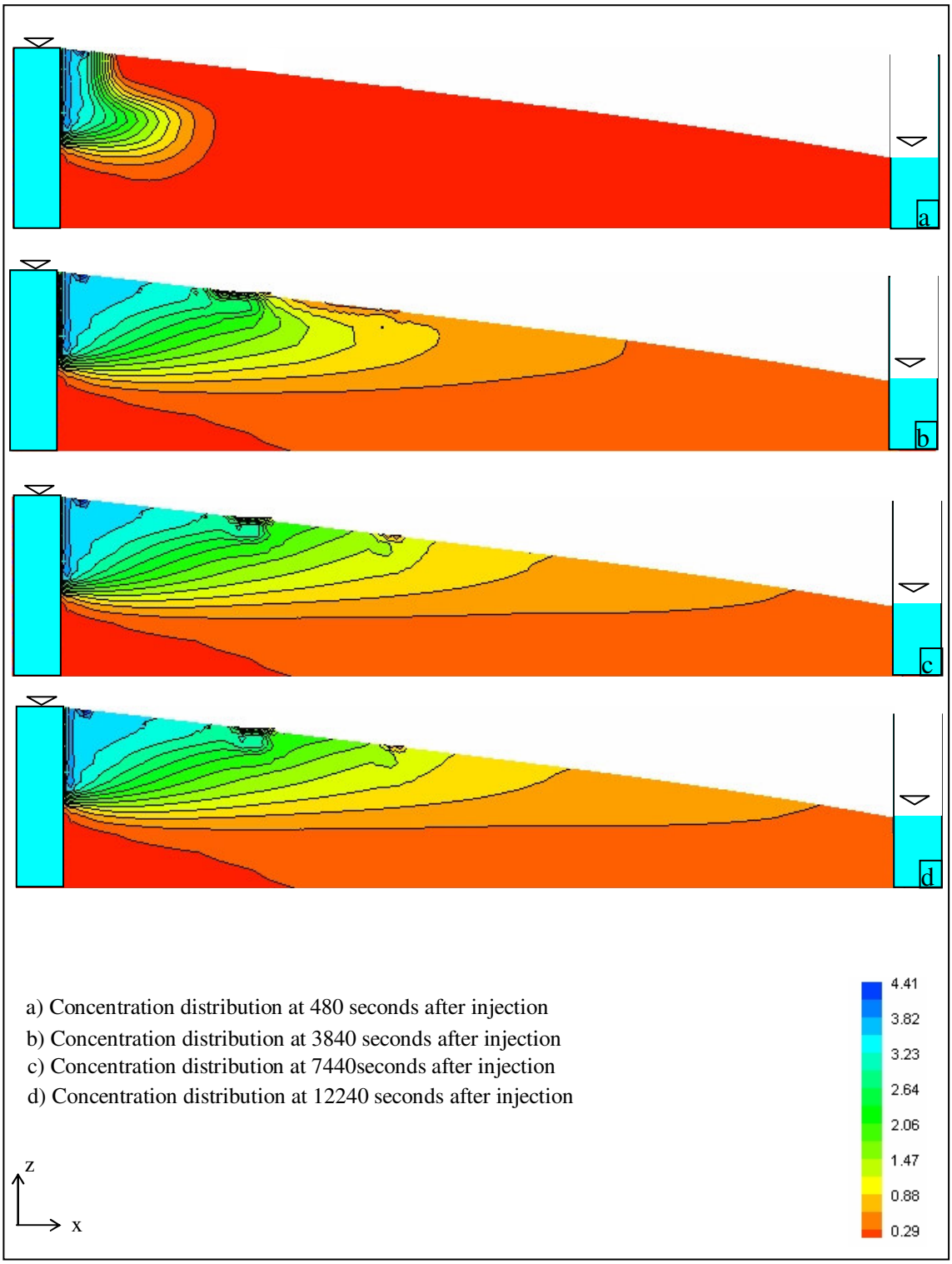


Figure 6.15 Longitudinal-sectional view of the plume distribution versus time in heterogeneous medium of three layers (second experiment)

As the present study is an inverse problem, the experimental concentration values concerning the last two experiments are used to obtain dispersivities from relevant equations by using trial and error method, and then these dispersivity values are used to calculate concentration values with conditions corresponding to the first experiment. These theoretical concentration values are compared with experimental ones for the sake of verification.

The dispersivities (for 3-5 mm quartz sand: $\alpha_x$=12.2 cm, $\alpha_y / \alpha_x$ = 0.21, $\alpha_z / \alpha_x$ = 0.05 , for 1-3 mm quartz sand: $\alpha_x$=5.5 cm, $\alpha_y / \alpha_x$ = 0.25, $\alpha_z / \alpha_x$ = 0.07 and for 0.6-1.2 mm quartz sand: $\alpha_x$ = 3.0 cm, $\alpha_y / \alpha_x$ = 0.18, $\alpha_z / \alpha_x$ = 0.055) obtained from last two experiments are used into the mass transport model to calculate concentrations corresponding to the first experiment. The observed and calculated concentrations are given in Figure 6.16 for some measurement points.

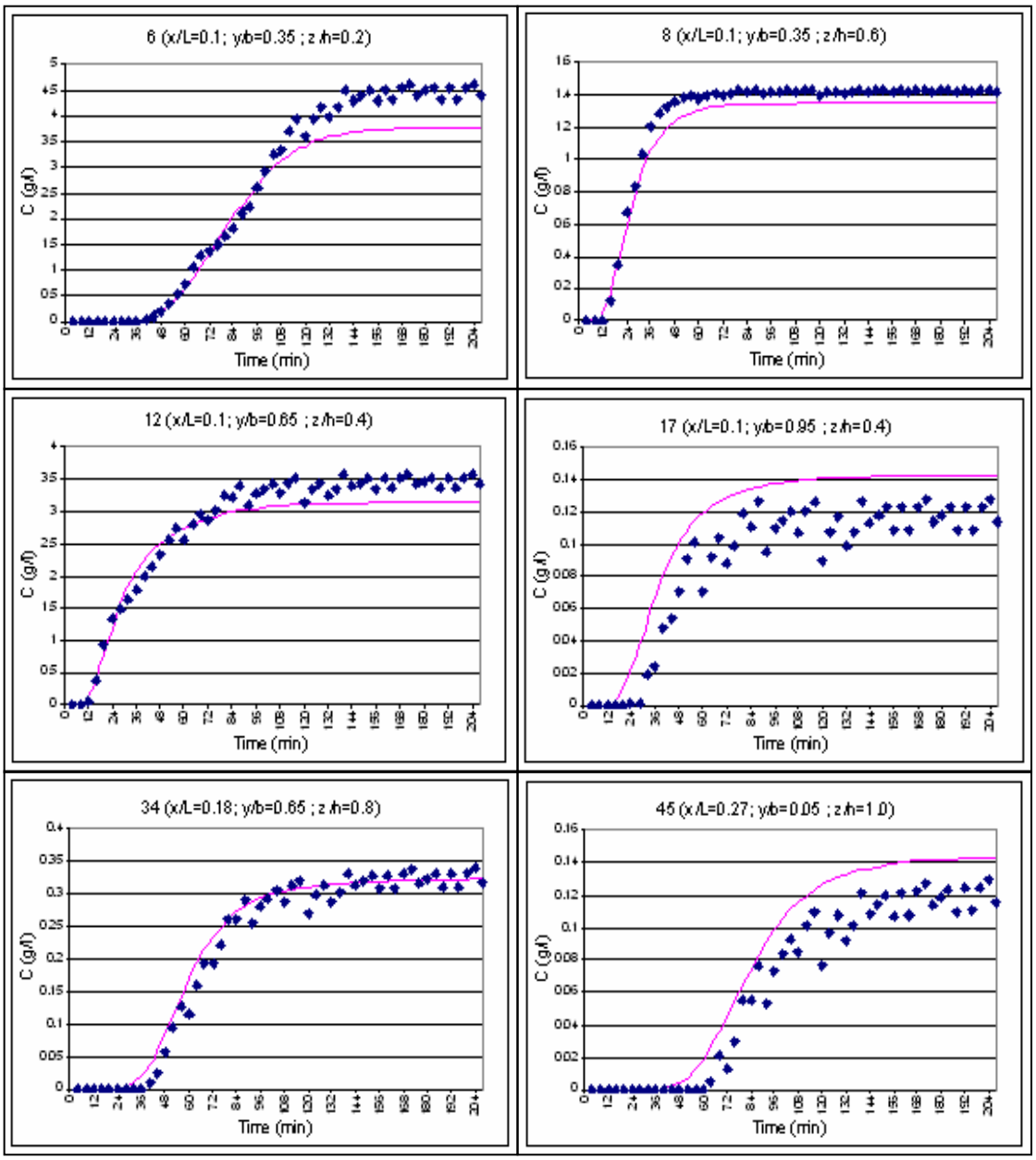


Figure 6.16 The observed (dots) and calculated (lines) concentrations of the first experiment in heterogeneous medium of three layers

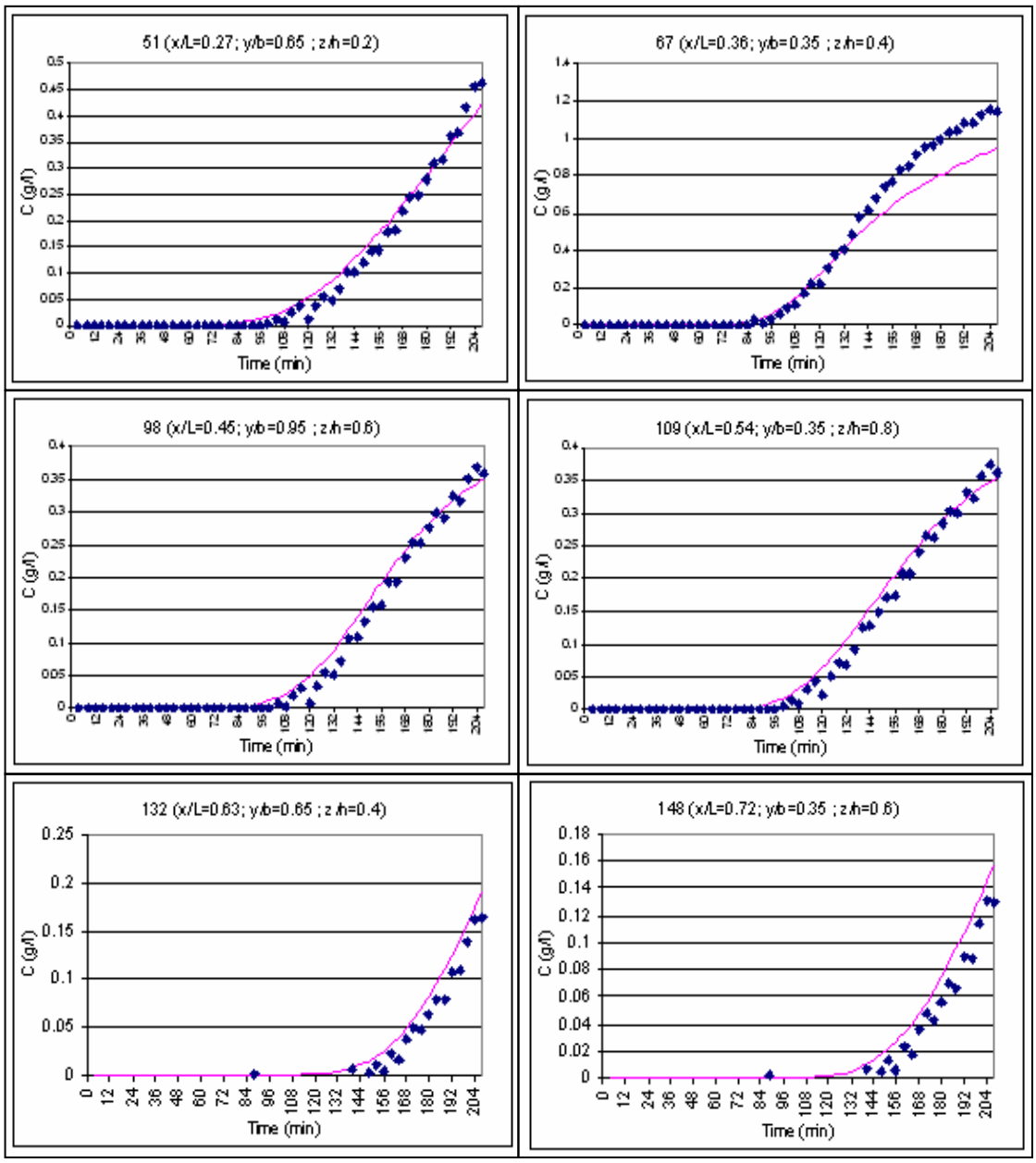


Figure 6.16 The observed (dots) and calculated (lines) concentrations of the first experiment in heterogeneous medium of three layers (continued)

# CHAPTER SEVEN
# CONCLUSION

In this study, an elaborate experimental system is designed and constructed in Hydraulics Laboratory of the Civil Engineering Department of Dokuz Eylül University, in order to study contaminant transport in homogeneous as well as heterogeneous media. First the contaminant transport is studied experimentally, and then the dispersivities in three dimensions for homogeneous and heterogeneous sandy aquifer are determined from laboratory tracer tests. The dispersivity parameters are obtained by trying several different combinations of their values in the related equations until one gets an acceptable accordance between the observed and computed breakthrough curves.

The values $\alpha_x$=12.2 cm, $\alpha_y / \alpha_x$= 0.22 and $\alpha_z / \alpha_x$= 0.05 give the best match between the observed and calculated breakthrough curves for the homogeneous aquifer constituted by using 3-5 mm quartz sand. These ratios are in the order of magnitude with those obtained from in-situ tests, given in the related literature.

According to experiments done in the heterogeneous aquifer dispersivity values of the 1-3 mm granular material are determined as $\alpha_x$=5.5 cm, $\alpha_y / \alpha_x$= 0.25 and $\alpha_z / \alpha_x$= 0.07. Dispersivity values $\alpha_x$= 3 cm, $\alpha_y / \alpha_x$= 0.18 and $\alpha_z / \alpha_x$= 0.055 give the best match between the observed and calculated breakthrough curves for the aquifer constituted by using 0.6-1.2 mm quartz sand. These ratios are also in the order of magnitude with those arisen from field tests.

As the studied subject is an inverse problem the dispersivity values obtained from the two experiments are used in the solution of the relevant equation with initial and boundary conditions corresponding to the third experiment for the sake of verification. The third experiment is the first and the last one in the case of homogeneous and heterogeneous porous media, respectively. The results are quite satisfactory.

It is revealed that the values of dispersivity depend on the diameter of the granular material and, they increase with the size of the granular material.

Various heterogeneous and anisotropic porous media - involving those corresponding to real site - can be formed in order to predict contaminant transport by means of mathematical models based on experiments performed on this experimental system.

This experimental system is designed to investigate contaminant transport in steady as well as unsteady flow, provided that some required measurement devices are provided. Consequently, it will also be beneficial to procure necessary instruments and pursue this study in the case of unsteady flow.

**REFERENCES**

Bear Jacob, Verruijt Arnold (1987). *Modeling Groundwater Flow and Pollution*. Reidel Publishing Company, Dordrecht, Holland.

Charbeneau Randall J. (2000). *Groundwater Hydraulics and Pollutant Transport*. Prentice Hall: Upper Saddle River, NJ.

Fetter (1993). *Contaminant Hydrogeology*. Prentice Hall: Upper Saddle River, NJ.

Ham P.A.S., Prommer H., Olsson A.H., Schotting R.J. , Grathwohl P. (2007). Predictive modelling of dispersion controlled reactive plumes at the laboratory-scale. Journal of *Contaminant Hydrology, 93*, 3014-315.

Huang K., Toride N., Van Genuchten M.TH. (1995). Experimental investigation of solute transport in large, homogeneous and heterogeneous, saturated soil columns. *Tranport in Porous Media, 18*, 283-302.

Kim D., Kim J., Yun S., Lee S. (2002). Determination of longitudinal dispersivity in an unconfined sandy aquifer. *Hydrological Processes, 16*, 1955-1964.

Kim S., Jo K., Kim D., Jury W.A. (2004). Determination of two-dimensional laboratory-scale dispersivities. *Hydrological Processes, 18*, 2475-2483.

Küreksiz, Ö., (2008) Non-darcian flow through rockfills, MS Thesis, Middle East Technical University, Department of Civil Engineering, Ankara Turkey.

Maineult A., Bernabe Y., Ackerer P. (2004). Electrical response of flow, diffusion, and advection in a laboratory sand box. *Vadose Zone Journal, 3*, 1180-1192.

Mascioli S., Benavente M., Martimez D.E. (2005). Estimation of transport hydraulic parameters in loessic sediment, Argentina: Application of column tests. *Hydrogeology Journal, 13,* 849-857.

McDonald, M. and Harbaugh A.W. (1988). *A modular three-dimensional finite difference groundwater flow model*. U.S. Geological Survey Techniques of Water Resources Investigations, Book 6.

Water.(n.d.). Retrieved August, 2008, from http://en.wikipedia.org/wiki/Water#Distribution_of_water_in_nature

Zheng C., Bennett G.D. (2002). *Applied Contaminant Transport Model.* John Wiley and Sons, Inc., New York.

Zheng C., P.P Wang. (1999) MT3DMS: *A modular three-dimensional multi-species model for simulation of advection, dispersion and chemical reactions of contaminants in groundwater systems: Documentations and User's guide*. SERDP-99-1, U.S. Army Engineer Research and Development Center, Vicksburg, MS.

# APPENDIX

The construction stages are explained below with illustrating photographs.

1. Construction of the brick piers according to the scheme given in Figure A.1


Figure A.1 Constructions of the brick piers

2. Placement of the metal sheets on the brick piers and welding of the plates in order to constitute a form for the concrete plate (Figure A.2).


Figure A.2 Constitution of the forms for the concrete plate


Figure A.2 Constitution of the forms for the concrete plate (continued)

3. Placement of the reinforcements to prevent probable cracks of the concrete plate (Figure A.3).


Figure A.3 Emplacement of the reinforcements

4. Pouring of the ready-mixed concrete of the plate which corresponds to the channel bottom (Figure A.4).


Figure A.4 Pouring of the ready-mixed concrete

5. Finishing of the concrete plate (Figure A.5).



Figure A.5 Finishing of the concrete plate

6. Drilling of the piezometer holes while the young concrete hardens (Figure A.6).


Figure A.6 The piezometer holes

7. Construction of the brick walls (Figure A.7).


Figure A.7 Construction of the brick walls


Figure A.7 Construction of the brick walls (continued)


Figure A.7 Construction of the brick walls (continued)

8. Placement of the perforated brick wall at upstream and downstream ends of the flume (Figure A.8).


Figure A.8 The upstream reservoir and the perforated wall

9. Plastering of the flume (Figure A.9).

Figure A.9 Plastering of the flume

10. Application of the water proof chemicals in order to prevent seepage from the flume (Figure A.10).


Figure A.10 Application of the water proof chemicals

11. Design and construction of the water supply tank equipped with pump, discharge pipe, and regulation valve (Figure A.11).


Figure A.11 The water supply tank

12. Placement of the chrome-nickel plate in the bottom of the flume (Figure A.12).


Figure A.12 The chrome-nickel plates

13. Fixation of the copper pipes (Figure A.13).


Figure A.13 The copper pipes

14. Manufacturing of the piezometers panel and connection with the copper tubes (Figure A.14)


Figure A.14 The panel of piezometers for reading the water levels

15. Fixation of the reinforcing steel profiles to overcome lateral pressure and to fasten the copper wires (Figure A.15).



Figure A.15 Fixation of the steel profiles

16. Construction of the sliding gate at the downstream end before the water supply tank (Figure A.16).

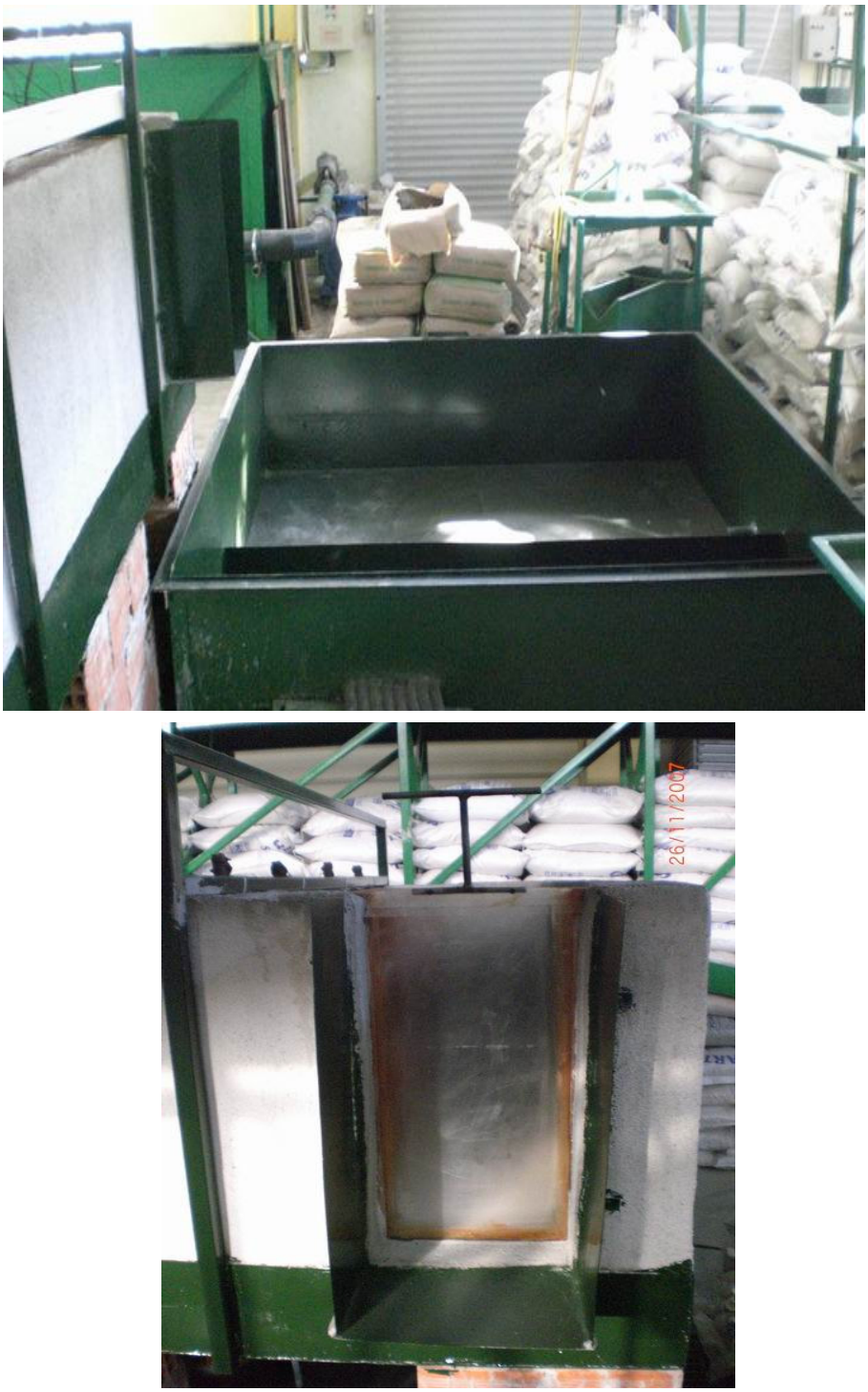


Figure A.16 The water supply tank and the gate of the downstream reservoir

17. Preparation and placement of the perforated plastic pipes (Figure A.17). The copper wires will be embedded in these pipes, to prevent hydrolysis.


Figure A.17 Preparation of the perforated plastic pipes



Figure A.17 Preparation of the perforated plastic pipes (continued)

18. Placement of the screens in front of each reservoir to prevent sand entry into the reservoir (Figure A.18).

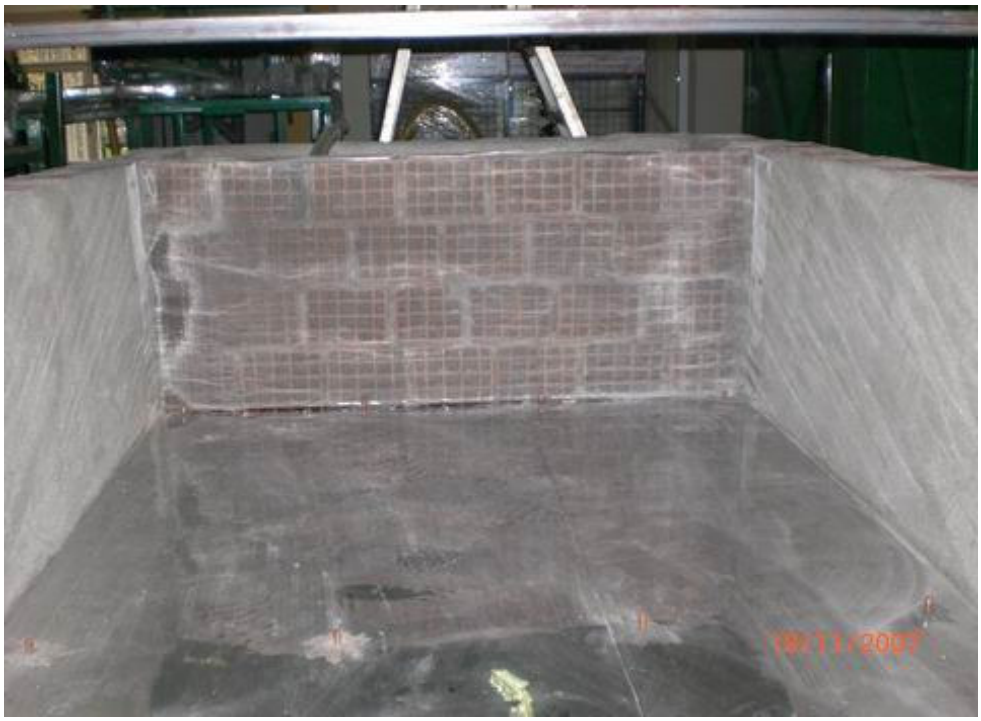

Figure A.18 Placement of the screens

19. Grouping by fives and numbering of the copper wires (Figure A.19).

Figure A.19 Grouping and numbering of the copper wires

20. Location of the perforated pipes and the copper wires (Figure A.20). The pipes are fastened and cables are soldered to the chrome-nickel plate to transmit the electricity.


Figure A.20 Location of the perforated pipes and the copper wires

21. Preparation and placement of the 1” pipes and the box (dimensions 15 cm by 55 cm by 30 cm) at upstream end to give tracer into the channel (Figure A.21).

Figure A.21 Placement of the pipes and the box to give tracer into the channel

22. Filling of the channel with grained material of 3-5 mm quartz coarse sand (Figure A.22).


Figure A.22 Filling of the channel with coarse sand

23. Fastening of the copper wires and their placement in the cable canal (Figure A.23).

Figure A.23 General view of the channel with armoured cables

24. Mounting of the valve at the downstream end of the channel to drain contaminated water (Figure A.24).

Figure A.24 The drain valve

25. Some seepage is observed when the water is pumped into the channel. Therefore some measures are taken by cutting metal sheet about 5 cm and slotting nearly 1 cm (Figure A.25).

Figure A.25 Cutting of the metal sheets and slotting of the wall in order to apply insulation material

26. Application of the insulation material (Ply-flex) into the slot (Figure A.26 and A.27)


Figure A.26 Application of the insulation material


Figure A.27 Application of the insulation liquid

27. Manufacturing and preparation of the scanner with 236 inputs to detect the electrical signals from the measurement points (Figure A.28).

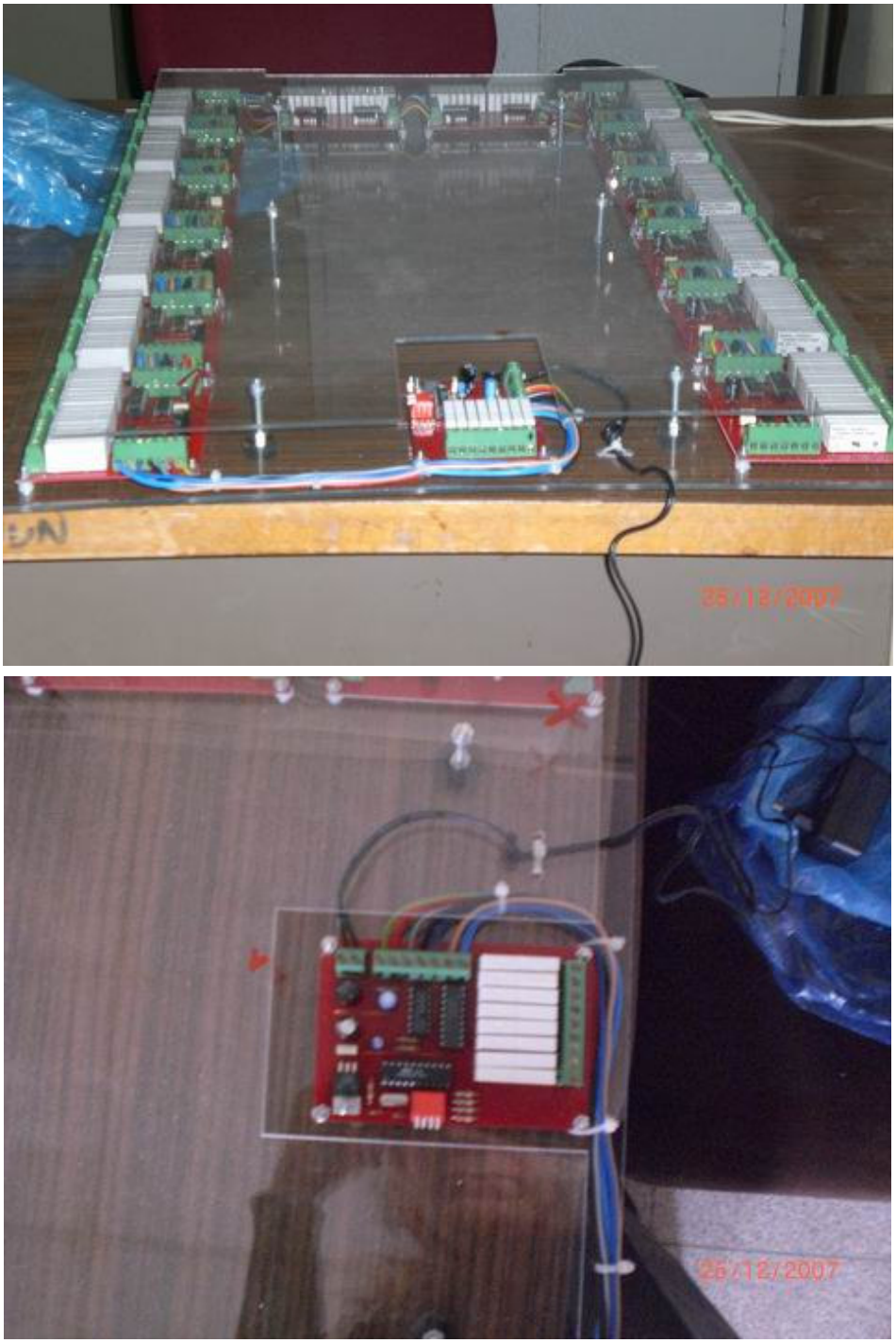

Figure A.28 Preparation of the signal detecting device with 236 inputs

28. Mounting of the signal detecting device and connection of the copper wires (Figure A.29).


Figure A.29 Mounting and connection of the copper wires

Figure A.29 Mounting and connection of the copper wires (continued)